The role of cytohesins and the ARNO-CNK1 complex in insulin signalling

Dissertation

zur

Erlangung des Doktorgrades (Dr. rer. nat.)

der Mathematisch-Naturwissenschaftlichen Fakultät

der Rheinischen Friedrich-Wilhelms-Universität Bonn

vorgelegt von

Christian Sieg

aus Oberhausen

Bonn, 2018

Angefertigt mit Genehmigung der Mathematisch-Naturwissenschaftlichen Fakultät
der Rheinischen Friedrich-Wilhelms-Universität Bonn

1. Gutachter: Prof. Dr. Michael Famulok

2. Gutachter: Prof. Dr. Matthias Geyer

Tag der Promotion: 27.08.2018

Erscheinungsjahr: 2018

Contents

List of Abbreviations

α-CT	C-terminal segment of the α chain
A_{280}	Absorption at 280 nm
A_{600}	Absorption at 600 nm
aa	Amino acid
AEBSF	4-(2-aminoethyl)benzenesulfonyl fluoride
AKAP	A-kinase anchoring protein
APS	Adaptor protein with PH and SH2 domains
ARF	ADP ribosylation factor
AS160	Akt substrate of 160 kDa
BRAG	Brefeldin-resistant Arf GEF
cAMP	3',5'-cyclic adenosine monophosphate
cc	Coiled-coil
CNK1	Connector enhancer of kinase suppressor of Ras 1
CoA	Coenzyme A
CBP	CREB-binding protein
CR	Cysteine-rich
CREB	Cyclic adenosine 3',5'-monophosphate response element-binding protein
CRAC	Conserved region among chordate
CRIC	Conserved region in CNK
DAG	Diacyl glycerol
Δcc	Construct with deleted coiled-coil domain
DEAE	Diethylaminoethyl
DGS-NTA(Ni)	1,2-dioleoyl-*sn*-glycero-3-[(N-(5-amino-1-carboxypentyl)iminodiacetic acid)succinyl] nickel salt
DLS	Dynamic light scattering
DMF	Dimethylformamide
DUF1170	Domain of unknown function 1170
EFA6	Exchange factor for Arf6
ER	Endoplasmic reticulum
ERGIC	ER-Golgi intermediate compartment
ERK	Extracellular-signal regulated kinase
Fbox8	F-box only protein 8
FnIII	Fibronectin type III
FRET	Förster resonance energy transfer

G protein	Guanine nucleotide-binding protein
GAP	GTPase-activating protein
GBF/BIG	Golgi BFA-resistance factor1/BFA-inhibited GEF
GEF	Guanine nucleotide exchange factor
GLP-1	Glucagon-like peptide-1
GRB	Growth factor receptor-bound protein
GRP1	General receptor for 3-phosphoinositides-1
GS	Glycogen synthase
GSH	Reduced glutathione
GSK3	Glycogen synthase kinase-3
GSP	Glycogen synthase phosphatase
GST	Glutathione S-transferase
HEPES	4-(2-Hydroxyethyl)-1-piperazineethanesulphonic acid
HIRcB	Rat fibroblasts overexpressing insulin receptor
HSL	Hormone-sensitive lipase
ICD	Intracellular domain
IEX	Ion exchange chromatography
IGFR	Insulin-like growth factor receptor
IMAC	Immobilised metal ion affinity chromatography
IPCEF1	Interaction protein for cytohesin exchange factors 1 (CNK3B)
IPTG	Isopropyl β-D-1-thiogalactopyranoside
IQGAP1	IQ motif containing GTPase activating protein 1
IR	Insulin receptor
IRS1	Insulin receptor substrate-1
ITC	Isothermal titration calorimetry
JM	Juxtamembrane
KC	Kinase core
K_D	Dissociation constant
kDa	Kilo Dalton
LB	Lysogeny broth
LC-MS	Liquid chromatography-mass spectrometry
Mant	2’/3’-O-N-Methyl-anthraniloyl
MAPK	Mitogen-activated protein kinase
MBP	Maltose-binding protein
MEK	MAPK/ERK kinase
MetAP	Methionine aminopeptidase

MST	Microscale thermophoresis
mTOR	Mammalian target of rapamycin
MW	Molecular weight
myr-ARF	Myristoylated ARF
NHS	N-Hydroxysuccinimide
Ni-NTA	Nickel nitrilotriacetic acid
NMT	N-myristoyltransferase
o/n	Overnight
p. a.	Pro analysi
P loop	Phosphate-binding loop
pbr	Polybasic region
PC	L-α-phosphatidylcholine
PDE	Phosphodiesterase
PDK1	3-phosphoinositide-dependent protein kinase-1
PDZ	Domain present in PSD-95/DLG-1/ZO-1/2
PE	L-α-phosphatidylethanolamine
PH	Pleckstrin homology
PI3K	Phosphatidylinositol-3-kinase
PI5K	Phosphatidylinositol-4-phosphate-5-kinase
PIP_2	L-α-phosphatidylinositol-4,5-bisphosphate
PIP_3	L-α-phosphatidylinositol-3,4,5-trisphospate
PKA	Protein kinase A
PKB	Protein kinase B
PS	L-α-phosphatidylserine
PSD	Pleckstrin and Sec7 domain containing
PSI	Pound per square inch
PTPase	Protein tyrosine phosphatase
pY	Phosphotyrosine
Rab	Ras related in brain
Ran	Ras related nuclear protein
Ras	Rat sarcoma
Rho	Ras homologous
rpm	Revolutions per minute
RT	Room temperature
RTK	Receptor tyrosine kinase
SAM	Sterile alpha motif

SEC	Size-exclusion chromatography
SDS	Sodium dodecyl sulphate
SDS-PAGE	SDS-polyacrylamide gel electrophoresis
SOS	Son of sevenless
Sulfo-SBED	Sulfosuccinimidyl-2-[6-(biotinamido)-2-(*p*-azidobenzamido) hexanoamido]ethyl-1,3´-dithiopropionate
TCEP	Tris(2-carboxyethyl)phosphine
TRIS	Tris(hydroxymethyl)aminomethane
UDP glucose	Uridine diphosphate glucose
UV	Ultraviolet

List of Figures

List of Tables

Zusammenfassung

Um auf externe Reize reagieren zu können und die Zellhomöostase aufrecht zu erhalten, ist die Regulation von Signalkaskaden für alle Organismen von großer Wichtigkeit. Bei Wirbeltieren stellt die Insulinsignalübertragung einen entscheidenden metabolischen Signalweg dar und eine Fehlregulation, wie sie zum Beispiel im Fall von Diabetes mellitus vorkommt, ist ein Gesundheitsrisiko in der alternden Gesellschaft. Die vorliegende Arbeit untersucht die Funktion von Cytohesinen und des Adapterproteins *Connector enhancer of kinase suppressor of ras 1* (CNK1) im Insulinsignalweg.

Bei Cytohesinen handelt es sich um Guaninnukleotid-Austauschfaktoren für ADP-Ribosylierungsfaktoren (Arf)-GTPasen, die an der Insulinsignalübertragung beteiligt sind. Zelluläre Daten weisen darauf hin, dass CNK1 einen Komplex mit dem Cytohesin *Arf nucleotide-binding site opener* (ARNO) bildet. Dieser Komplex soll für die Translokation von ARNO zur Plasmamembran notwendig sein und wirkt an der Signalweiterleitung vom Insulinrezeptor zum zentralen Effektor Proteinkinase B (PKB) mit.

Um die Rolle von ARNO innerhalb des Insulinrezeptor (IR)-Netzwerkes genauer zu verstehen, wurden in dieser Arbeit biochemische und biophysikalische Untersuchungen durchgeführt. Eine direkte Interaktion zwischen ARNO und dem IR wurde nicht nachgewiesen, jedoch konnte die Interaktion zwischen ARNO und CNK1 detailliert aufgeklärt werden. *Pull-down* Experimente, analytische Gelfiltration und isotherme Titrationskalorimetrie zeigten die direkte Interaktion der beiden Proteine über deren *coiled-coil*-Domänen. Proteinkristalle wurden generiert, die aufgrund schlechter Beugung von Röntgenstrahlen jedoch keine Strukturbestimmung ermöglichten. Um den Effekt der Komplexbildung auf die katalytische Aktivität von ARNO zu untersuchen, wurden Guaninnukleotid-Austauschreaktionen mit myristoylierten Arfs an Liposomen etabliert. In Einklang mit der Literatur lokalisiert wildtyp CNK1 nicht an Membranen und hatte keinen Einfluss auf den ARNO-vermittelten Nukleotidaustausch. Da sowohl aktiviertes CNK1 als auch ARNO an der Zellmembran lokalisiert sind, wurde CNK1 über einen Polyhistidin-Tag künstlich an funktionalisierte Liposomen gekoppelt. Trotz der erfolgreichen Liposomen-Lokalisation, konnte unter diesen Bedingungen kein Austausch gemessen werden, weshalb die Auswirkung der Interaktion auf die ARNO-Aktivität mit einem anderen Verfahren untersucht werden muss.

Mechanistisch ist es wahrscheinlich, dass CNK1 die Konzentration ARNO und hiermit aktiven Arfs an der Plasmamembran erhöht, was wiederum PIP_2-vermittelt das Insulinsignal verstärkt. Lysin-Acetylierung innerhalb der PH-Domäne von CNK1 ist ein möglicher Rekrutierungsmechanismus, der durch weitere Studien bestätigt werden muss.

Abstract

The tight regulation of signalling cascades is of crucial importance for organisms in order to react to external stimuli and maintain homeostasis. Insulin signalling is a key metabolic pathway in vertebrates and dysregulation as seen in the case of diabetes mellitus poses a major health risk to the ageing society. This work aims at a deeper understanding of the underlying intracellular signalling cascade, especially of the cytohesin-CNK1 complex.

Cytohesins are guanine nucleotide exchange factors for GTPases of the ADP-ribosylation factor (Arf) family and were shown to be involved in insulin signalling. Cellular data further suggest that the adaptor protein Connector enhancer of kinase suppressor of ras 1 (CNK1) forms a complex with the cytohesin Arf nucleotide-binding site opener (ARNO). This complex is required for the translocation to the plasma membrane and signal transduction from the insulin receptor to its downstream effector protein kinase B (PKB).

To characterise interaction partners of ARNO and elucidate its mode of action within the insulin receptor (IR) signalling network, biochemical and biophysical approaches were undertaken. A direct interaction of ARNO with the IR could not be demonstrated, however this study characterises the interaction between ARNO and CNK1 in depth. Using pull-down, analytical size-exclusion chromatography and isothermal titration calorimetry approaches, a direct physical interaction between ARNO and CNK1 was shown. Furthermore, the interaction site was mapped to the respective coiled-coil domains of both proteins. Structural studies resulted in the generation of protein crystals, which however did not allow for structure determination due to poor X-ray diffraction. To elucidate the effect of complex formation on the catalytic activity of ARNO, an exchange assay using liposomes and myristoylated Arfs was established. The localisation as well as the effect of CNK1 on the exchange rate was tested *in vitro*. As expected, wildtype CNK1 did not localise to membranes and also did not affect ARNO-catalysed exchange. Since activated CNK1 as well as ARNO are membrane-bound, CNK1 was artificially tethered to functionalised liposomes via a hexahistidine-tag. Although the liposome tethering was successful, no exchange could be monitored under these conditions, and hence the consequences of the interaction on the exchange rate remain to be investigated using a modified approach.

Possibly, CNK1 helps localise cytohesins to the plasma membrane which increases the concentration of activated Arf. Sustained Arf activity leads to higher levels in phosphatidyl-inositol-4,5-bisphosphate (PIP_2) and increased IR signalling. Lysine acetylation within the PH domain of CNK1 might be an important factor to direct CNK1 to the membrane and drive signalling but further studies need to confirm the specific mode of action.

1 Introduction

1.1 Intracellular signalling

For a multicellular organism, signal transmission, integration and processing are vital to react to external stimuli. Signals can be conveyed electrically via the nervous system or by soluble chemical messengers such as hormones and paracrine mediators. Once the messenger molecule has reached its target cell, it exerts its action by binding to a specific receptor. If the messenger molecule is membrane permeable like steroid hormones, the receptor can be located inside the cell (Germain *et al.* 2006). More often however, the mediating molecule cannot penetrate the cellular barrier and therefore binds to a receptor located within the cell membrane. Those transmembrane receptors consist of extra- and intracellular domains as well as a membrane-spanning domain to receive and transmit a signal.

Most transmembrane receptors can be assigned to one of three categories: ion channels, G protein-coupled receptors and enzyme-linked receptors. The acetylcholine receptor is a typical example for an ion channel receptor which allows cations to pass when ligands such as acetyl choline (and many more) bind (Karlin 2002). G protein-coupled receptors are seven-pass transmembrane proteins and transfer the signal via the activation of an intracellular trimeric guanine nucleotide-binding protein (G protein). A light-sensitive G protein-coupled receptor is the rhodopsin photoreceptor located in the retina (Garriga and Manyosa 2002). Ligand binding to an enzyme-linked receptor activates enzymatic activity in the receptor itself or an associated protein via the induction of conformational changes. Typically, this leads to the activation of a kinase as in the case of the insulin receptor (Kasuga *et al.* 1982, Hubbard 2013).

1.1.1 Intracellular signal transmission

Once a receptor is activated, intracellular signalling molecules assist in relaying the signal to target proteins. Those signalling molecules can be so called “second messengers” like water-soluble 3’,5’-cyclic adenosine monophosphate (cAMP), Ca^{2+} or the lipid-soluble diacyl glycerol (DAG) (Newton *et al.* 2016). Phosphatidylinositol-3,4,5-trisphospate (PIP_3) produced by phosphatidylinositol-3-kinase (PI3K) and cAMP constitute important second messengers in insulin signalling (Ruderman *et al.* 1990, Cohen 2006).

Furthermore, proteins and protein complexes are major constituents of signalling cascades. The interplay of those components leads to signal transmission, amplification, integration and finally the desired effect. Proteins involved in signalling cascades can covalently modify other proteins (such as kinases), work as molar switches (GTPases) or

assist in the assembly of large signalling complexes (scaffold proteins). Finally, the signalling process results in alterations of gene expression, metabolism or cell shape to encounter the stimulus. Importantly, this is not a unidirectional process with clear beginning and end. The components are interconnected and several feedback mechanisms lead to signal attenuation and termination. In the case of the insulin receptor (IR), which is a receptor tyrosine kinase, protein tyrosine phosphatases (PTPases) stop the signalling once the ligand has dissociated (Sugimoto *et al.* 1994).

1.1.2 Protein-protein interactions

The molecular basis of signal transmission between proteins is their physical interaction and possibly covalent modification. Interaction with a binding partner can change the catalytic activity, alter the accessibility for other factors or simply shift the subcellular localisation and hence allow new functions. A modular set of specialised binding domains has evolved and was shown to be crucial for the majority of protein-protein interactions within signalling cascades. Important examples with relevance for this work are highlighted in the following paragraphs.

Activation of signalling proteins often involves protein phosphorylation by kinases. The Src homology 2 (SH2) and phosphotyrosine-binding (PTB) domains both recognise phosphotyrosines in peptide sequences (Sadowski *et al.* 1986, Kavanaugh and Williams 1994). SH2 domains consist of about 100 amino acids and were found in many signalling proteins such as the p85α subunit of PI3K (Russell *et al.* 1992, Booker *et al.* 1992). The PTB domains are structurally more diverse than SH2 domains and can be further classified. The insulin receptor substrate-1 (IRS1) binds via PTB to the activated, phosphorylated IR (Eck *et al.* 1996) and gave rise to the group of IRS-type PTB domains.

Src homology 3 (SH3) domains are protein interaction modules of about 60 amino acids and bind to short proline-rich hydrophobic patches via their hydrophobic core (Yu *et al.* 1992). The function is not comprehensively understood but SH3 domains seem to play a role in protein localisation and the assembly of signalling protein complexes (Schlessinger 1994). The previously mentioned PI3K p85α subunit for example, also contains an SH3 domain apart from its two SH2 domains (Koyama *et al.* 1993).

Another domain similar to the SH2 and SH3 domains in respect to its sequence homology and overall functionality was discovered shortly afterwards, the pleckstrin homology (PH) domain (Musacchio *et al.* 1992, Haslam *et al.* 1993). In contrast to the aforementioned domains, PH domains primarily bind phosphorylated phosphoinositides but they also serve as protein-protein interaction modules (Harlan *et al.* 1994, Wang *et al.* 1994). Both

cytohesins and Connector enhancer of KSR 1 (CNK1), which this study focusses on, possess PH domains (Kolanus *et al.* 1996, Jaffe *et al.* 2004).

Further, Domain present in PSD-95/DLG-1/ZO-1/2 (PDZ domains) comprise a heterogeneous group of modules which bind either C-terminal protein sequences or internal polypeptides with varying binding specificities (Ponting *et al.* 1997). CNK1 possesses a PDZ domain consisting of 90 amino acids (Jaffe *et al.* 2004).

Finally, the coiled-coil (cc) domain is introduced. First described by Francis Crick in the early 1950s, this motif usually consists of two to five α-helices wound around each other in a left-handed helix termed “supercoil” (Crick, F. H. C. 1953, Mason and Arndt 2004). The supercoil is formed by a seven-residue repeat which is commonly denoted $[abcdefg]_n$. Here, a and d are typically nonpolar residues located at the inside of the helix while e and g are solvent exposed residues which account for the specificity between the helices (Mason and Arndt 2004). 3-5 % of all amino acids in proteins form a coiled-coil motif and so do cytohesins and CNK1 (Mason and Arndt 2004, Wolf *et al.* 1997, Chardin *et al.* 1996, Fritz and Radziwill 2011). Fig. 1-1 shows the parallel dimeric coiled-coil of yeast transcription factor GCN4.

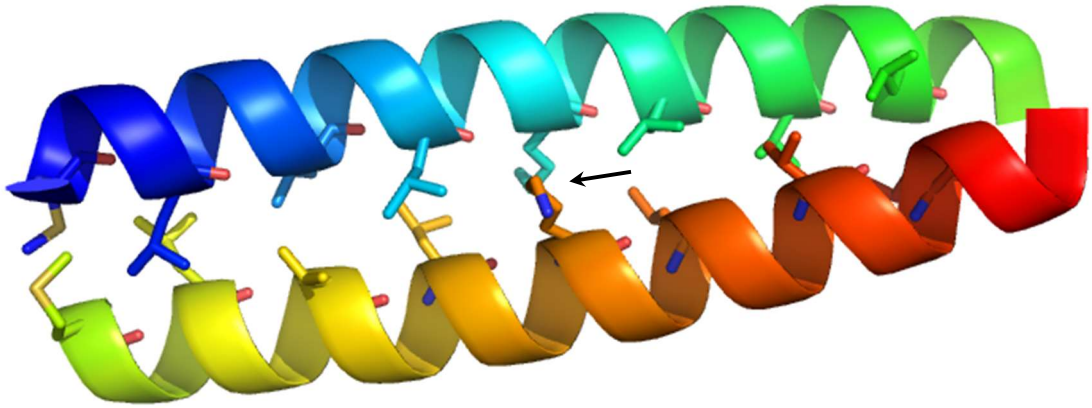

Fig. 1-1: The coiled-coil domain in the yeast leucine zipper GCN4. If the lysine at position 16 (arrow, asparagine in the wildtype protein, an “a” position according to cc nomenclature) is mutated to glutamine, also trimers can form apart from the shown dimer. The structure is depicted in cartoon representation with the hydrophobic a and d positions shown as sticks (PDB-ID 1ZIK, Gonzalez *et al.* 1996).

1.1.3 The function of scaffold proteins

Scaffold proteins are usually rich in the protein interaction motifs described above since one of their main tasks is to mediate binding of at least two other proteins involved in a signalling cascade. Protein scaffolds can localise a complex to a certain cellular compartment but are usually devoid of catalytic activity themselves. At least four distinct functions for scaffold proteins were identified: The assembly of a signalling complex, the

determination of the subcellular localisation, the coordination of positive and negative feedback and the protection of activated signalling molecules from inactivation (Shaw and Filbert 2009).

The most fundamental function of scaffold proteins is the assembly of different components of a signalling cascade, which can lead to improved efficiency as well as specificity. Targeting a complex to a certain localisation was shown for the A-kinase anchor proteins (AKAPs), which tether cAMP-dependent protein kinase A (PKA) to different sites in the cell (Wong and Scott 2004, Hirsch *et al.* 1992). An example for feedback coordination is the mitogen-activated protein kinase (MAPK) cascade. The cascade involves the initial activation of a small G protein followed by three subsequent kinases. It was suggested, that the scaffold protein Ste5 could enhance kinase specificity and also limit the amplification of the signal (Burack and Shaw 2000). Finally, proteins can be protected from inactivation by scaffolds. Especially the shielding effect on phosphorylated proteins was studied and mathematically modelled. In these cases, phosphatases cannot access the phosphorylation site and the signal is maintained (Locasale *et al.* 2007).

CNK1, 14-3-3 proteins and IQGAP1 are important scaffolds involved in insulin signalling and will be discussed later in chapter 1.4 (Lim *et al.* 2010, Craparo *et al.* 1997, Chawla *et al.* 2017).

1.2 Insulin signalling

Energy metabolism is an essential task which has to be tackled by every organism from bacteria and paramecium to blue whale. Glucose can be generated from higher molecular weight nutrients and is a key energy source for many organisms. In vertebrates, a system based on the two hormones insulin and glucagon has evolved to regulate the blood glucose level and was intensively studied in mammals (Navarro *et al.* 1999). A tightly-regulated blood glucose level is vital for organismal survival and growth and its regulation is outlined in the subsequent chapters.

1.2.1 Blood glucose homeostasis

The normal fasting plasma glucose concentration is < 110 mg/dL (6.1 mM) in human; fasting plasma glucose of ≥ 126 mg/dL (7.0 mM) defines diabetes mellitus (WHO and IDF 2006). Low blood glucose levels are critical since the brain uses glucose almost as its sole energy source (Mergenthaler *et al.* 2013). Hypoglycaemia hence causes functional brain failure and profound and prolonged hypoglycaemia (usually of iatrogenic origin) results in brain death (Cryer 2007).

Diabetes mellitus is a major health risk and 415 million adults were estimated to suffer from diabetes mellitus worldwide including 193 million undiagnosed cases (International Diabetes Federation 2015). Insufficient treatment results in complications ranging from pregnancy complications, diabetic foot syndrome and chronic kidney disease to retinopathy (International Diabetes Federation 2015). Obviously, the function of the human body is highly dependent on a tightly controlled blood glucose level and therefore a sophisticated regulatory system has evolved.

The most important components in blood glucose regulation are the two peptide hormones insulin and glucagon (fig. 1-2). When the blood glucose level rises, for example after food intake, β cells of the pancreas produce the anabolic insulin. This leads to glucose uptake by muscle and liver cells and storage in the form of glycogen. Additionally, adipocytes store energy in form of triglycerides. When the blood glucose level decreases, α cells of the pancreas produce catabolic glucagon. This causes glycogenolysis and gluconeogenesis in order to maintain blood sugar levels.

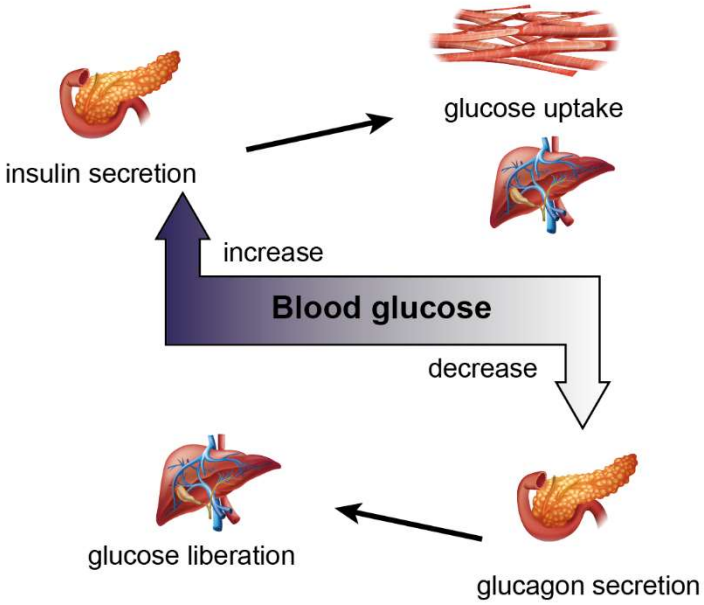

Fig. 1-2: The blood glucose level is tightly controlled by insulin and glucagon. If the blood glucose level rises, for example after food intake, β cells of the pancreas produce insulin. In turn, glucose is taken up by liver and muscle cells and can be stored as polymeric glycogen. When the blood glucose level falls, α cells of the pancreas produce glucagon which leads to glycogenolysis and a following increase in blood glucose levels. Graphics taken from colourbox.de.

It could later be shown that additional hormones finetune the actions of insulin and glucagon. Amylin is also produced in pancreatic β cells and suppresses postprandial glucagon secretion (Moore and Cooper 1991). Glucagon-like peptide-1 (GLP-1) is produced in L-cells of the intestine and enhances insulin effects (Nauck *et al.* 1993).

1.2.2 Insulin

During this work, the intracellular insulin signalling network was further investigated which is the reason why I will focus on this part of the blood glucose homeostasis in the following.

Insulin was discovered in 1922 and pancreatic extracts were used for patient treatment just one year afterwards (Macleod 1922, Ward and Lawrence 2011). The amino acid sequence of insulin was solved in the early 1950s and insulin became the first protein to be sequenced (Sanger and Tuppy 1951a, Sanger and Tuppy 1951b, Sanger and Thompson 1953a, Sanger and Thompson 1953b). Insulin consists of a 21 amino acid A-chain and a 30 amino acid B-chain. Both chains are connected via two disulphide bridges between CysA7 and CysB7 as well as CysA20 and CysB19. Additionally, there is an intramolecular disulphide bridge between CysA6 and CysA11.

The three-dimensional structure of hexameric porcine insulin was determined in 1969 and the authors found that “in each molecule the A chain is a compact unit around which the B chain is wrapped” (Adams *et al.* 1969). A more recent structure of porcine insulin is shown in fig. 1-3. Note, that the structure of insulin changes upon receptor binding and this flexibility is required for receptor interaction (Derewenda *et al.* 1991).

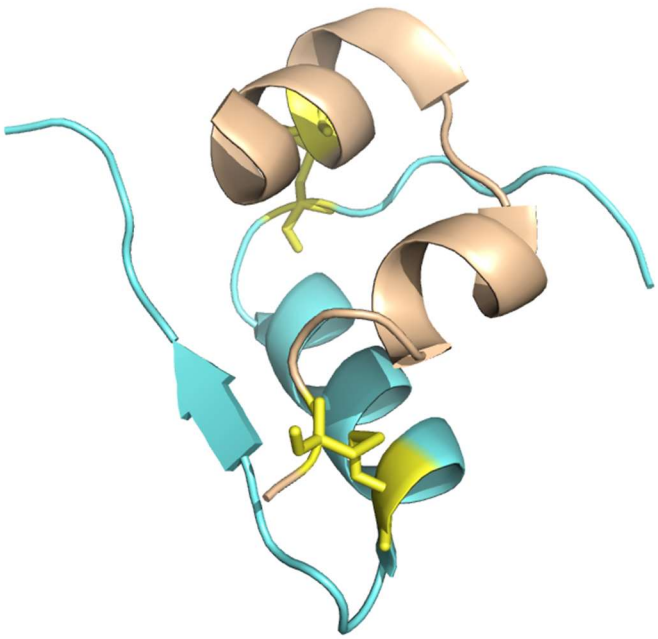

Fig. 1-3: The three-dimensional structure of porcine insulin. The A-chain (ochre) is linked to the B-chain (light blue) via two disulphide bridges. The structure is depicted in cartoon representation with the intramolecular disulphide bridges shown as yellow sticks (PDB-ID 4INS, Baker *et al.* 1988).

1.2.3 The insulin receptor

It took over thirty years from the first postulation that insulin interacted with the cell membrane in order to facilitate sugar uptake into cells in 1949 until the general composition of the receptor was elucidated (Levine and Goldstein 1949, Massague *et al.* 1980). The receptor is a heterotetramer which is formed of two extracellular α subunits and two β subunits, which consist of an extracellular and an intracellular part. The α subunits are connected via several disulphide bonds and each α subunit is linked to a β subunit by another disulphide bond (Sparrow *et al.* 1997). Fig. 1-4 shows the three-dimensional structure of the receptor.

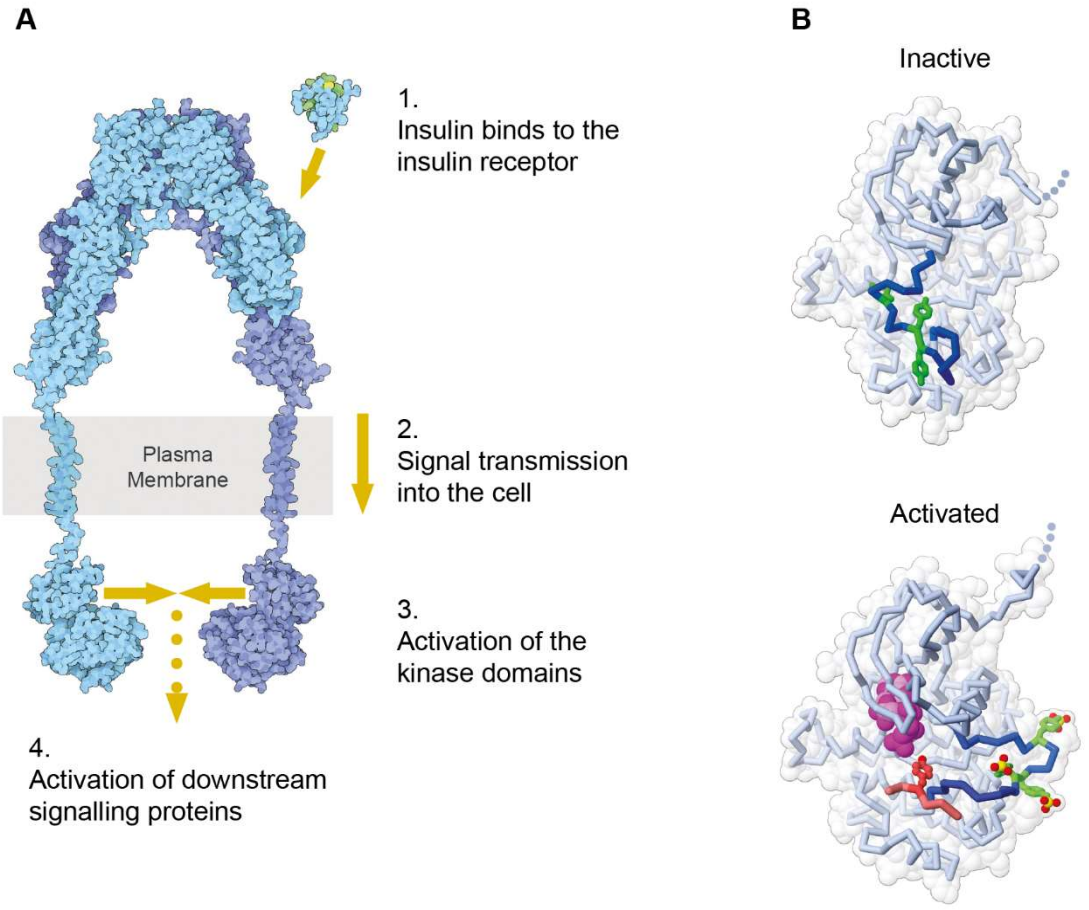

Fig. 1-4: The three-dimensional structure of the insulin receptor. A | Reconstruction of the complete insulin receptor from solved partial structures. One heterodimer consisting of an α and a β subunit is shown in light blue, the other in dark blue. Insulin PDB-ID 1TRZ (Ciszak and Smith 1994), extracellular domain (ectodomain) PDB-ID 3LOH (Croll *et al.* 2016), transmembrane domain PDB-ID 2MFR (Li *et al.* 2014), intracellular kinase domain PDB-ID 1IRK (Hubbard *et al.* 1994). **B |** The inactive and activated intracellular (kinase) domain (ICD) of the insulin receptor. Tyrosines 1158, 1162 and 1163 (green) situated in the activation loop (blue) are phosphorylated (red and yellow). Hence, the kinase can bind ATP (magenta) to phosphorylate substrates (red). Inactive IR-ICD PDB-ID 1IRK (Hubbard *et al.* 1994), active, triple phosphorylated IR-ICD PDB-ID 1IR3 (Hubbard 1997). The activation mechanism is further described in the text. Adapted from PDB 2016.

The IR is a receptor tyrosine kinase with the catalytic sites located in either of the two intracellular β chains. Upon insulin binding, the kinase domains trans-phosphorylate each other within a region called activation loop which in turn enables effector binding and phosphorylation (Kasuga *et al.* 1982, Hubbard 1997).

In the following, I will briefly go through some structural features of the different receptor domains and comment on the activation mechanism. The three-dimensional structure of the receptor ectodomain was solved in 2006 (McKern *et al.* 2006). The receptor is heavily glycosylated (Cosgrove *et al.* 1995) and consists of (starting from the extracellular N-terminus) a leucine-rich repeat domain (L1), a cysteine-rich region (CR), a second leucine-rich repeat domain (L2) and three fibronectin type III (FnIII-1, FnIII-2, FnIII-3) domains as well as an insert domain (ID) within the FnIII-2 domain (Ebina *et al.* 1985, Ward and Lawrence 2011). The ID domain also encompasses a critical α-chain (αCT) segment. The dimer “adopts a folded-over conformation that places the ligand-binding regions in juxtaposition”, which turned out to be different from previous models (McKern *et al.* 2006). A revised structure revealed further details and improved some model weaknesses but confirmed the overall “inverted V” structure (Croll *et al.* 2016). Recently, a structure of insulin bound to its primary receptor binding site could be solved using truncated IR constructs (Menting *et al.* 2013). Insulin interacts with the αCT segment and induces a conformational change but there is also minor contact to L1. “The αCT segment displaces the B-chain C-terminal β-strand [of insulin] away from the hormone core, revealing the mechanism of a long-proposed conformational switch in insulin upon receptor engagement” (Menting *et al.* 2013). Two insulin molecules can bind to a heterotetramer IR with high affinity, further binding sites require higher concentrations leading to negative cooperativity (Ward *et al.* 2013, Meyts 2015).

The structure of the transmembrane region embedded in micelles was solved by nuclear magnetic resonance (NMR) studies and showed a well-defined helical structure, which is crucial for relaying the signal to the cell interior (Li *et al.* 2014).

The first crystal structure of the intracellular kinase domain of the IR was obtained in the mid-1990s (Hubbard *et al.* 1994). Typical for kinases, the ICD consists of an N-terminal and a C-terminal lobe. In the inactive state, Tyr1162 interacts with the catalytic site as a pseudo-substrate. It cannot be phosphorylated because the activation loop prevents proper Mg^{2+}-ATP binding by the catalytic Asp1150 (fig. 1-4). Three years later, the structure of the activated kinase was determined in the same group and revealed the activation mechanism (Hubbard 1997). In the active state, the activation loop undergoes a large conformational change allowing autophosphorylation of Tyr1158, Tyr1162 and

Tyr1163 by the second dimer (in trans) as well as access for Mg^{2+}-ATP and substrate proteins like IRS1. How insulin binding exactly elucidates theses conformational changes is still under investigation and no structure of the complete receptor exists yet. Negative regulators like adaptor protein with PH and SH2 domains (APS) were found to bind directly to the phosphotyrosines in the activation loop via their SH2 domains (Hu *et al.* 2003). Another important mechanism in downstream signalling is the phosphorylation of Tyr972, which is localised in the juxtamembrane (JM) region. IRS proteins bind to the IR via their PTB domains to this phosphotyrosine after receptor activation (Gustafson *et al.* 1995). In contrast to other RTKs, The JM of IR has an inhibitory function. It is exerted via Tyr984, which is no phosphorylation site (Li *et al.* 2003b, Hubbard 2004).

1.2.4 Intracellular insulin signalling pathway

A pubmed search for “insulin signal[l]ing” yields more than 34000 research articles which demonstrates the large scope of this topic. It is furthermore clear that many interesting aspects of insulin signalling cannot be covered in depth in this work since the field is very wide. I would like to refer the reader to four comprehensive review articles, which also served as the basis for this chapter (Cohen 2006, Saltiel 2016, Wilcox 2005, Ward and Lawrence 2011).

It took many years from the identification of insulin in 1922 (Macleod 1922) to the elucidation of the main involved intracellular factors. The main function of insulin is lowering the blood glucose levels by enhancing the conversion of glucose to its storage forms. In muscle and adipose tissue, glucose is converted to glucose 6-phosphate by hexokinase and in the liver by glucokinase. Glucose is finally stored as glycogen in muscle and the liver or as triglycerides in fat tissue. The key enzyme for glycogen storage is the glycogen synthase (GS), which catalyses the last step of glycogen formation, the coupling of uridine diphosphate glucose (UDP-glucose) to a pre-existing glycogen molecule. An excess of glucose 6-phosphate activates GS. Further it was found in muscle, that insulin stimulates GS by converting a less active, phosphorylated GS into its dephosphorylated form and hence implied that kinases/phosphatases are part of the insulin signalling cascade (Villar-Palasi and Larner 1960). How does insulin cause the conversion of glucose to its storage form glycogen by GS activation on a molecular level?

The signal to store glucose in form of glycogen starts with insulin binding to its receptor (fig. 1-5). As described in detail in chapter 1.2.3, the IR is a receptor tyrosine kinase (RTK) which is autophosphorylated upon conformational changes within the activation loop (Hubbard 1997). The phosphorylated IR now serves as a docking site for adaptor proteins like IRS1, which is in turn phosphorylated (White *et al.* 1985, Sun *et al.* 1993).

SH2 domain-containing proteins can now bind the phosphorylated IRS1. This is the case for the regulatory p85 subunit of PI3K, which recruits the functional kinase to the plasma membrane (Ruderman *et al.* 1990). PI3K converts the membrane lipid phosphatidylinositol-4,5-bisphosphate (PIP_2) into the second messenger phosphatidylinositol-3,4,5-trisphosphate (PIP_3), whose concentration increases as a result. Hence, 3-phosphoinositide-dependent protein kinase-1 (PDK1) as well as protein kinase B (PKB) bind to PIP_3 via their PH domains (Komander *et al.* 2004, James *et al.* 1996). PDK1 phosphorylates PKB at Thr308 which greatly enhances kinase activity of PKB (Alessi *et al.* 1997). Additionally, PKB is activated by a phosphorylation at Ser473 by mammalian target of rapamycin (mTOR), which is still subject of current investigation (Sarbassov *et al.* 2005).

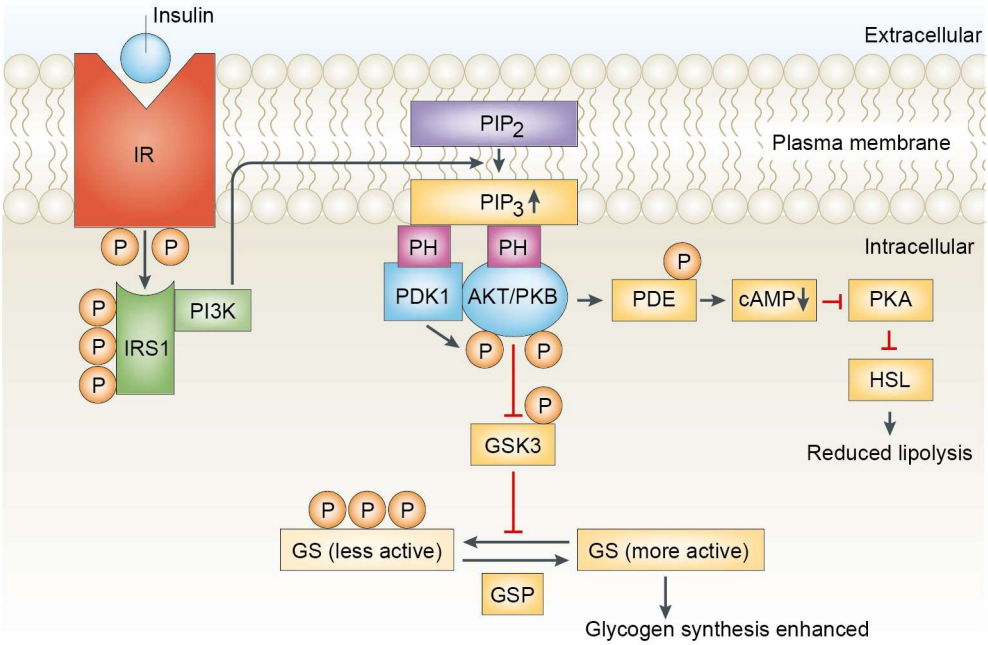

Fig. 1-5: The intracellular insulin signalling network. The signalling cascade is described in the text. IR, insulin receptor; IRS1, insulin receptor substrate-1; PI3K, phosphatidylinsositol-3-kinase; PIP_2, phosphatidylinositol-4,5-bisphosphate; PIP_3, phosphatidylinositol-3,4,5-trisphosphate; PDK1, 3-phosphoinositide-dependent protein kinase-1; PKB, protein kinase B; GSK3, glycogen synthase kinase-3; GS, glycogen synthase; GSP, glycogen synthase phosphatase; PDE, phosphodiesterase; cAMP, cyclic AMP; PKA, protein kinase A; HSL, hormone-sensitive lipase. Adapted from Cohen 2006.

As one of the last steps, active PKB inhibits glycogen synthase kinase-3 (GSK3) by phosphorylating GSK3α at Ser21 and GSK3β at Ser9 (Cross *et al.* 1995). With GSK3 inactivated, the glycogen synthase (GS) gets dephosphorylated by glycogen synthase phosphatase (GSP) which activates GS and finally leads to the accumulation of glycogen.

In contrast to muscle cells, energy is stored in form of lipids in adipocytes. Insulin enhances lipid synthesis and inhibits lipolysis (Saltiel 2016). PKB phosphorylates a phosphodiesterase (PDE), which is activated and causes a drop in cAMP concentration (fig. 1-5, Kitamura *et al.* 1999, Ahmad *et al.* 2009). Thus, protein kinase A (PKA) is less active and the hormone-sensitive lipase (HSL) remains in its non-phosphorylated, inactive state. This results in blocked lipolysis (Anthonsen *et al.* 1998, Strålfors *et al.* 1984). PKB also phosphorylates the transcription factor FoxO1 which excludes it from the nucleus and stops expression of gluconeogenetic and lipolytic genes (Gross *et al.* 2009).

Another extremely important effect of insulin is the translocation of glucose transporters, namely GLUT-4 to the cell membrane in muscle cells and adipocytes. This leads to enhanced glucose uptake into the tissue and hence a decrease in blood glucose level. While it is clear that insulin and muscle activity trigger the translocation, the exact mechanism is still under investigation. Apparently, PKB phosphorylates the GTPase activating protein AS160 which leads to the inactivation of several Rab GTPases (Sano *et al.* 2003). AS160 was shown to enhance the insulin-stimulated GLUT-4 exocytosis but does not affect down-regulation by endocytosis (Zeigerer *et al.* 2004).

Insulin stimulation also modulates gene expression, cell proliferation and differentiation. For those effects, a further signalling pathway is essential, the mitogen-activated protein kinase (MAPK) signalling cascade (Avruch 1998). Binding of IRS or SHC to the activated IR also recruits the adaptor protein growth factor receptor-bound protein-2 (GRB2). GRB2 in turn recruits son of sevenless (SOS), which is an exchange factor for the small GTPase RAS, the start of the MAPK cascade (Pronk *et al.* 1993). RAS activates the Raf kinase by membrane recruitment, which then phosphorylates MAPK/ERK kinase (MEK) and finally activates the effector kinase extracellular-signal regulated kinase (ERK).

Taken together, hallmarks of insulin signalling are complex kinase cascades involving lipid and nucleotide-based second messengers. The kinase PKB is central in the mediation of metabolic insulin effects.

1.3 Small GTPases and their guanine nucleotide exchange factors

As already pointed out in chapter 1.1, guanine nucleotide-binding proteins (G proteins or GTPases) constitute an important class of signalling molecules. They can be grouped into two classes: Heterotrimeric G protein-coupled receptors and monomeric small G proteins. As the name suggests, the first class consists of three subunits (α, β and γ), which associate with a seven-transmembrane-span receptor. Upon receptor activation, G_α

separates from the $G_{\beta\gamma}$ complex and both are responsible for further signal transduction (activation mechanism reviewed in Oldham and Hamm 2008).

Most of the small monomeric G proteins belong to the Rat sarcoma (Ras) superfamily with more than 150 members in human, which can further be subdivided into the five classes: Ras, Ras homologous (Rho), Ras related in brain (Rab), Ras related nuclear protein (Ran) and ADP ribosylation factor (Arf) (Wennerberg *et al.* 2005). As mentioned before, small GTPases are involved in several occasions in the insulin signalling pathway such as GLUT-4 exocytosis and MAPK signalling (Sano *et al.* 2003, Pronk *et al.* 1993).

Ras proteins are further implicated in many diseases such as cancer and also psychiatric disorders and are therefore a subject of intensive research (Simanshu *et al.* 2017). Rho GTPases are particularly well known for their involvement in actin organisation and cell migration; RhoB was shown to regulate membrane trafficking, cell proliferation, DNA repair and apoptosis (Vega and Ridley 2016). Rab GTPases are key regulators of vesicular transport mechanisms and vesicle budding. Different isoforms were found to localise to specific compartments (Goody *et al.* 2017). Ran proteins on the other hand are primarily engaged in nuclear-cytoplasmic transport (Nagai and Yoneda 2012). Finally, ARF GTPases are involved in vesicular trafficking and are discussed in detail in chapter 1.3.1.

GTPases can be regarded as a molecular switch: In their basal state, they are in their inactive, GDP-bound conformation (fig. 1-6).

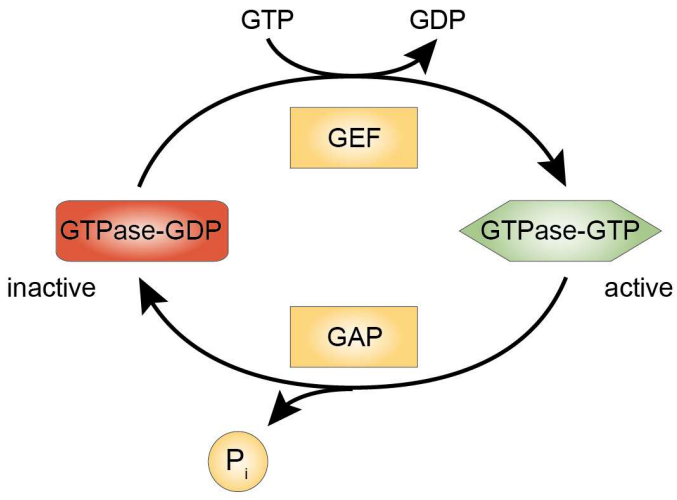

Fig. 1-6: GTPases act as molecular switches. The GDP-bound GTPase is considered its inactive state since it is usually not involved in signal transmission. Guanine nucleotide exchange factors (GEFs) expel the bound GDP which enables GTP binding. The active, GTP-bound form has a largely different three-dimensional structure and can now interact with effector proteins. The signal is terminated with the help of GTPase-activating proteins (GAPs), which stimulate the GTPase activity. The GTP γ-phosphate is hydrolysed and released and the GTPase returns to its GDP-bound, inactive state.

Guanine nucleotide exchange factors (GEFs) displace the nucleotide and GTP, which is at a ten times higher concentration in cells than GDP, binds to the GTPase (Traut 1994, Vetter and Wittinghofer 2001). The evoked conformational change enables binding of effector proteins and downstream signalling. GTPase-activating proteins (GAPs) accelerate the intrinsically low GTPase activity which leads to the hydrolysis of GTP to GDP and the GTPase returns to its inactive state.

All small GTPases possess a nucleotide binding and hydrolysis function which is located in the around 20 kDa large “G domain” with a universal structure and switch mechanism. The domain consists of a “mixed six-stranded β sheet and five helices located on both sides” (Vetter and Wittinghofer 2001). The Asn/Thr-Lys-Xaa-Asp motif (Xaa: any amino acid) in conjunction with the phosphate-binding loop (P loop) are most important for nucleotide binding (Vetter and Wittinghofer 2001, Saraste *et al.* 1990) alongside with Mg^{2+} (Lenzen *et al.* 1998). Small GTPases are characterised by two “switch regions” first discovered in Ras, which show increased flexibility and enable effector binding (Milburn *et al.* 1990, Farrar *et al.* 1997). While the different GDP-bound G proteins show a large structural variety, GTP-bound G proteins are stunningly similar to enable effector binding (Sprang 1997). Vetter compares the changes after nucleotide hydrolysis to “a loaded-spring mechanism where release of the γ-phosphate after GTP hydrolysis allows the two switch regions to relax into the GDP-specific confirmation” (Vetter and Wittinghofer 2001). The switching mechanism is exemplified for ARF1 in fig. 1-7 B.

While this is the classical view on GTPase biology, the distinction of inactive GDP-bound GTPase and active GTP-bound GTPase became blurry during the last years. Novel binding partners of GDP-bound Rab27a in pancreatic β cells were identified and Rab27a-GDP controls endocytosis of the secretory membrane (Yamaoka *et al.* 2015).

1.3.1 ADP ribosylation factor (ARF) GTPases

In the following, I will focus on the group of ARF-GTPases since they were an important subject of investigation in this study. ARF-GTPases were discovered in the mid-1980s as a cofactor required for cholera toxin to ADP-ribosylate the stimulatory regulatory element of adenylate cyclase and cause its toxic effect (Kahn and Gilman 1986). Further, its ability to bind GDP and GTP was described (Kahn and Gilman 1986, O'Neal *et al.* 2005) and it is this characteristic which confers the function as a molecular switch to the protein.

In mammals, there are six ARFs which are grouped into three classes according to their sequence homology: Class I comprises ARF1, ARF2 (missing in human) and ARF3, class II comprises ARF4 and ARF5, while the sole member of class III is ARF6 (Kahn *et al.* 2006). Class I ARFs enable the assembly of coat protein complexes on budding

vesicles within the secretory pathway. ARF1 was shown to be involved in COPI as well as clathrin coat formation (Serafini *et al.* 1991, Austin *et al.* 2000, Ren *et al.* 2013). Class II ARFs were less intensely studied but evidence accumulates that ARF4 regulates retrograde endosome-to-Golgi transport and intraorganellar traffic in the ER-Golgi intermediate compartment (ERGIC) in conjunction with class I ARFs (Nakai *et al.* 2013, Ben-Tekaya *et al.* 2010). ARF6, alongside ARF1, is the best characterised ARF. It regulates endosomal traffic and membrane remodelling (reviewed in D'Souza-Schorey and Chavrier 2006).

In order to fulfil this multitude of crucial functions, ARFs show several structural features, which also distinguish them from other small GTPases (fig. 1-7).

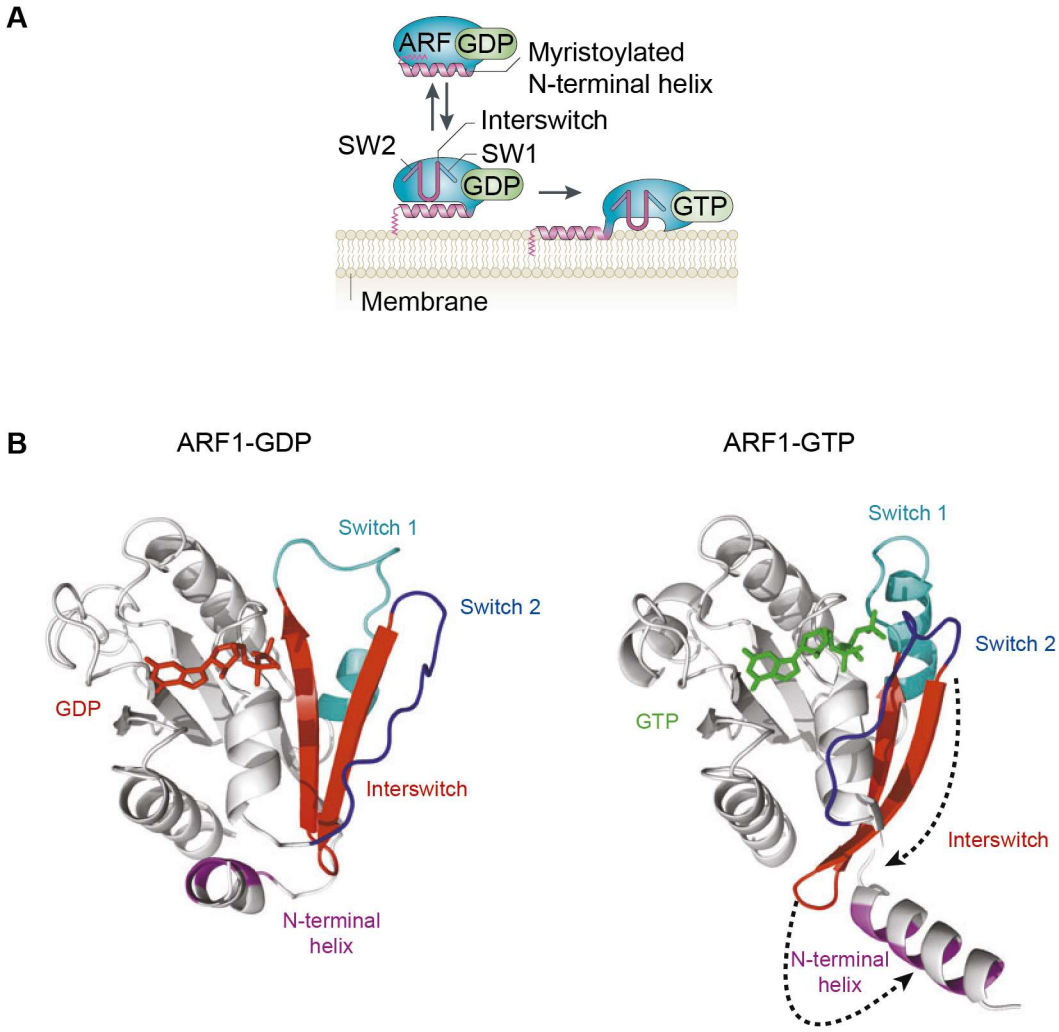

Fig. 1-7: Activation of ARF GTPases. A | Schematic representation of ARF activation. GTP binding liberates the N-terminally myristoylated amphipathic helix, which enables membrane association. SW1/2, switch 1/2. Adapted from Donaldson and Jackson 2011. **B** | Comparison of ARF1-GDP and ARF1-GTP shows the large structural change. The interswitch region pushes the N-terminal helix out. ARF1-GDP PDB-ID 1HUR (Amor *et al.* 1994), ARF1-GTP PDB-ID 1O3Y (Shiba *et al.* 2003). Adapted from Gillingham and Munro 2007.

At their N-terminus, ARFs possess an amphipathic helix. After methionine processing, the N-terminal glycine is modified with a lipid, a C14 myristoyl group (Kahn *et al.* 1988). Both elements facilitate membrane tethering of ARFs (Amor *et al.* 1994). The N-terminal helix further locks the GTPase in its GDP-bound inactive conformation (Amor *et al.* 1994, Liu *et al.* 2009).

Upon GDP to GTP exchange, the region between switch 1 and switch 2, called "interswitch", changes conformation. These two newly oriented β sheets in turn displace the N-terminal helix form a hydrophobic pocket, leading to facilitated membrane attachment (Antonny *et al.* 1997). ARF6 however is associated with membranes also in its GDP bound form (Macia *et al.* 2004).

1.3.2 Sec7 domain exchange factors and GAPs control ARF GTPases

The aforementioned activation process, the exchange of GDP for GTP, is triggered by guanine nucleotide exchange factors (GEFs) of the Sec7 family. They are named after their catalytic Sec7 domain, which is homologous to the yeast ARF GEF sec7p (Achstetter *et al.* 1988). Based on domain organisation, the 15 human ARF GEFs can be grouped into five classes (tab. 1-1). The fact that 15 activating proteins exist for only five human ARF GTPases suggests that ARF activity needs to be tightly controlled in time and space.

Tab. 1-1: Human ARF GEF families. All GEF proteins possess the catalytic Sec7 domain. GBF/BIG, Golgi BFA-resistance factor 1/BFA-inhibited GEF; EFA6, exchange factor for Arf6; PSD, pleckstrin and Sec7 domain containing; BRAG, Brefeldin-resistant Arf GEF; Fbox8, F-box only protein 8. Taken from Casanova 2007.

Family	Human proteins
GBF/BIG	GBF1, BIG1, BIG2
Cytohesins	Cytohesin-1, Cytohesin-2 (ARNO), Cytohesin-3 (GRP1), Cytohesin-4
EFA6/PSD	EFA6A (PSD), EFA6B (PSD4), EFA6C (PSD2), EFA6D (PSD3)
BRAGs	BRAG1, BRAG2 (GEP100), BRAG3
Fbox	Fbox8

The Sec7 domain consists of approximately 200 amino acids and its catalytic activity depends on a "glutamic finger" within a hydrophilic loop, which was shown by mutational studies and confirmed by X-ray crystallography (Cherfils *et al.* 1998, Béraud-Dufour *et al.* 1998, Renault *et al.* 2003). In cytohesins, the catalytic Sec7 domain is flanked by an N-terminal coiled-coil domain which serves as an interaction module and the C-terminal PH domain, which binds phosphoinositides (Klarlund *et al.* 2000) (fig. 1-8).

Fig. 1-8: Modular structure of cytohesins. Cytohesins have a molecular weight of approximately 45 kDa and possess an N-terminal coiled-coil (cc) domain, a central Sec7 domain and a C-terminal pleckstrin homology (PH) domain. There is also a polybasic region (pbr) at the very C-terminus.

In the cytohesin ARNO, Glu156 destabilises GDP and Mg^{2+} bound to ARF1 and thus allows GTP to bind, which is approximately at a ten times higher intracellular concentration than GDP (Béraud-Dufour *et al.* 1998, Renault *et al.* 2003, Traut 1994) (fig. 1-9).

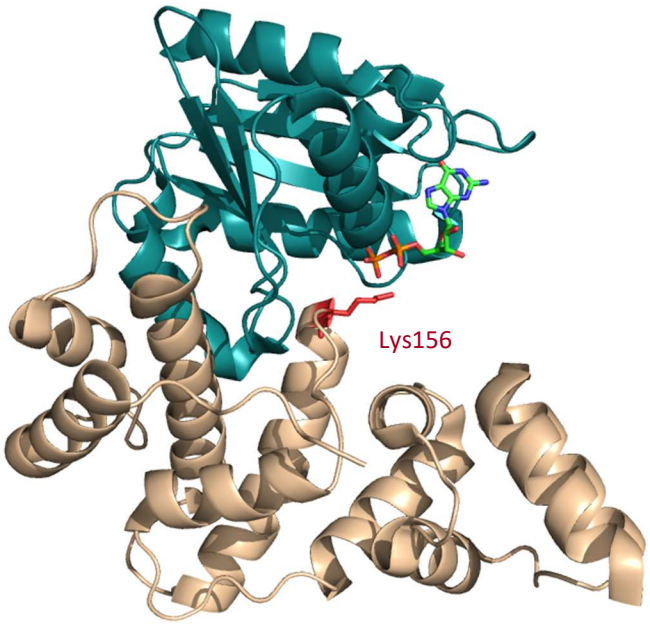

Fig. 1-9: Complex of NΔ17ARF1-GDP and the catalytically inactive $ARNO_{E156K}$ charge reversal mutant. GDP (green carbon atoms, stick representation) is bound to the truncated ARF1 (turquoise, cartoon representation). The ARNO Sec7 domain (ochre, cartoon representation) is associated with the N-terminally truncated GTPase but since the catalytic Glu156 is mutated to Lys (red sticks), the complex is stabilised and the nucleotide cannot be displaced. PDB-ID 1R8S (Renault *et al.* 2003).

Since the intrinsic GTPase activity of ARFs is comparatively low, GAPs are needed to end ARF signalling. This GAP activity was first discovered in bovine brain extracts (Randazzo and Kahn 1994). A specific ARF GAP domain was described just one year later and subsequently discovered in a heterogeneous group of 24 mammalian proteins with a large variety in structure and size (Cukierman *et al.* 1995, Gillingham and Munro 2007). The domain comprises approximately 140 amino acids and is characterised by four cysteine residues which form a zinc finger. A conserved arginine inserts into the active site and

might directly participate in GTP hydrolysis, although opposing models have been suggested (Mandiyan *et al.* 1999, Goldberg 1999).

1.3.3 Membranes and feedback loops influence ARF activity

Since ARF GTPases as well as their exchange factors interact with membranes in their active states, it comes as no surprise that there is a well-orchestrated interplay between the proteins and the membrane which is crucial for the regulation of activity.

ARF GTPases are controlled by a double layer of autoinhibition. First, the myristoylated N-terminal helix has to be displaced from its hydrophobic pocked by membrane binding since the helix occludes the binding site for the GTP γ-phosphate (Amor *et al.* 1994, Liu *et al.* 2009). Second, the reorientation of the interswitch region remodels the GTP-binding site and also helps in displacing the N-terminal helix and hence secures membrane attachment (Antonny *et al.* 1997). The necessity of membranes to relieve autoinhibition was demonstrated by the fact that the isolated Sec7 domain cannot promote nucleotide exchange on full-length myristoylated ARF in absence of membranes (Chardin *et al.* 1996). Hence, membranes prime the GTPase by spontaneous and transient attachment.

Additionally, membranes are also required for an effective orientation and close proximity of ARF and GEF. Cytosolic GEFs of the cytohesin family are autoinhibited by a C-terminal polybasic region (pbr) (DiNitto *et al.* 2007). However, two mechanisms target cytohesins to the membrane. The PH domain binds to phosphoinositides, namely phosphatidylinositol-4,5-bisphosphate (PIP_2) and phosphatidylinositol-3,4,5-trisphosphate (PIP_3) (Chardin *et al.* 1996, Klarlund *et al.* 2000). Furthermore, the positively charged pbr interacts with negatively charged lipid headgroups like phosphatidylserine (Macia *et al.* 2000). The extent of membrane influence becomes apparent when comparing catalytic efficiencies. K_{cat}/K_M for an ARNO construct composed of Sec7 and PH domain increases by four orders of magnitude for myr-ARF1 compared to the soluble NΔ17ARF1 (Nawrotek *et al.* 2016).

The notion that ARF does not only represent a substrate of ARNO but can also recruit ARNO as an effector to the plasma membrane and hence change its activity was introduced about 10 years ago (Cohen *et al.* 2007). The interaction was found to depend on the ARNO PH domain, phosphoinositides and ARF6 being in its GTP-bound state. Compared to this cellular study, the mechanism was further dissected biochemically using liposomes and purified myristoylated ARFs (Stalder and Antonny 2013). ARF6-GTP stimulated ARNO at nanomolar concentrations and also ARF1-GTP contributed to a positive feedback loop.

1.4 Cytohesins and scaffold proteins in insulin signalling

There are about 20000 human protein-coding genes and the resulting gene products are situated inside of a cell which is crowded with other proteins and macromolecules such as nucleic acids (Ezkurdia *et al.* 2014). Scaffold proteins, which were introduced in chapter 1.1.3, have evolved to orchestrate and finetune protein-protein interactions in this setting. Before focussing on CNK1, which is the central scaffold protein in this study, I would like to mention some other examples of scaffold proteins in insulin signalling.

The probably best-known scaffold in insulin signalling is IRS1 (White *et al.* 1985). The PTB domain of IRS1 binds the JM region of the activated phosphorylated insulin receptor (Eck *et al.* 1996). IRS1 is then phosphorylated and serves as a docking platform for further proteins and hence fulfils the classical role of an adaptor protein (Sun *et al.* 1993). One of those interacting proteins belongs to a further group of scaffold protein itself, the 14-3-3 proteins (Craparo *et al.* 1997). 14-3-3 proteins were later shown to be involved in GLUT-4 recycling by interacting with the phosphorylated Rab GAP AS160 (Ramm *et al.* 2006).

IQ motif containing GTPase activating protein 1 (IQGAP1) binds to the IR as well as to IRS1 and is required for PKB and MAPK downstream signalling (Chawla *et al.* 2017). As pointed out in chapter 1.2.4, the GRB2 scaffold is another factor involved in the MAPK signalling branch of insulin action (Pronk *et al.* 1993). GRB scaffolds are also implicated in insulin signal termination. GRB14 acts as a pseudosubstrate for the IR and inhibits its activity (Depetris *et al.* 2005). Further, GRB10 and GRB14 bind with their different domains to an IR-Ras-phosphoinositide complex thus limiting signal propagation (Depetris *et al.* 2009).

The CNK family of scaffold proteins and their involvement in cytohesin-dependent insulin signalling will be discussed in depth in the following chapters.

1.4.1 The CNK family of scaffold proteins

Five mammalian Connector enhancer of kinase suppressor of Ras (CNK) proteins have been described, which are all characterised by a plethora of interaction domains (Fritz and Radziwill 2011). Fig. 1-10 illustrates the modular structure of CNK1 including the classical interaction modules sterile alpha motif (SAM), PDZ and cc. CNK2A (MAGUIN-1), CNK2B (MAGUIN-2) and CNK3A furthermore possess a central domain of unknown function 1170 (DUF1170). CNK3A lacks the C-terminal PH and cc domain, while the last member, CNK3B (IPCEF1) lacks the N-terminus and consists of a PH domain, a serine-rich region and a conserved region among chordate (CRAC).

Relatively little research has been conducted on this protein family but a substantial body of knowledge arises from research performed in the Radziwill group. They found CNK1 to be involved in MAPK signalling by showing that it regulates Src-mediated Raf1 kinase activation (Ziogas *et al.* 2005). Further, CNK1 was established as a new PKB interaction partner which promotes cell proliferation through FoxO signalling (Fritz *et al.* 2010).

Fig. 1-10: Modular structure of CNK1. SAM, sterile alpha motif; CRIC, conserved region in CNK; PDZ, Domain present in PSD-95/DLG-1/ZO-1/2; PH, pleckstrin homology; cc, coiled-coil.

Also the group of Alan Hall expanded the knowledge of CNK1, especially its involvement in signalling downstream of Rho GTPase. CNK1 is an effector of Rho-GTP and the CNK1 PH domain is required for Rho interaction. CNK1 bridges the interaction with Rho and Ras effectors and might therefore mediate the crosstalk between both pathways (Jaffe *et al.* 2004). The involvement in the MAPK signalling was further substantiated by the identification of the Rho-specific GEFs Net1 and p115RhoGEF as well as two kinases of the JNK MAP kinase pathway (MLK2 and MKK7), which all interact with CNK1 (Jaffe *et al.* 2005).

1.4.2 Cytohesins in insulin signalling

The link between insulin signalling and cytohesins was first discovered in the late 1990s when it was shown that ARNO, Cytohesin-3 and ARF6 are recruited to the cell membrane upon insulin stimulation (Venkateswarlu *et al.* 1998, Shome *et al.* 1997, Langille *et al.* 1999). Analyses of downstream signalling afterwards revealed that ARNO mediates the activation of ARF and phospholipase D (Li *et al.* 2003a).

More information on cytohesin-dependent insulin signalling could be obtained by using a chemical GEF activity inhibitor termed SecinH3 specific for cytohesins (Hafner *et al.* 2006, Fuss *et al.* 2006). In *Drosophila melanogaster*, mutations in the cytohesin homologue *steppke* as well as chemical inhibition by SecinH3 led to slowed growth in all key fly development stages. Impaired insulin signalling was identified to cause the effects as shown by reduced PKB activation and expression profile analysis of insulin-dependent transcription (Fuss *et al.* 2006).

Also when SecinH3 was fed to mice, a diabetic-like phenotype including insulin resistance and reduced expression in of glycolytic, fatty acid and ketone body metabolism genes in the liver was evoked (Hafner *et al.* 2006). This further confirmed the involvement of cytohesins also in mammalian insulin signalling. Since SecinH3 inhibited IRS1 but not IR

phosphorylation, Hafner and colleagues concluded that cytohesins are involved in the early steps of the signalling cascade after IR activation.

Cytohesins were also implicated in GLUT-4 regulation. PKB phosphorylates Cytohesin-3 and promotes GLUT-4 recycling via its effector ARF6 (Li *et al.* 2012).

It was also found that the involvement of cytohesins is not limited to the downstream effects of IR but cytohesins also mediate insulin-like growth factor receptor (IGFR) signalling in a prostate cancer cell line (Weizhong *et al.* 2011).

1.4.3 The involvement of CNK1 in insulin signalling

Cytohesins were discovered as a major interaction partner of the previously introduced scaffold protein CNK1 (chapter 1.4.1) by using a pull-down/mass spectrometry approach. The C-terminal domain of CNK1 and the coiled-coil domain of cytohesins were required to facilitate the membrane recruitment of ARNO upon insulin stimulation (Lim *et al.* 2010). The authors postulated a direct protein-protein interaction, which was however not strictly proven since the results were obtained by co-immunoprecipitations from cell lysates. The authors report that the CNK1-cyothesin interaction is critical for the activation of the PI3K/PKB downstream cascade from IR and IGFR and that microenvironments with elevated PIP_2 levels are essential for signal transmission. The question of how CNK1 is localised to the membrane is not addressed; their developed model is depicted in fig. 1-11.

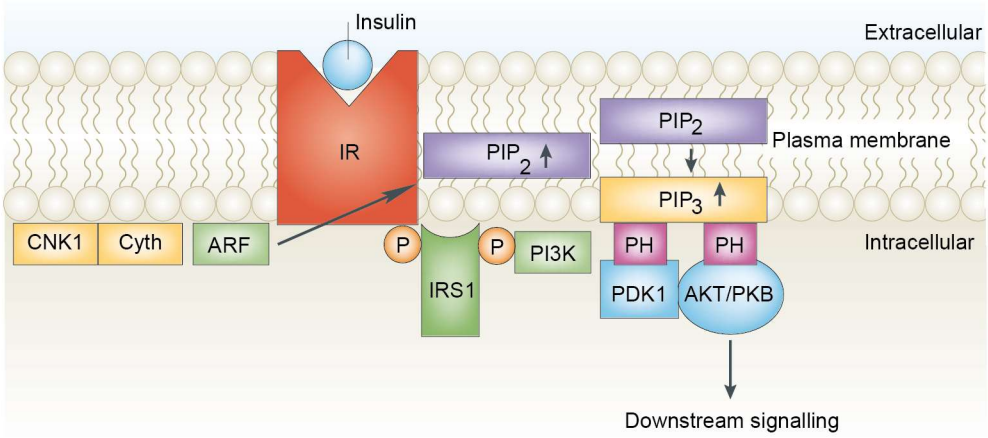

Fig. 1-11: Model of CNK1-cytohesin involvement in insulin signalling. CNK1 recruits cytohesins to the plasma membrane in an insulin-dependent manner. Activated ARF leads to increased PIP_2 production via allosteric activation of phosphatidylinositol-4-phosphate-5-kinase (PIP5K). Increased PIP_2 levels subsequently facilitate IRS1 binding and enhance the signalling cascade. IR, insulin receptor; IRS1, insulin receptor substrate-1; PI3K, phosphatidylinsositol-3-kinase; PIP_2, phosphatidylinositol-4,5-bisphosphate; PIP_3, phosphatidylinositol-3,4,5-trisphosphate; PDK1, 3-phosphoinositide-dependent protein kinase-1; PKB, protein kinase B. Adapted from Lim *et al.* 2010 and Cohen 2006.

2 Aim of the Project

A detailed understanding of complex signalling networks is the fundamental prerequisite for the development of therapeutics in many areas. Insulin signalling is a key metabolic pathway with high significance and dysregulation is associated with diabetes mellitus, a disease affecting hundreds of millions of people worldwide (WHO and IDF 2006).

This works aims at understanding the molecular basis of certain insulin signalling components. In particular, cytohesins, which are guanine nucleotide exchange factors for Arf GTPases, and the scaffold protein CNK1 were investigated. The involvement of cytohesins in insulin signalling is subject to research since the late 1990s (Venkateswarlu *et al.* 1998, Shome *et al.* 1997) and pharmacological blockage of cytohesins induces a diabetic-like phenotype in mice (Hafner *et al.* 2006). CNK1 forms a complex with cytohesins and positively regulates insulin signalling (Lim *et al.* 2010).

In order to understand the mode of action, respective components were heterologously expressed and analysed by biochemical means. It was assessed whether the cytohesin ARNO directly interacts with the insulin receptor and changes its activity. The interaction between ARNO and CNK1 was characterised via pull-down assays, analytical size-exclusion chromatography and isothermal titration calorimetry. Crystallisation approaches were undertaken to determine the three-dimensional structure of the complex.

It was hypothesised that CNK1 directly affects the catalytic activity of ARNO. To test this hypothesis, the localisation to membranes was evaluated in liposome flotation assays and a liposome-dependent nucleotide exchange assay was established using myristoylated ARFs. Since it is activated, membrane-bound CNK1 which most likely exerts its action within the cell, different strategies were employed to tether CNK1 to liposomes and evaluate the effect on the localisation and catalytic activity of ARNO.

3 Results

3.1 Influence of cytohesins on the insulin receptor activity

The involvement of cytohesins in the insulin signalling pathway was first discovered in 1998 (Venkateswarlu *et al.* 1998). Specifically, the translocation of the cytohesin ARNO to the cell membrane upon insulin stimulation was described. Li and colleagues subsequently postulated a direct interaction between ARNO and the insulin receptor (IR) (Li *et al.* 2003a). However, their approach, performing immunoprecipitation experiments of the insulin receptor α subunit from HIRcB cell lysates and analysing bound ARNO constructs, does not allow conclusions about direct interactions. The question of mediating co-factors or proteins remains to be addressed.

Two ground-breaking publications from 2006 shed further light on the involvement of cytohesins in insulin signalling by making use of the chemical GEF activity inhibitor SecinH3 (Hafner *et al.* 2006, Fuss *et al.* 2006). Hafner and co-workers proposed a physical association between a cytohesin-ARF complex with the insulin receptor-IRS complex since activation of insulin receptor substrate-1 (IRS1) was hampered by SecinH3 and both complexes were co-immunoprecipitated.

To test whether the involvement of cytohesins is rooted in an enhanced IR activity, *in vitro* autophosphorylation assays were performed in this work. Further, diverse biochemical interaction studies were carried out in order to investigate the possibility of a direct interaction between the insulin receptor intracellular domain (IR-ICD) and ARNO.

3.1.1 Quality control of purified proteins

In order to ascertain the proper folding and structural integrity of the heterologously expressed and purified components for the succeeding studies, their catalytic activities were tested using appropriate *in vitro* assays. The IR-ICD was obtained via Sf9 cell expression followed by immobilised metal ion affinity chromatography (IMAC) and size-exclusion chromatography (SEC) purification. ARNO was heterologously expressed in *E. coli* and also purified via IMAC. After enzymatic affinity tag removal, the protein was subjected to SEC as a last purification step.

Upon binding of insulin to the IR, the adjacent kinase domains of the IR-ICD trans-phosphorylate each other at three tyrosine residues within the activation loop at positions Tyr1158, Tyr1162 and Tyr1163 (Hubbard 1997). Addition of high concentrations of magnesium (30 mM $MgCl_2$) typically leads to receptor aggregation followed by autophosphorylation (Herrera and Rosen 1986). Using this approach, the activity of the IR-ICD was tested (fig. 3-1 A). Antibodies specific to the phosphotyrosines (pY) in the

activation loop as well as a general pY antibody could detect activation of the IR within one minute after ATP/$MgCl_2$ addition.

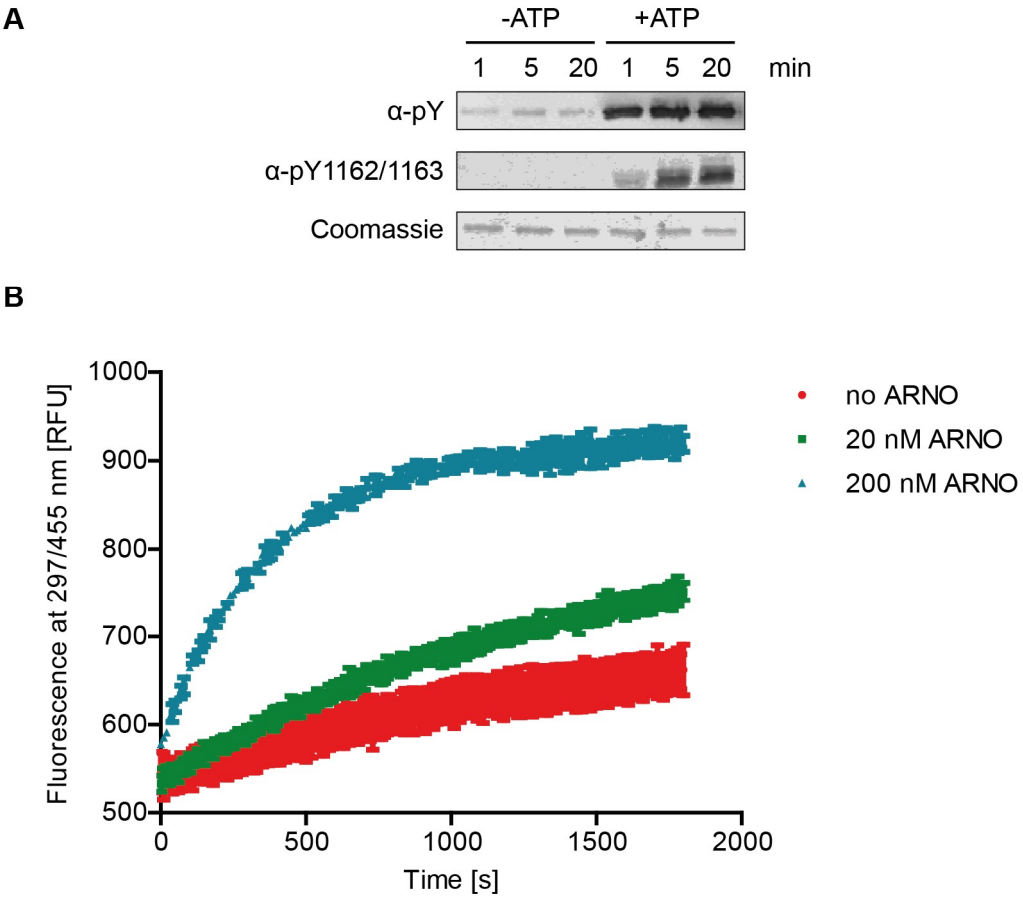

Fig. 3-1: IR-ICD and ARNO are catalytically active. A | 525 nM IR-ICD was mixed with 30 mM $MgCl_2$ and 1 mM ATP and samples were taken at the indicated time points. The samples were applied to 10 % SDS-PAGE, transferred via western blot and detected with α-pY and α-pY1162/1163 antibodies. **B** | 20 nM and 200 nM ARNO catalyse the GDP to Mant-GTP exchange on 400 nM NΔ17ARF1. The exchange reaction was monitored by Mant-FRET at 297/455 nm.

ARNO catalyses the exchange of GDP to GTP on small GTPases of the ADP ribosylation factor (ARF) family leading to their activation (Kolanus 2007). The activity of heterologously expressed ARNO was tested using a Mant-GTP binding assay. The exchange of GDP to Mant-GTP on the soluble, N-terminally truncated NΔ17ARF1 was measured by monitoring the Mant-FRET fluorescence increase. Clearly, ARNO possesses exchange activity and can thus be used for the following analyses (fig. 3-1 B).

3.1.2 Autophosphorylation of IR-ICD remains constant upon ARNO presence

To investigate if ARNO or its non-auto inhibited truncation ARNOΔpbr (DiNitto *et al.* 2007) directly influence the autophosphorylation and hence activation of IR-ICD, an *in vitro* setup was chosen. Previously, the catalytic activity of ARNOΔpbr was also confirmed using the Mant-GTP binding assay (data not shown). As described in chapter 5.2.11, $MgCl_2$ induces

receptor autophosphorylation and the extent of tyrosine phosphorylation was evaluated via western blot analysis. Fig. 3-2 shows that the activation takes place fast and the amount of pY remains constant after 15 sec.

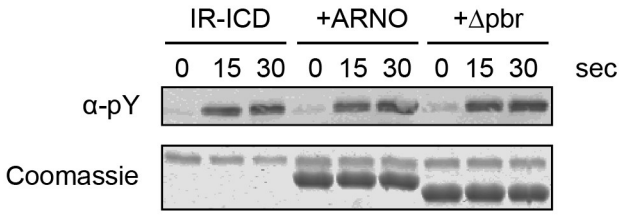

Fig. 3-2: IR-ICD autophosphorylation remains constant upon ARNO addition. 525 nM IR-ICD was mixed with a tenfold ARNO excess, 30 mM $MgCl_2$ and the reaction was started with 1 mM ATP. Samples were taken at the indicated time points and applied to 10 % SDS-PAGE, transferred via western blot and detected with α-pY antibody.

Autophosphorylation remained constant in presence or absence of ARNO constructs. This finding indicates that the receptor activation is independent from ARNO in this setting. That is in line with studies performed in HepG2 cells showing that neither autophosphorylation of the IR nor its density on the cell surface was affected by blocking cytohesins (Hafner *et al.* 2006).

3.2 Physical interaction of ARNO and the insulin receptor

As previously described, experimental data show that ARNO is involved in the early steps of insulin signalling and therefore a direct physical interaction has been proposed (Li *et al.* 2003a, Hafner *et al.* 2006). In this thesis, diverse biochemical and biophysical methods were applied to investigate the possibility of a direct protein-protein interaction.

3.2.1 Label transfer and microscale thermophoresis suggest interaction of ARNO and the insulin receptor

Chemical crosslinking constitutes a means of covalently linking interaction partners which are in close proximity. Apart from stable interactions, this enables the detection of transient protein-protein interactions, which are otherwise hard to identify (Das and Fox 1979, Arora *et al.* 2017).

For the current investigation, the trifunctional crosslinking reagent Sulfo-SBED was used. It consists of a biotin moiety, a sulfonated N-hydroxysuccinimide (Sulfo-NHS) active ester and a photoactivatable aryl azide (see chapter 5.2.13). In a first step, the compound is coupled via its NHS group to primary amines of one of the interaction partners. The modified protein is then incubated with its putative interaction partner and the aryl azide is activated by UV light, interacting with diverse functional groups in vicinity. Cleaving the disulphide bridge within the crosslinker finally separates the crosslinked proteins and

transfers the biotin group, which can be detected via western blot using streptavidin (Alley *et al.* 2000).

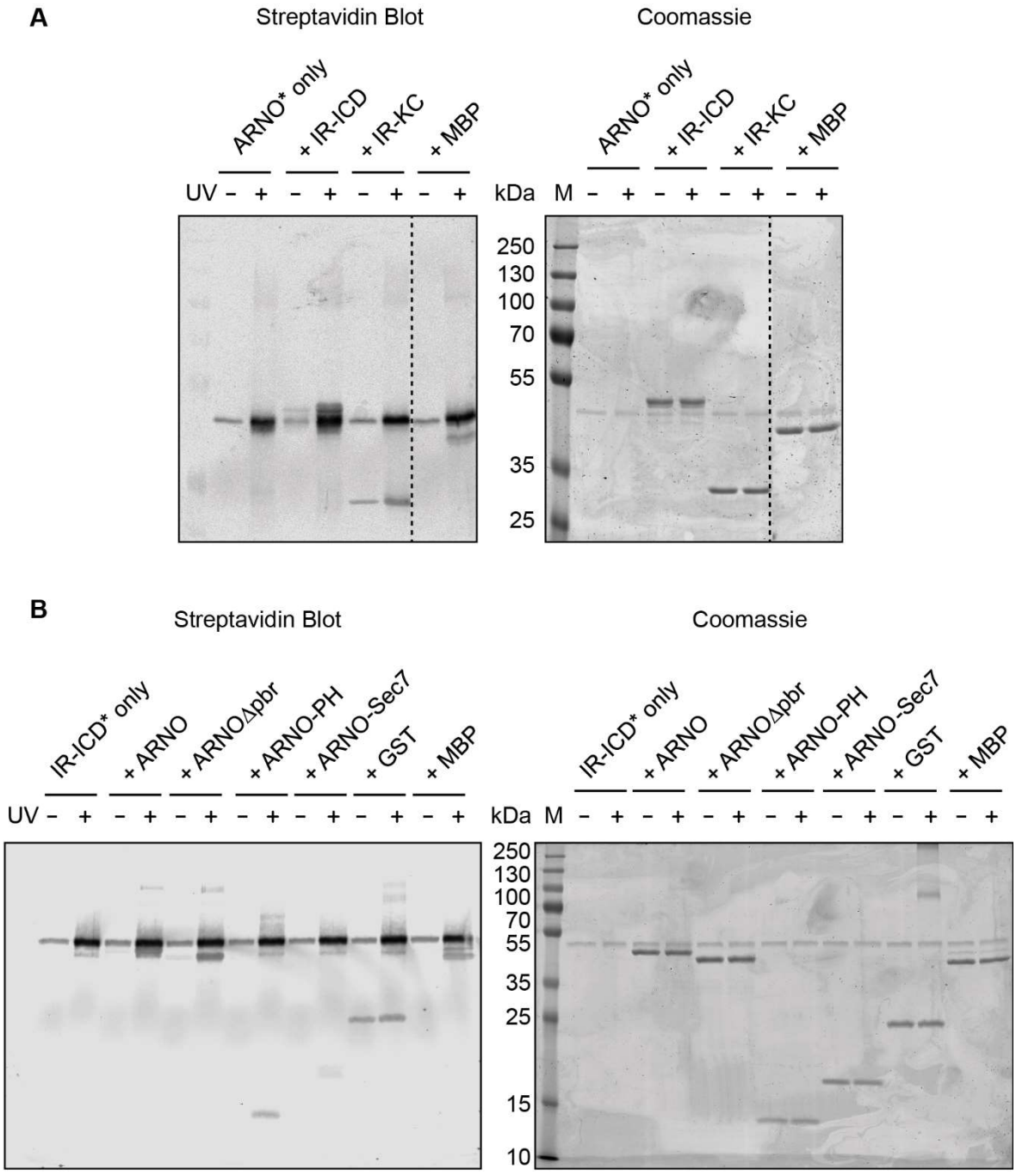

Fig. 3-3: Label transfer suggests interaction between ARNO and IR-ICD. A | 250 nM Sulfo-SBED modified ARNO (indicated with the asterisk) was incubated with 1 µM IR-ICD, IR-KC and MBP. After 3 min UV irradiation, the disulphide bonds were reduced with 100 mM DTT and the samples were applied to 10 % SDS-PAGE. The proteins were transferred via western blot and detected with fluorescently labelled streptavidin. **B** | The label transfer is bidirectional. 250 nM Sulfo-SBED modified IR-ICD (indicated with the asterisk) was incubated with 1 µM ARNO constructs or negative controls GST and MBP. After 3 min UV irradiation, the disulphide bonds were reduced with 100 mM DTT and the samples were applied to 12.5 % SDS-PAGE. The proteins were transferred via western blot and detected with fluorescently labelled streptavidin.

In a first step, the label transfer from labelled ARNO to IR-ICD, the kinase core of IR lacking the C-terminal tail (IR-KC) and the negative control maltose-binding protein (MBP) was investigated (fig. 3-3 A).

The strongest label transfer was observed from ARNO to IR-ICD. Of note, the label was also transferred to IR-KC and to a lesser extent to MBP. Fig. 3-3 B shows the reverse setup, where IR-ICD was initially labelled. Although the transfer seems most intense to ARNO and ARNOΔpbr, there is clearly also a label transfer to the control proteins including GST. This indicates that the conditions, although optimised with reduced irradiation/incubation times and presence of detergent, were not selective enough to clearly prove a specific interaction.

Another means of interaction analysis is microscale thermophoresis (MST). Here, the changes in migration behaviour of fluorescently labelled particles upon ligand binding are exploited to quantify binding affinities. This technology utilises the fact that molecules migrate in a temperature gradient depending on their size, charge and hydration shell and at least one of those parameters changes upon ligand binding (Jerabek-Willemsen *et al.* 2011, Seidel *et al.* 2013).

The binding behaviour of the complete intracellular domain (IR-ICD) and the kinase core (IR-KC) to ARNO were compared. While no saturable interaction of ARNO with IR-KC can be seen, an interaction with IR-ICD seems possible and a dissociation constant (K_D) of around 7 µM was inferred (fig. 3-4). In order to further test this finding, pull-down, analytical size-exclusion chromatography and ITC experiments were performed.

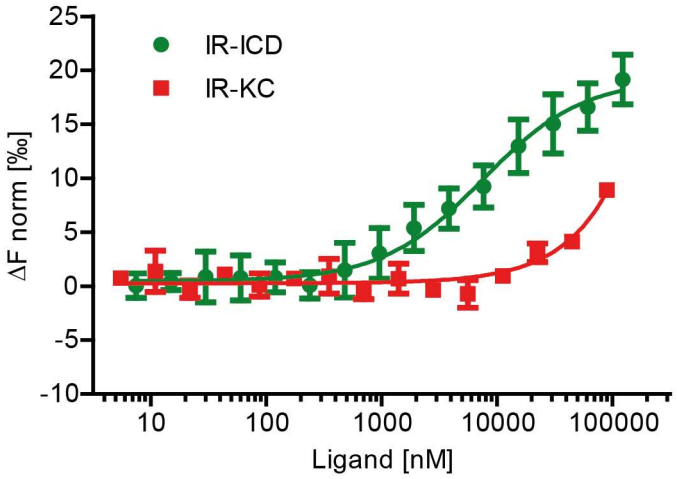

Fig. 3-4: MST differentiates interaction of ARNO with IR-ICD and IR-KC. Both IR constructs were serially diluted (from 100 µM to 5 nM) and mixed with a constant concentration of 100 nM fluorescein labelled ARNO. The measurement was performed in duplicate with 40 % LED power and 10 % MST power. The normalised changes in fluorescence (thermophoresis including t-jump) are plotted against the logarithmic concentration of IR-ICD/IR-KC and the data is fitted using a model derived from the law of mass action. Error bars represent the standard deviation, n = 2.

3.2.2 Further analytical methods fail to confirm the interaction between IR-ICD and ARNO

Pull-down experiments are a well-established procedure to detect new or confirm putative protein-protein interactions. Similar to immunoprecipitations, a “bait” protein is immobilised on a solid support like functionalised polymeric beads and bound partners are analysed after incubation and washing steps (Einarson *et al.* 2007).

In this case, glutathione sepharose beads were loaded with either GST or GST-tagged IR-ICD. ARNO was added in a fivefold molar excess and the bead-bound proteins were analysed via SDS-PAGE (fig. 3-5). While GST and GST-IR-ICD can be recovered in the eluate fraction, ARNO remains unbound in the supernatant fraction. Hence, this pull-down does not indicate an interaction of ARNO and GST-IR-ICD.

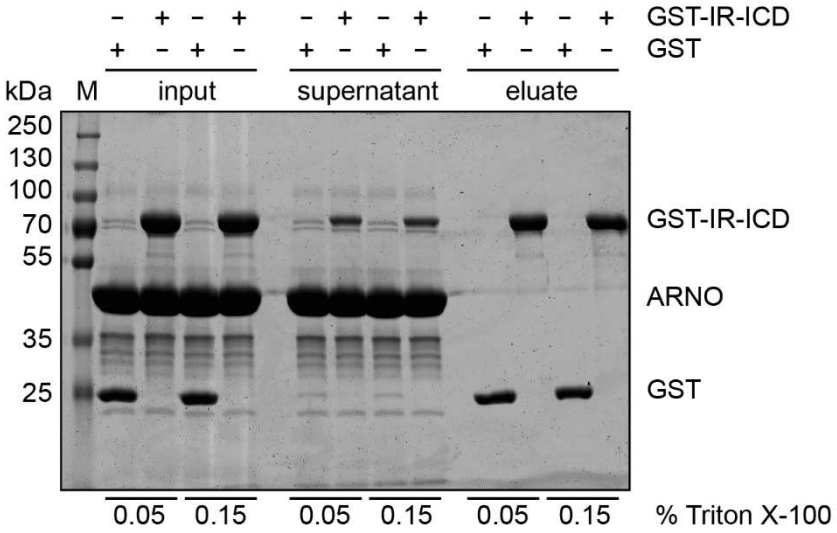

Fig. 3-5: Pull-down shows no interaction between ARNO and GST-IR-ICD. 5 µM GST or 5 µM GST-IR-ICD were incubated with 25 µM ARNO and 10 µL glutathione sepharose 4B beads for 30 min at room temperature (RT) while shaking. After washing, the bound proteins were eluted with 50 mM reduced glutathione (GSH). The input, supernatant after beads incubation and the eluate fractions were analysed via 10 % SDS-PAGE and stained with Coomassie blue. Neither at 0.05 % nor at 0.15 % Triton X-100 ARNO bound to GST-IR-ICD.

Another method of detecting molecular complex formation is the analytical size-exclusion chromatography (SEC). SEC, also termed gel filtration, separates molecules due to their hydrodynamic radius, which corresponds well with the molecular weight of globular proteins (Hong *et al.* 2012). While small molecules pass through all pores of the beads and have an accordingly long retention time, larger molecules do not enter the matrix and elute early.

Initially, ARNO and IR-ICD were analysed separately. ARNO eluted at 12.1 mL, IR-ICD at 14.2 mL (fig. 3-6). Compared with the molecular weight standard, this hints at monomeric

IR-ICD and probably dimeric ARNO. Note that ARNO elutes at a higher molecular weight as expected for a 93 kDa dimer (calculated MW according to standard 134 kDa). However, the coiled-coil dimerisation motif most likely conveys a non-globular but rather extended quaternary structure to the protein resulting in a higher hydrodynamic radius.

When an equimolar mixture of ARNO and IR-ICD were applied to the column, the elution profile resembled exactly the profile of the single proteins. This argues against complex formation. In this case, a higher molecular weight complex would have been expected to elute earlier.

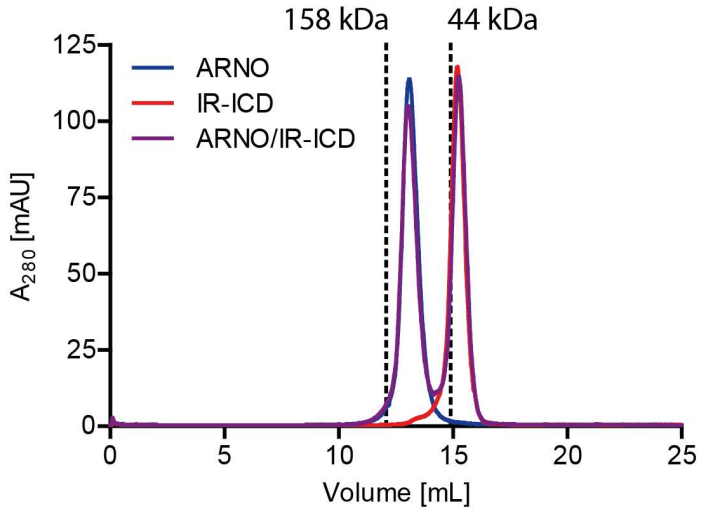

Fig. 3-6: Analytical size-exclusion chromatography suggests no interaction between ARNO and IR-ICD. 100 µL of 50 µM ARNO, 50 µM IR-ICD and a mixture of 50 µM ARNO/50µM IR-ICD were applied to a Superdex 200 10/300 GL gel filtration column. The elution profile of the mixture exactly matches the profile of the individual proteins, arguing against complex formation. The dotted lines indicate the elution maxima of a molecular weight standard.

To broaden the analytical spectrum further, isothermal titration calorimetry (ITC) was also tested to investigate the interaction between ARNO and IR-ICD. The basic principle is to measure the required energy to keep the temperature of a reference and a reaction chamber constant after repeated addition of a defined amount of a ligand to the molecule in the reaction chamber (Pierce *et al.* 1999, Ladbury 2004). This in turn allows to obtain the complete thermodynamic description of a given interaction including the K_D value, enthalpy and entropy.

After overnight dialysis, the experiment was carried out at 15 °C. Seven times higher concentrated IR-ICD was injected into the chamber containing ARNO (fig. 3-7). As a control, also a buffer to buffer injection was performed. The heat development of both experiments was in a similar range and therefore binding cannot be shown.

Taken together, the interaction analyses could not confirm a stable interaction between IR-ICD and ARNO. However, transient interactions cannot be ruled out, which constitute a large proportion of protein-protein interactions in cellular signalling complexes (Perkins *et al.* 2010).

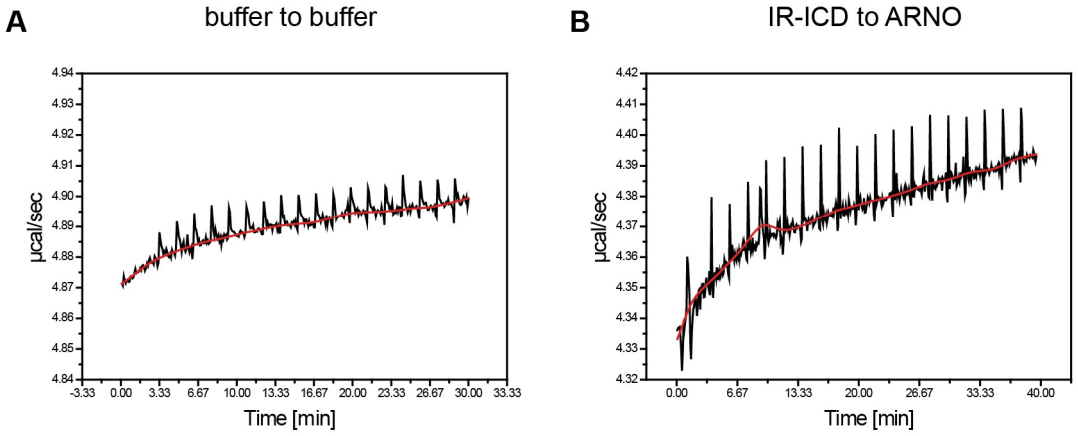

Fig. 3-7: ITC shows no interaction between IR-ICD and ARNO. 211 µM IR-ICD was added into 32 µM ARNO in 18 injections of 2 µL. The measurement was performed at 15 °C after protein dialysis overnight. The heat development for the IR-ICD to ARNO injection is in a similar range as for the buffer to buffer control and no binding can be inferred.

3.3 Biochemical characterisation of the ARNO-CNK1 complex

Identifying and characterising the individual components of complex signalling cascades is a challenging but inevitable task on the road to a comprehensive understanding of cellular processes and the development of targeted therapies. So far, several studies have been undertaken on cellular and organismal level to decipher the involvement of cytohesins in insulin signalling (Venkateswarlu *et al.* 1998, Li *et al.* 2003a, Hafner *et al.* 2006, Fuss *et al.* 2006, Lim *et al.* 2010). While binding of ARNO to the IR remains uncertain (chapter 3.2), using a pull-down approach coupled to mass spectrometry analysis, Lim and colleagues identified cytohesins as a major interaction partner of the scaffold protein connector enhancer of kinase suppressor of Ras 1 (CNK1). Moreover, they showed that the C-terminal domain of CNK1 and the coiled-coil domain of cytohesins are required to facilitate the membrane recruitment of ARNO upon insulin stimulation (Lim *et al.* 2010). Therefore, they conclude that both proteins interact with each other directly. However, taken into account that the experiments were based on co-immunoprecipitations from cell lysates, this conclusion can be described as daring although definitively standing to reason.

I therefore set out to study the putative ARNO-CNK1 interaction in more depth, including the mapping of involved domains and K_D determination. The chosen *in vitro* approach is suitable to rule out the necessity of cellular cofactors and enables the analysis of the interaction in a defined environment.

3.3.1 The cc domains of CNK1 and ARNO are required for the interaction

Since Lim and colleagues had reported the importance of the ARNO cc domain and the CNK1 C-terminal domain comprising a cc domain (Lim *et al.* 2010), I speculated that the interaction is dependent on both cc domains and therefore created cc deletion mutants of either proteins (termed Δcc).

In a pull-down setup, GST-ARNO and GST-ARNOΔcc were incubated with CNK1 and CNK1Δcc in presence of glutathione sepharose beads and the bound proteins were analysed via SDS-PAGE after washing steps (fig. 3-8). The GST pull-down using purified proteins reveals that ARNO and CNK1 interact directly without the requirement of additional proteins. Further, it shows that the cc domains of both GST-ARNO and CNK1 are required for the interaction. When either of the cc domains is lacking, no binding could be detected.

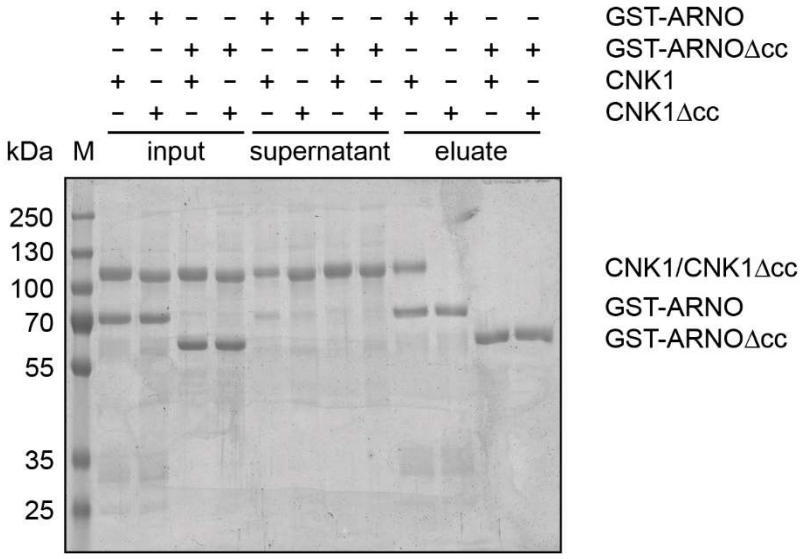

Fig. 3-8: The coiled-coil domains of ARNO and CNK1 are needed for the protein-protein interaction. 1 µM GST-ARNO constructs and 1 µM CNK1 constructs were mixed with 10 µL glutathione sepharose 4B beads in buffer containing 0.15 % Triton X-100 and incubated for 3 h at 4 °C. Bound proteins were eluted with 50 mM GSH, resolved by 10 % SDS-PAGE and stained with Coomassie blue.

3.3.2 The ARNO cc domain is necessary and sufficient for the CNK1 interaction

Next, it was tested whether the ARNO cc domain is sufficient for CNK1 interaction. Therefore, the interaction of GST-ARNO, the ARNO cc domain fused to GST (GST-ARNO-cc) and ARNO lacking the cc domain fused to GST (GST-ARNOΔcc) with CNK1 was evaluated using the pull-down approach described above. Expectedly, GST-ARNO interacts with CNK1 while GST-ARNOΔcc does not (fig. 3-9). It is also obvious, that the ARNO cc domain alone is able to interact with CNK1. However, the amount of CNK1

pulled is slightly less arguing for a somewhat weaker affinity compared to full-length ARNO.

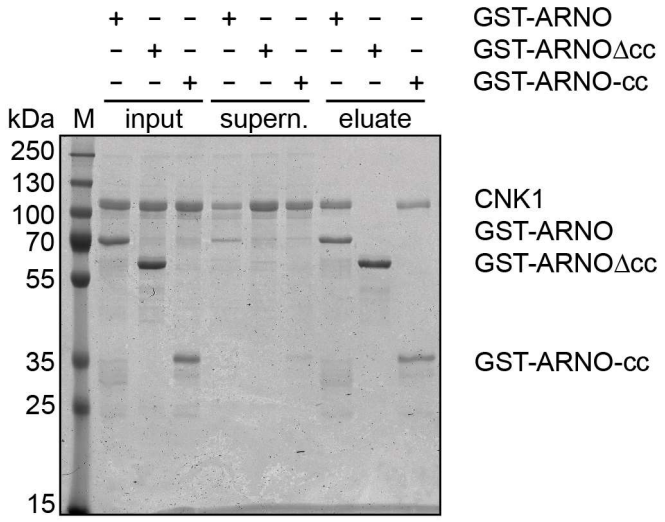

Fig. 3-9: The ARNO cc domain is necessary and sufficient for CNK1 interaction. 1 µM GST-ARNO constructs and 1 µM CNK1 were mixed with 10 µL glutathione sepharose 4B beads in buffer containing 0.15 % Triton X-100 and incubated for 3 h at 4 °C. Bound proteins were eluted with 50 mM GSH, resolved by 10 % SDS-PAGE and stained with Coomassie blue. GST-ARNO and GST-ARNO-cc interact with CNK1 while GST-ARNOΔcc does not bind CNK1.

3.3.3 The CNK1 cc domain is sufficient for ARNO interaction

Using the pull-down method, it was further investigated, whether the cc domain of CNK1 is sufficient for the interaction with ARNO. To ensure that the interaction is independent from the tag fused to the protein, a second tag apart from GST was also used. The so called HaloTag® is a 34 kDa mutated hydrolase (haloalkane dehalogenase), which covalently binds to a chloroalkane ligand (Zhang *et al.* 2006). The His272 to Phe mutation within the catalytic triad renders the formed ester bond between the HaloTag® and its ligand unhydrolysable. Since the HaloTag® fusion protein is covalently attached to the beads, elution, i.e. boiling the beads in sample buffer containing a high concentration of SDS, only yields the interacting protein but not the HaloTag® fusion protein itself.

For protein purification purposes, the CNK1 cc domain was fused to MBP connected via a linker including a TEV cleavage site. Since the fusion protein is larger and hence easier to detect than the 7.4 kDa cc domain only, pull-down experiments with the MBP fusion protein and also the isolated CNK1 cc domain were performed.

GST-ARNO interacts with MBP-CNK1-cc as well as CNK1-cc but not with the negative controls MBP and the insulin receptor C-terminus (fig. 3-10). If GST was bound to the beads as a control, no unspecific binding with any proteins could be observed. Using the same setup, the experiment was repeated with the HaloTag® ARNO fusion (fig. 3-11).

Here, the results resembled exactly the GST pull-down findings: Halo-ARNO interacts with CNK1-cc whether it is fused to MBP or not and does not interact with the control proteins. Beads just covered with the Halo protein do not interact with MBP-CNK1-cc nor CNK1-cc. It has to be noted that Halo-ARNO and Halo are absent in the analysed eluate fractions since the HaloTag® attaches covalently to the HaloLink™ resin. The CNK1-cc band is visualised weakly due to its small size and lack of high resolution in the SDS-PAGE.

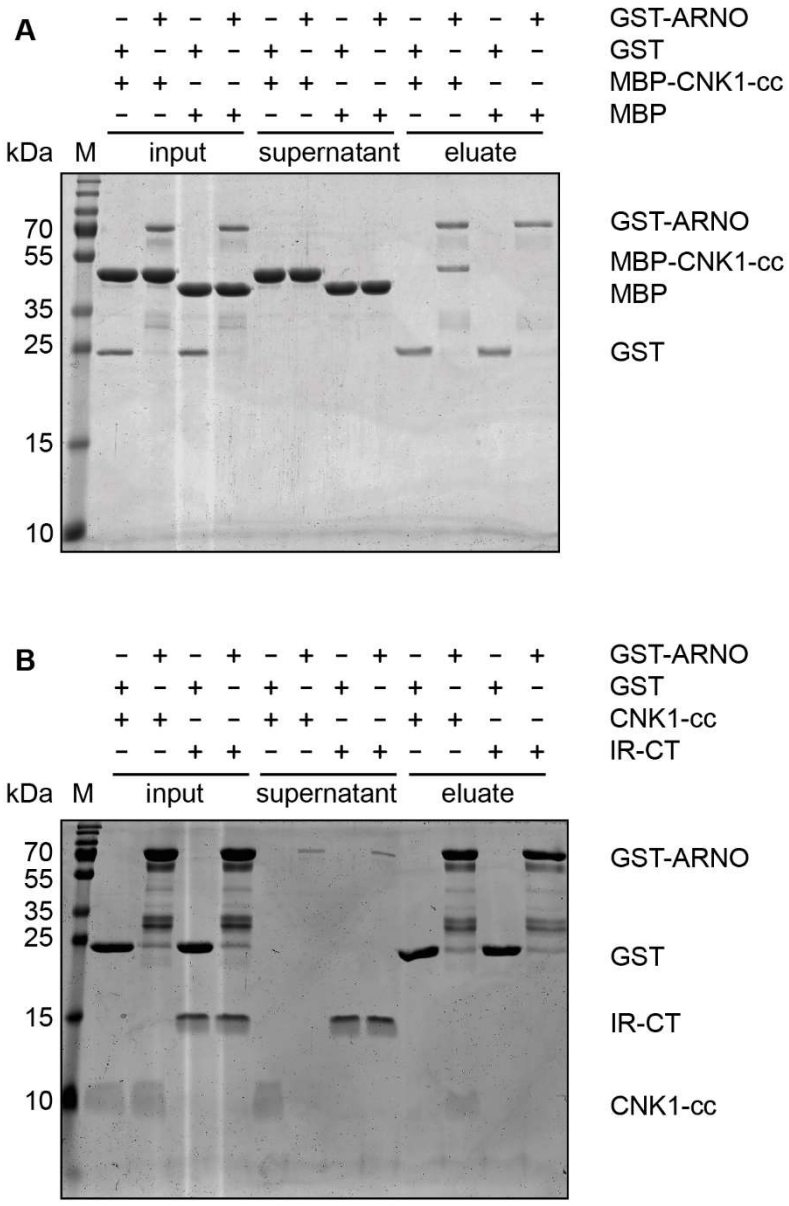

Fig. 3-10: GST-pull-down shows that CNK1-cc is sufficient for ARNO interaction. A | 1 µM GST-ARNO or 1 µM GST was mixed with 5 µM MBP-CNK1-cc or 5 µM MBP and 10 µL glutathione sepharose 4B beads. The samples were prepared in buffer containing 0.15 % Triton X-100 and incubated for 3 h at 4 °C. Bound proteins were eluted with 50 mM GSH, resolved by 12.5 % SDS-PAGE and stained with Coomassie blue. **B** | 5 µM GST-ARNO or 5 µM GST was mixed with 5 µM CNK1-cc or 5 µM insulin receptor C-terminus (IR-CT) as negative control and 10 µL glutathione sepharose 4B beads. The samples were prepared in buffer containing 0.15 % Triton X-100 and incubated for 3 h at 4 °C. Bound proteins were eluted with 50 mM GSH, resolved by 15 % SDS-PAGE and stained with Coomassie blue.

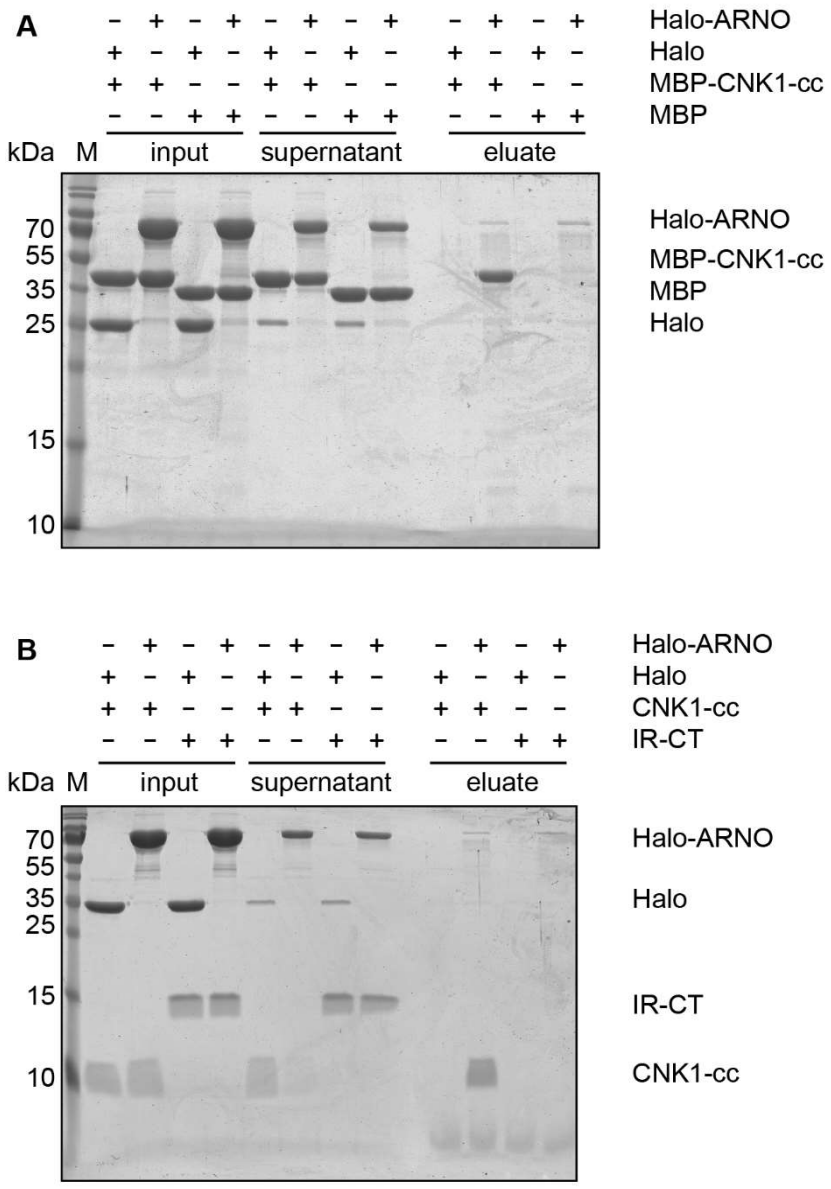

Fig. 3-11: HaloTag® pull-down supports that CNK1-cc is sufficient for ARNO interaction. **A** | 5 µM Halo-ARNO or 5 µM Halo was mixed with 5 µM MBP-CNK1-cc or 5 µM MBP and 10 µL HaloLink™ resin. The samples were prepared in buffer containing 0.15 % Triton X-100 and incubated for 4 h at 4 °C. Bound proteins were eluted by boiling the sample in SDS-PAGE loading buffer, resolved by 12.5 % SDS-PAGE and stained with Coomassie blue. **B** | 5 µM Halo-ARNO or 5 µM Halo was mixed with 5 µM CNK1-cc or 5 µM insulin receptor C-terminus (IR-CT) and 10 µL HaloLink™ resin. The samples were prepared in buffer containing 0.15 % Triton X-100 and incubated for 4 h at 4 °C. Bound proteins were eluted by boiling the sample in SDS-PAGE loading buffer, resolved by 15 % SDS-PAGE and stained with Coomassie blue.

Taken together, the pull-down analyses showed that the CNK1 cc domain is sufficient to interact with ARNO independent of the tags used for the pull-down.

3.3.4 Analytical SEC and ITC confirm the ARNO-CNK1 interaction

Having mapped the binding site of both proteins to their respective cc domains, the question of affinity and stoichiometry remained. Additionally, the interaction should be confirmed by independent techniques.

Analytical SEC was applied to validate the ARNO-CNK1 interaction (fig. 3-12). When applied separately to the column, CNK1 and ARNO eluted at 12.3 mL and 11.6 mL, respectively. According to a molecular weight standard, this corresponds to dimeric CNK1 and ARNO, which is also at least dimeric (see chapter 5.2.14). The fact that CNK1 possesses a cc domain as well as a sterile alpha motif (SAM), both of which are able to drive dimerisation, supports this notion (Mason and Arndt 2004, Stapleton *et al.* 1999). When CNK1 and ARNO were applied in a 1:1 molar ratio, a new peak at an elution volume of 10.6 mL emerged, indicating the formation of a higher molecular weight complex. SDS-PAGE analysis of the peak fractions confirmed that it contained CNK1 as well as ARNO (fig. 3-12 A). Notably, a fraction of ARNO remained unbound, which can be deduced by the small peak remaining at the retention volume of ARNO and by the corresponding SDS-PAGE fraction. This peak got even more pronounced, when a 2:1 molar mixture of ARNO to CNK1 was analysed (data not shown). On the other hand, it vanished at the expense of an even higher complex peak when a 1:2 molar ratio of ARNO to CNK1 was subjected to the column. This result led to the hypothesis, that ARNO and CNK1 form a 1:2 complex. Expectedly, no complex formation was observed when ARNOΔcc was incubated with CNK1 (fig. 3-12 B).

A similar experiment was also performed to confirm that the CNK1 cc domain is sufficient for the interaction with ARNO (fig. 3-13). The cc domain in MBP-CNK1-cc does not lead to dimerisation, as the protein elutes close to the expected molecular weight of the monomer at 14.3 mL. The MBP-CNK1-cc fusion protein eluted together with ARNO. Clearly, the CNK1-cc domain is responsible for complex formation, as MBP alone does not co-elute with ARNO (fig. 3-13 B). However, using the MBP-CNK1-cc fusion protein, no hint for the formation of a 2:1 complex could be obtained.

In summary, the analytical SEC experiments confirmed the interaction between ARNO and CNK1 and raise the possibility of the formation of a 1:2 complex. SEC also validated the finding that the CNK1 cc domain is sufficient for the ARNO interaction. As a next step, ITC experiments were performed. They offer two advantages: First, ITC enables the deduction of the K_D value and hence the quantification of the affinity. Second, apart from binding enthalpy and entropy, also the stoichiometry of the interaction can be obtained to test the analytical SEC findings.

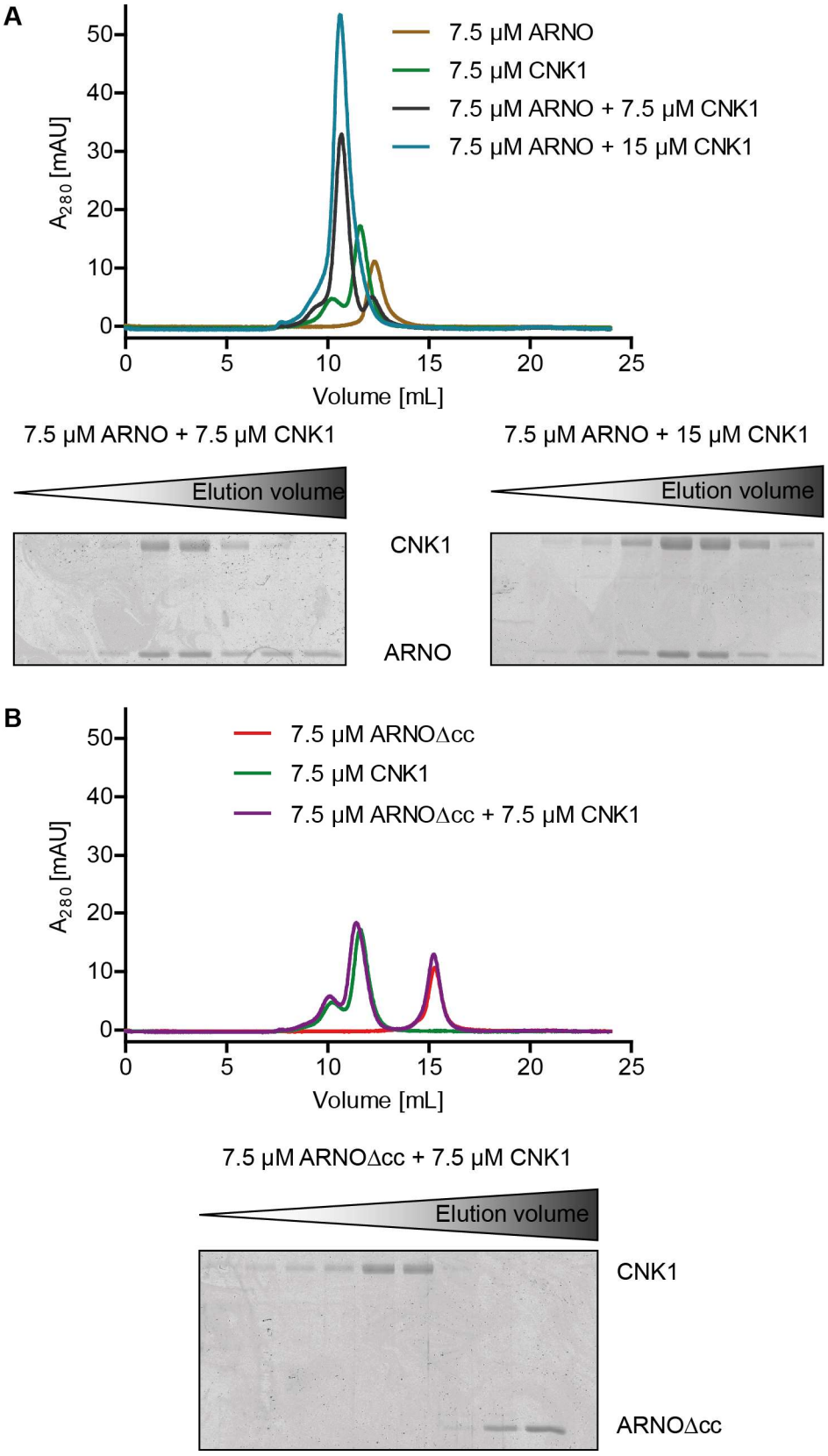

Fig. 3-12: Analytical SEC confirms the interaction of ARNO and CNK1. 100 µL of the indicated concentrations of ARNO, ARNOΔcc and CNK1 and respective mixtures were analysed via analytical SEC using a Superdex 200 10/300 GL at a flow rate of 0.4 mL/min. **A** | The ARNO-CNK1 complex elutes at a lower retention time and the presence of both proteins could be verified by 10 % SDS-PAGE/Coomassie blue staining. **B** | The ARNO construct lacking the cc domain does not interact with CNK1.

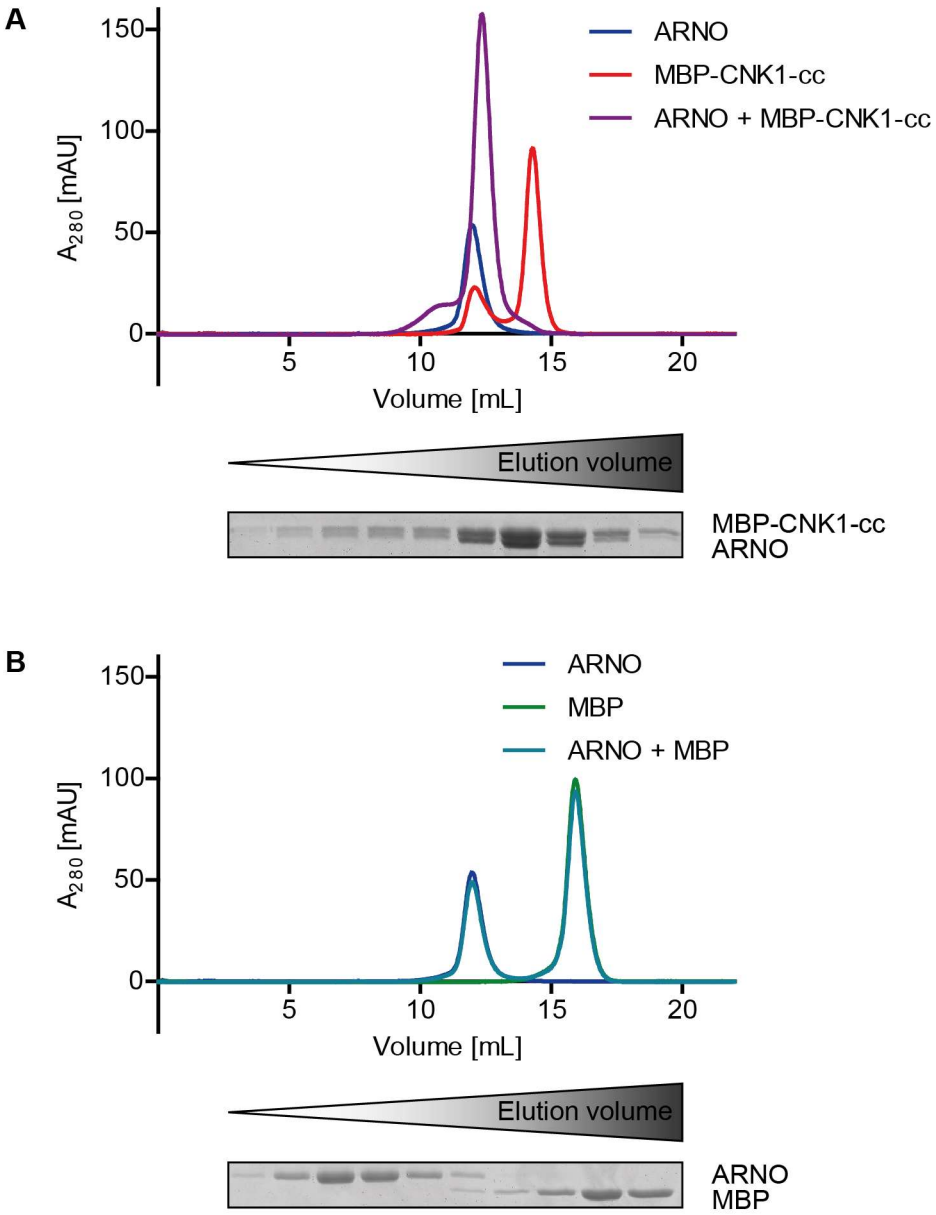

Fig. 3-13: Analytical SEC confirms that the CNK1 cc domain is sufficient for ARNO interaction. 100 µL of 30 µM ARNO, 30 µM MBP-CNK1-cc and 30 µM MBP as well as respective mixes were analysed via analytical SEC using a Superdex 200 10/300 GL at a flow rate of 0.4 mL/min. **A** | The presence of both MBP-CNK1-cc and ARNO could be verified by 10 % SDS-PAGE/Coomassie blue staining. The MBP-CNK1-cc peak at 14.3 mL completely vanished. **B** | ARNO does not interact with the negative control MBP.

As a final tool for interaction analysis, ITC measurements were performed. When ARNO was injected into CNK1, the interaction could be confirmed (fig. 3-14 A). Furthermore, the stoichiometry of 2 CNK1 molecules binding 1 ARNO molecule, as suggested by analytical SEC, was verified. The K_D value was determined as 2.6 nM ± 0.9 nM indicating a highly affine interaction. Note however, that the signal-to-noise ratio is rather weak and the steepness of the curve with only one point in the transition zone limits the accuracy of the measurement. This limitation can in principle be circumvented by lowering the

concentrations of the reactants in the syringe and the chamber. However, this also reduces the signal intensity and thereby further deteriorates the signal-to-noise ratio. Thus, it was decided to also test the interaction between MBP-CNK1-cc and ARNO, which might have a slightly lower affinity. In this case, higher concentrations can be used leading to a better signal intensity (fig. 3-14 B).

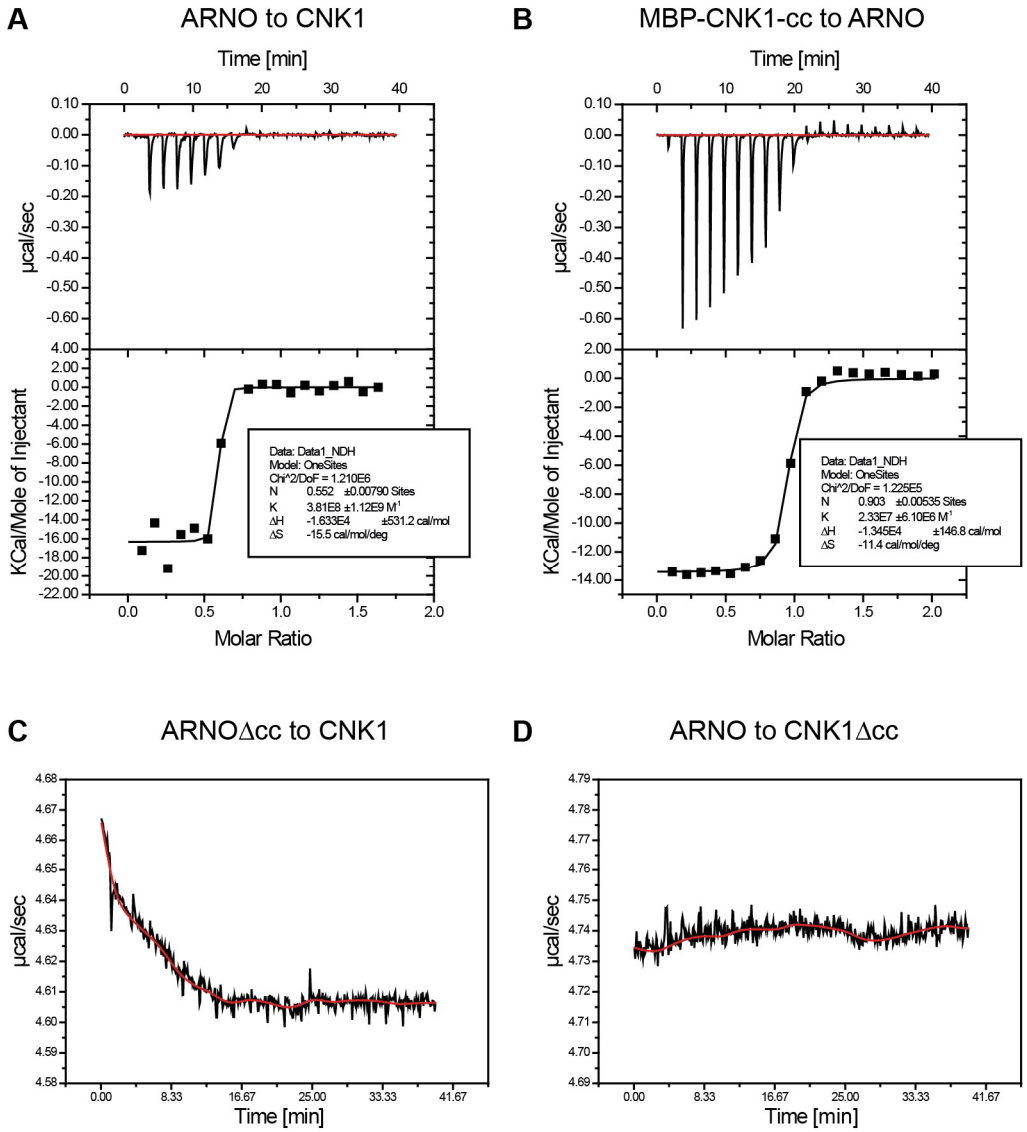

Fig. 3-14: ITC experiments confirm the interaction of ARNO with CNK1 and MBP-CNK1-cc. **A** | 101 µM ARNO were injected into 12 µM CNK1 at 25 °C using proteins previously dialysed against the same buffer overnight. The K_D value could be determined as 2.6 ± 0.9 nM. **B** | 244 µM MBP-CNK1-cc were injected into 23 µM ARNO at 25 °C using proteins previously dialysed against the same buffer overnight. Injections of MBP-CNK1-cc into buffer were subtracted. The K_D value could be determined as 43 ± 164 nM. **C** | 95 µM ARNOΔcc was injected into 11 µM CNK1 at 25 °C using proteins previously dialysed against the same buffer overnight. No interaction was observed. **D** | 70 µM ARNO was injected into 11 µM CNK1 at 25 °C using proteins previously dialysed against the same buffer overnight. No interaction was observed.

Indeed, compared to full-length CNK1, the affinity of MBP-CNK1-cc was lower with a K_D of 43 nM ± 164 nM. As in the analytical SEC experiments, a 1:1 complex is suggested for the MBP-CNK1-cc interaction with ARNO. Both interactions are enthalpically driven as can be deduced from the negative change in enthalpy (ΔH). As negative controls, the titration of ARNOΔcc into CNK1 and ARNO into CNK1Δcc were performed (fig. 3-14 C and D). In line with the previous experiments, no interactions were found.

3.4 Crystallisation of ARNO-CNK1 complexes

One way of understanding the foundation of biomolecular interactions is the elucidation of the three-dimensional structure. X-ray crystallography has long been the only means of structure determination at atomic resolution but is now complemented by nuclear magnetic resonance techniques (Rupp 2009). Additionally, single particle cryo-electron microscopy has become yet another powerful tool for 3D structure reconstruction (Wang and Wang 2017). Due to better availability and compatibility with the molecular weight of ARNO-CNK1 complexes, crystallisation trials were undertaken to decipher the molecular interaction of ARNO and CNK1.

3.4.1 Generation of complexes for crystallisation

Obtaining diffracting protein crystals is the prerequisite for structure determination via X-ray crystallography. At the same time, it constitutes one of the most challenging steps in the process. Two general concepts were employed to increase the likelihood of crystal formation: First, different truncation constructs of ARNO and CNK1 were used. Protein crystals can only form if intermolecular interactions of neighbouring proteins in the crystal lattice enable an ordered alignment. To allow for different crystal arrangements, the shortened ARNOΔpbr and ARNO-cc-Sec7 constructs were used alongside full-length ARNO. Additionally, either the isolated cc domain of CNK1 or full-length CNK1 were co-crystallised with the different ARNO constructs. Second, a high degree of homogeneity helps avoiding crystal defects and therefore raises the chances of crystal formation. Sample uniformity was enhanced by applying the complex to a size-exclusion chromatography step prior to crystallisation. This removes high molecular weight aggregates and also reduces the amount of protein not forming a complex. Although I had the possibility of setting up and evaluating several crystal screens, most of this work was performed by Dr Kanchan Anand, Karlsruhe Institute of Technology/University of Bonn. I am very grateful for her advice and help.

Fig. 3-15 shows the purity of the complexes obtained by size-exclusion chromatography and respective crystals which could be produced using the sitting and hanging drop methods. Especially the complex formed of ARNO-cc-Sec7 and CNK1-cc reached high

purity. Although crystals showed blue colour when treated with IZIT dye, strengthening the probability of being protein crystals, they did not diffract X-rays when tested at a synchrotron beamline. To improve the quality of crystals, several techniques were used, e.g. dehydration, various types of seeding, the use of different precipitant ratios and also hanging drop crystallisation. Further improvement at different levels is possible, such as the exploration of different constructs and more crystallisation conditions, which help in obtaining better quality single crystals.

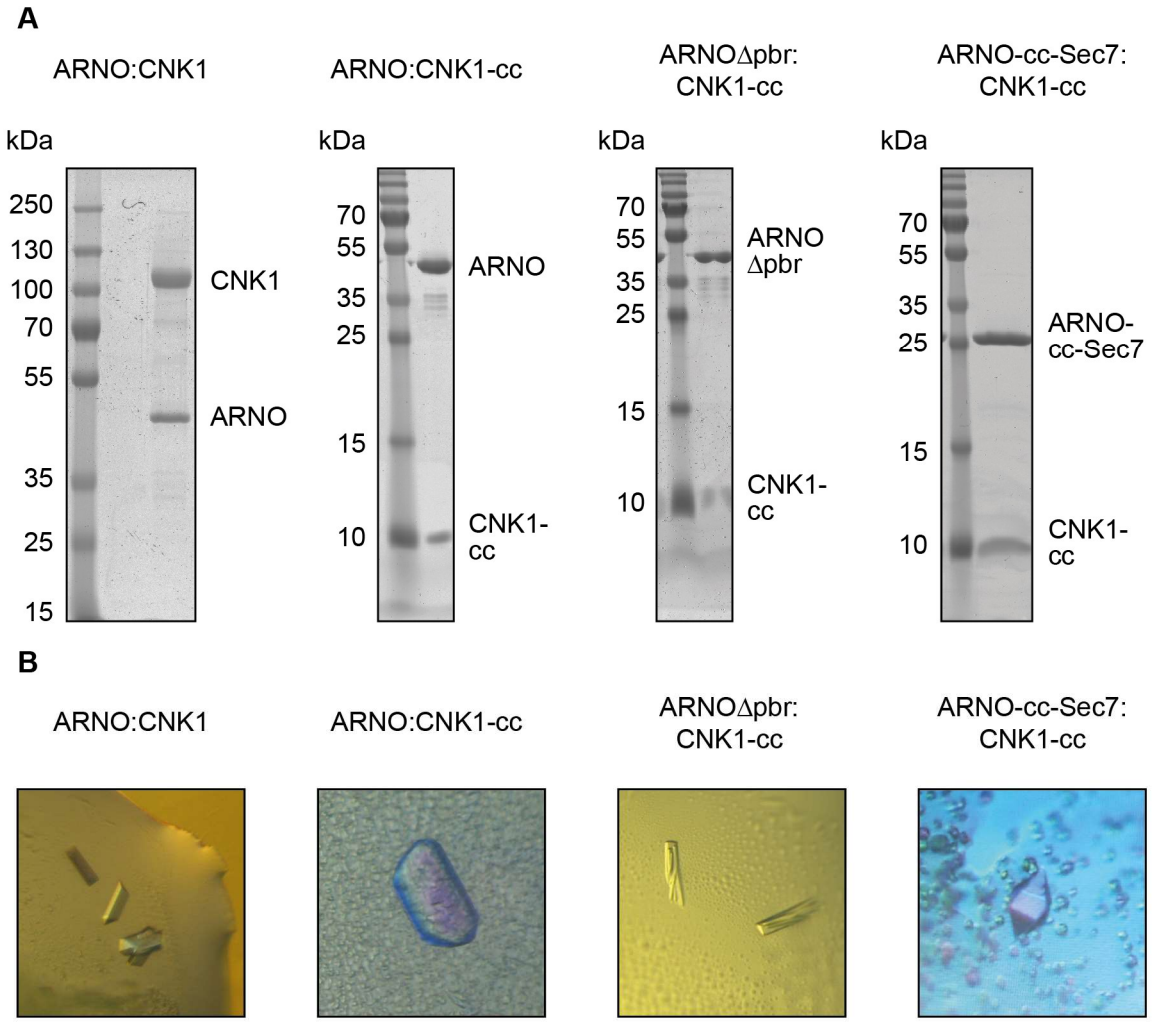

Fig. 3-15: Crystallisation of diverse ARNO-CNK1 complexes. A | The crystallisation complexes were obtained by mixing the respective proteins and applying them to the HiLoad 16/600 Superdex 200 pg or HiLoad 16/600 Superdex 75 pg (for ARNO-cc-Sec7/CNK1-cc). The final samples were applied to 15 % SDS-PAGE (10 % for ARNO/CNK1) and stained with Coomassie blue. **B** | The shown crystals were grown in the hanging drop vapour diffusion method at 10 °C under the following conditions: ARNO:CNK1, 1 M ammonium phosphate dibasic, 0.1 M imidazole/HCl, pH 8, 0.2 M sodium chloride; ARNO:CNK1-cc, 12.5 % PEG 1000, 12.5 % PEG 3350, 12.5 % 2-methyl-2,4-pentanediol, 0.03 M sodium nitrate, 0.03 M sodium phosphate, dibasic, 0.03 M ammonium sulphate, 0.1 M HEPES/MOPS, pH 7,5; ARNOΔpbr:CNK1-cc, 0.1 M sodium citrate, pH 6.5, 0.2 M ammonium acetate, 5 % ethylene glycol, 15 % low and medium MW PEG mix; ARNO-cc-Sec7:CNK1-cc, 0.1 M sodium citrate, pH 6.5, 20 % PEG 6000, 0.2 M zinc chloride. The typical crystal size was 50-150 µm x 40-50 µm x 20-30 µm.

3.5 The influence of CNK1 on the ARNO exchange activity

Having established the binding mode of CNK1 and ARNO, the next question was to decipher the underlying mechanism of the ARNO-CNK1 complex in insulin signalling. Endogenous CNK1 is found exclusively in the cytoplasm of serum-starved cells and insulin stimulation redistributes a fraction to the cell membrane (Lim *et al.* 2010). Earlier studies showed that the presence of another CNK protein, CNK3B, also termed IPCEF1, enhances ARNO exchange activity towards ARF6 in a radioactive GTPγS *in vitro* binding assay (Venkateswarlu 2003). Since active ARFs are localised via their N-terminal amphipathic helix and myristoyl moiety to membranes, myristoylated ARF1 and ARF6 were purified and the effect of CNK1 on ARNO-mediated exchange was studied in a lipid environment.

3.5.1 Purification of myristoylated ARF1 and ARF6

ARF proteins are myristoylated *in vivo* to facilitate membrane localisation (D'Souza-Schorey and Chavrier 2006, Kahn *et al.* 1988). N-Myristoylation refers to the addition of a 14 carbon atom saturated fatty acid to the N-terminal glycine of proteins (Wright *et al.* 2010). While ARF6 is permanently tethered to membranes independent of the bound nucleotide (Macia *et al.* 2004), ARF1 is cytoplasmic in its GDP-bound inactive state and localises to the plasma membrane upon GTP binding (Donaldson and Jackson 2011, Antonny *et al.* 1997, Duijsings *et al.* 2009, Chun *et al.* 2008).

Two different methods have been described to produce myristoylated ARFs (myr-ARF) in a heterologous expression system. Traditionally, ARFs are co-expressed with an N-myristoyltransferase (NMT) in *E. coli* in presence of sodium myristate. The myristoylated protein is subsequently isolated via ammonium sulphate precipitation, followed by anion exchange chromatography or gel filtration (Franco *et al.* 1995, Ha *et al.* 2005). Due to low yields, a different approach was developed for ARF6. Here, the non-myristoylated ARF6 and NMT are expressed separately. The proteins are then mixed in presence of myristoyl-Coenzyme A (myristoyl-CoA) and the myristoylated ARF is recovered by ammonium sulphate precipitation (Padovani *et al.* 2013).

To purify myristoylated ARF1, a modified protocol of Franco and colleagues was used (Franco *et al.* 1995). In short, non-tagged ARF1 was co-expressed with the pHV738 plasmid, which I obtained as a generous gift from Prof Richard A. Kahn, Emory University Atlanta (Van Valkenburgh and Kahn 2002). The plasmid bears the sequence of the human NMT1 under control of the IPTG inducible tac promotor as well as the *E. coli* methionine aminopeptidase (MetAP) under control of its endogenous promotor. 60 min after addition of sodium myristate and NMT induction, ARF1 expression from the

pMON5840-ARF1wt vector was induced. The pMON5840-ARF1wt plasmid was a generous gift from Prof Felix Wieland, Heidelberg University and Dr Frank Adolf. The cell lysate was precipitated at 35 % ammonium sulphate to enrich myristoylated ARF1, desalted, applied to anion exchange chromatography and, as a last step, purified by SEC. The result is depicted in fig. 3-16.

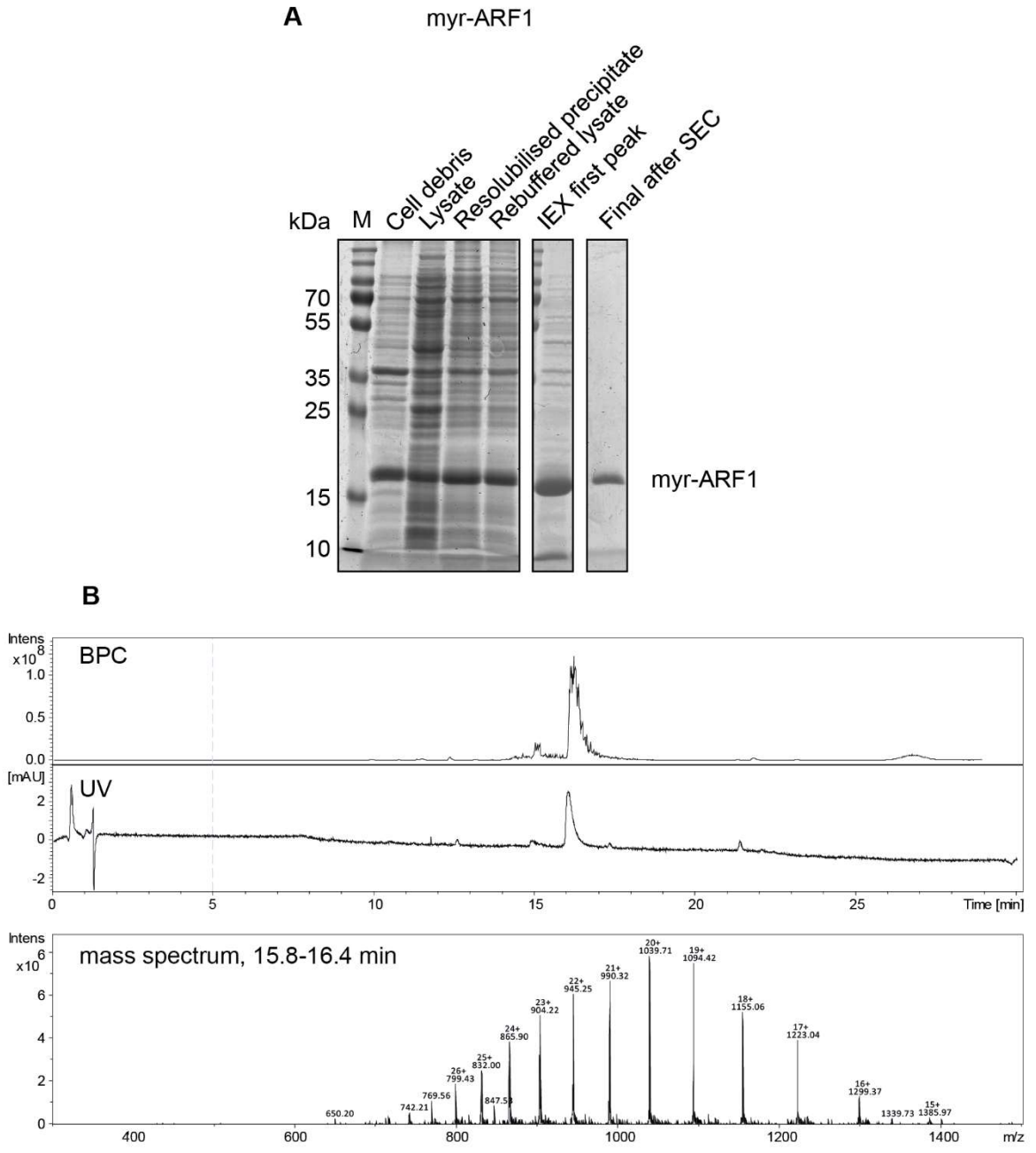

Fig. 3-16: Purification of myr-ARF1. A | The lysate was precipitated at 35 % ammonium sulphate and then resolubilised (resolubilised precipitate) and rebuffered (rebuffered lysate). The first peak of the Diethylaminoethyl (DEAE) sepharose anion chromatography contained the target protein which could be further purified by SEC. Respective fractions were analysed via 12.5 % SDS-PAGE and Coomassie stain. **B** | Mass spectrometric analysis of the final sample confirmed the successful myristoylation. The mass spectrum obtained at 16 min was deconvoluted leading to a mass of 20774.2 Da, which is in good accordance with the theoretical MW of 20775.9 Da for myr-ARF1.

While the resolubilised ammonium sulphate precipitate still contained many contaminants, the first peak of the anion exchange chromatography eluate yielded a relatively pure sample, which was further purified and rebuffered using SEC. Following analysis of the final sample by liquid chromatography-mass spectrometry (LC-MS) confirmed the protein identity to be myr-ARF1. No considerable amounts of non-myristoylated ARF1 were detected.

For the purification of myr-ARF6, the *in vitro* myristoylation approach was pursued (Padovani *et al.* 2013). First, hexahistidine-tagged ARF6 and NMT were expressed in *E. coli* and purified separately via IMAC and SEC (fig. 3-17 A and B). The yield for NMT was comparatively low but since only small amounts are needed for myristoylation, this constitutes a negligible issue.

As described in more detail in chapter 5.2.7, ARF6 was then myristoylated *in vitro*. 100 µM ARF6 was mixed with 1 µM NMT and 160 µM myristoyl-CoA. The mixture was incubated at room temperature for 4.5 h. To separate myr-ARF6 from non-myristoylated ARF6, myr-ARF6 was recovered by 30 % ammonium sulphate precipitation and was then rebuffered by overnight dialysis. To confirm the myristoylation, the final sample was analysed via LC-MS (fig. 3-17 C). The myristoylated protein could be detected, while no traces of non-myristoylated ARF6 were found.

Since the purification of non-myristoylated ARFs is easier and leads to a higher yield, it was also tested whether ARF1 could be myristoylated *in vitro* using the published approach (Padovani *et al.* 2013). However, no myristoylated protein could be obtained. The reason is unclear but could be a non-accessible N-terminal glycine. Also, pre-loading ARF1 with GTP could not change this (data not shown). Of note, other groups have tried to avoid the need for the sophisticated and time-consuming purification of myr-ARFs. They have replaced the lipid modification by a simple histidine-tag which allows them to tether GTPases to nickel-lipid containing membrane systems (Peurois *et al.* 2017).

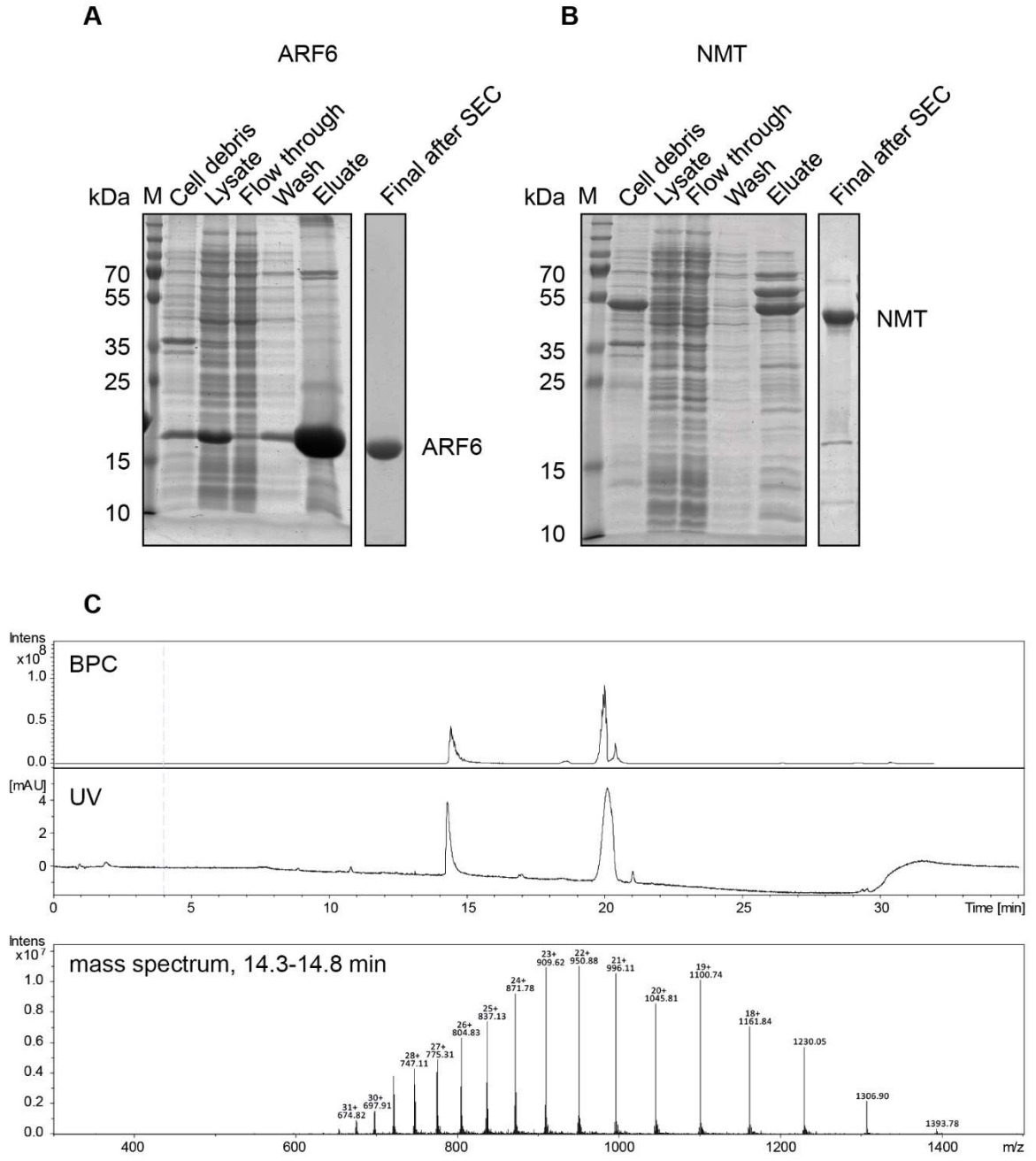

Fig. 3-17: Purification and *in vitro* myristoylation of ARF6. A and B | The cleared lysate was applied to Protino® nickel nitrilotriacetic acid (Ni-NTA) resin. After wash steps with 20 mM imidazole, the proteins were eluted with 250 mM imidazole. Finally, ARF6 was applied to a HiLoad™ 16/600 Superdex 75 pg and NMT to a HiLoad™ 16/600 Superdex 200 pg column. Respective fractions were analysed via 12.5 % SDS-PAGE and Coomassie stain. **C** | After *in vitro* myristoylation and ammonium sulphate precipitation, mass spectrometric analysis of the final sample confirmed the successful myristoylation of ARF6. The mass spectrum obtained at 14 min was deconvoluted leading to a mass of 20897.7 Da, which is in good accordance with the theoretical MW of 20897.0 Da for myr-ARF6. The peak at 20 min did not match a protein spectrum. The characteristic steps of 44 Da rather point to the presence of polyethylene glycol.

3.5.2 Creating a lipid system for nucleotide exchange assays

ARFs are localised to biological membranes in their active state via their N-terminal amphipathic helix and myristoylation (Donaldson and Jackson 2011, Franco *et al.* 1995, Antonny *et al.* 1997). In order to study ARFs in solution, N-terminal truncations have been generated. These GTPases do not localise to membranes, however studies showed that the catalytic activity of exchange factors towards soluble ARFs and membrane-bound myr-ARFs differ significantly by more than two orders of magnitude (Padovani *et al.* 2014). Since the membrane environment changes kinetics to a large extent, I chose to work with myristoylated ARFs and a suitable lipid system. Several lipid systems, like detergent micelles (Tanford and Reynolds 1976), bicelles (Sanders and Landis 1995) and nanodiscs (Bayburt and Sligar 2003) are available to study membrane or membrane-associated proteins. For ARFs, the vast majority of published *in vitro* data so far has been generated using liposomes (Robbe and Antonny 2003). Since this system has proven to work particularly well for ARF GTPases, it was chosen for subsequent activity and localisation studies.

Liposomes are spherical-shaped vesicles formed of at least one lipid bilayer (Laouini *et al.* 2012, Akbarzadeh *et al.* 2013). They were prepared following the general protocol as described for ARF activity studies (Robbe and Antonny 2003, Stalder *et al.* 2011) with a defined composition of 20 % L-α-phosphatidylethanolamine (PE), 30 % L-α-phosphatidylserine (PS), 48 % (or 50 %) L-α-phosphatidylcholine (PC) and 2 % (or no) L-α-phosphatidylinositol-4,5-bisphosphate (PIP_2). Briefly, a total of 2 mM lipids was mixed in 2 mL chloroform/methanol and the solvent was evaporated in a pointed hand vice. The lipids were rehydrated in 1 mL buffer, subjected to five freeze-thaw cycles and extruded through a polycarbonate membrane with a pore size of 100 nm. The liposomes were stored at room temperature until use.

The dynamic light scattering (DLS) method was used to assess the size distribution of the liposomes. It enables the deduction of the particle size by measuring the diffusion speed due to Brownian motion (Stetefeld *et al.* 2016).

Fig. 3-18 shows that the liposomes possessed a uniform size of around 130 nm and that the size remained constant over a period of 11 days. In order to avoid ageing and oxidation of the lipids, the liposomes were used for a maximal period of four days after production.

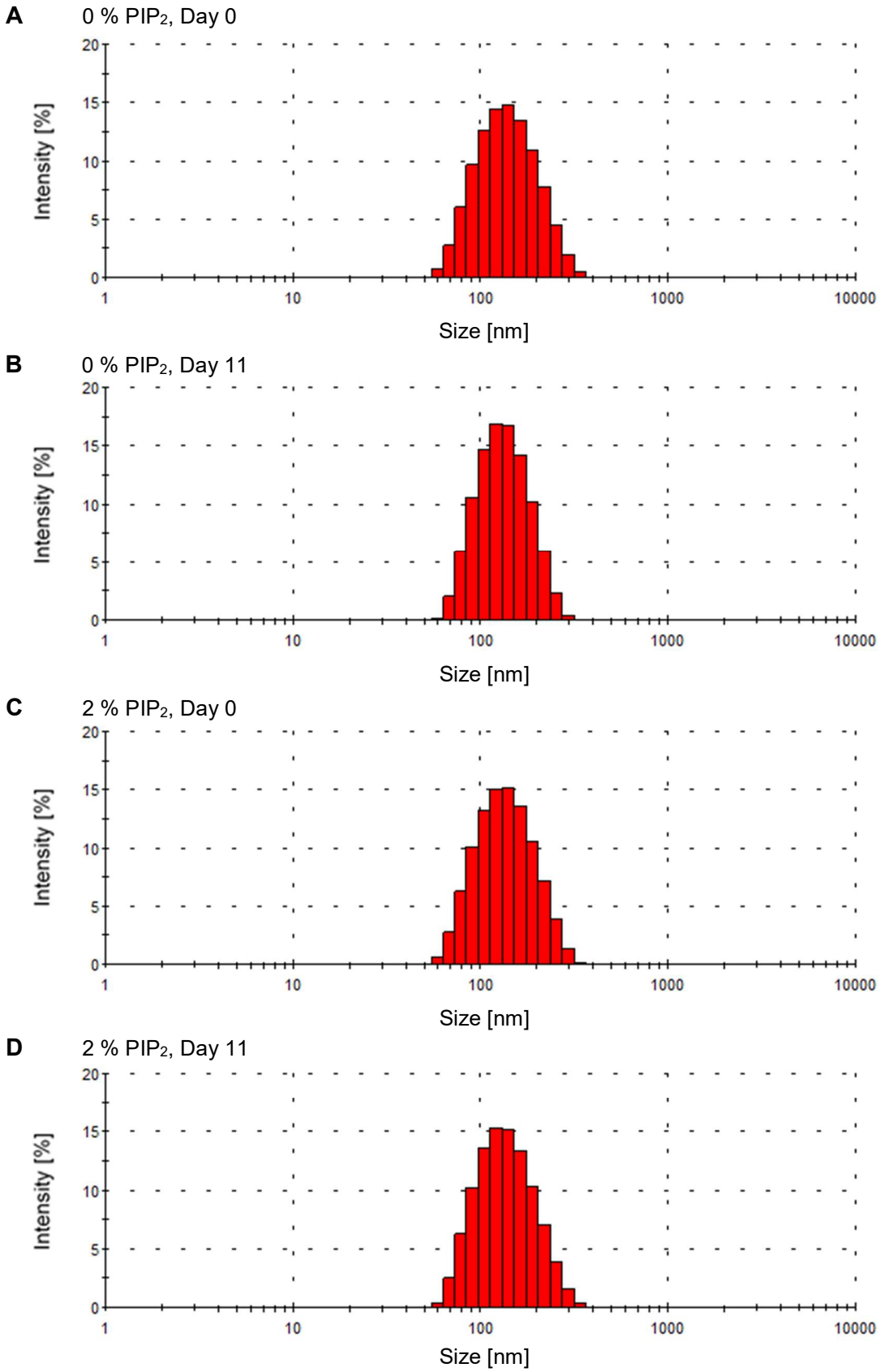

Fig. 3-18: DLS analysis of liposomes confirms their expected size. The prepared liposomes were diluted 1:100 and measured in the DLS Zetasizer nano Series S. The averages of 3 measurements, each consisting of 15 runs of the same sample are shown in the intensity representation.

3.5.3 Establishing a nucleotide exchange assay for myr-ARF1 and myr-ARF6

Assessing the catalytic activity of exchange factors on ARF GTPases can be performed by several means. Initially, the GDP to GTP exchange was monitored through binding or release of radioactively labelled nucleotides such as [^{35}S]GTPγS and [^{3}H]GDP (Kahn and Gilman 1986, Franco *et al.* 1995). At the same time, it was discovered that the intrinsic tryptophan fluorescence of ARFs increases upon GTP binding, which can be exploited to monitor catalytic activity (Kahn and Gilman 1986, Antonny *et al.* 1997). Additionally, the binding or release of fluorescently labelled nucleotide analogues can be measured (as performed in Stalder *et al.* 2011).

Testing several different exchange assay formats, the Mant-GDP release assay proved to work most stably with the experimental setup using a Tecan plate reader. Thus, it was chosen for the following analyses. When Mant-GDP is bound to the GTPase, excited tryptophan residues transfer energy to the Mant moiety via FRET. The radiationless energy transfer results in a high emission fluorescence signal at around 450 nm when the tryptophans are exited at approximately 280 nm.

For establishing the assay, the general scheme was adopted from Stalder *et al.* 2011. However, several adjustments had to be made because the original experiments were conducted using a fluorescence spectrophotometer and a cuvette setup. In this work on the other hand, a Tecan plate reader equipped with a fluorescence module was used. Notably, microtiter plates with a modified non-binding surface need to be used. This avoids sticking of the proteins as well as the Mant-nucleotide to the plastic, which would otherwise result in a drop of signal intensity.

Fig. 3-19 shows that 1 nM of ARNO is sufficient to elucidate a Mant-GDP to GTP exchange in presence of liposomes (200 µM total lipid concentration) and 100 µM GTP. While myr-ARF1 could be pre-incubated with GTP for temperature adaptation to 37 °C, this could not be done with myr-ARF6. For myr-ARF6, the spontaneous exchange of Mant-GDP to GTP in absence of exchange factor was too high, which can be deduced by the red curve in fig. 3-19 B. Therefore, the exchange was initiated by ARNO addition without prior temperature equilibration.

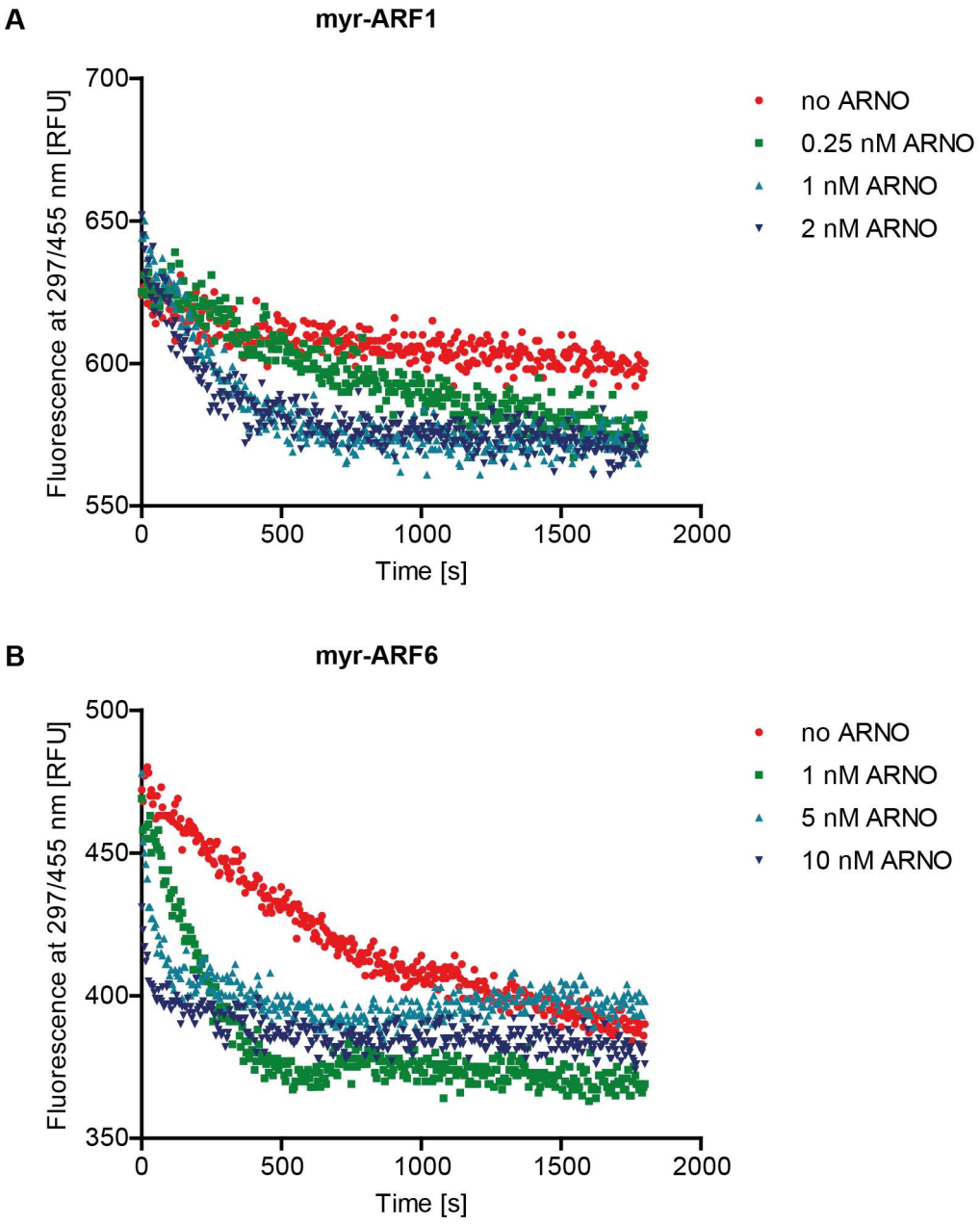

Fig. 3-19: Development of a Mant-GDP release ARNO activity assay for myr-ARF1 and myr-ARF6. 400 nM myr-ARF1 or myr-ARF6 were pre-loaded with 1 µM Mant-GDP. The exchange reaction in presence of liposomes (2 % PIP_2, 200 µM total lipid concentration) and 100 µM GTP was initiated by the addition of the indicated concentrations of ARNO. The reaction was performed at 37 °C and monitored by the decreasing Mant-FRET. **A** | For myr-ARF1, the sample was incubated at 37 °C for 20 min prior to the addition of ARNO to allow for complete temperature equilibration. 1 nM ARNO elicits the desired exchange and was chosen for the next experiments. **B** | Since the intrinsic exchange without exchange factor for myr-ARF6 is higher than for myr-ARF1, the measurement was started immediately. 1 nM ARNO elicits the desired exchange and was chosen for the next experiments.

3.5.4 The impact of CNK1 on the ARNO exchange activity

CNK1 depletion inhibits insulin signalling as shown by a reduced phosphorylation of IRS1 and PKB (Lim *et al.* 2010). One possible explanation for the involvement of CNK1 is the direct alteration of the ARNO exchange activity as shown for CNK3B (Venkateswarlu 2003). To test this hypothesis, exchange assays as described above using 1 nM ARNO were performed and CNK1 was titrated from 1 nM to 20 nM. Additionally, the experiment was repeated in triplicate for a fixed concentration of 2 nM CNK1. The experiments were performed on myr-ARF1 (fig. 3-20) as well as myr-ARF6 (fig. 3-21).

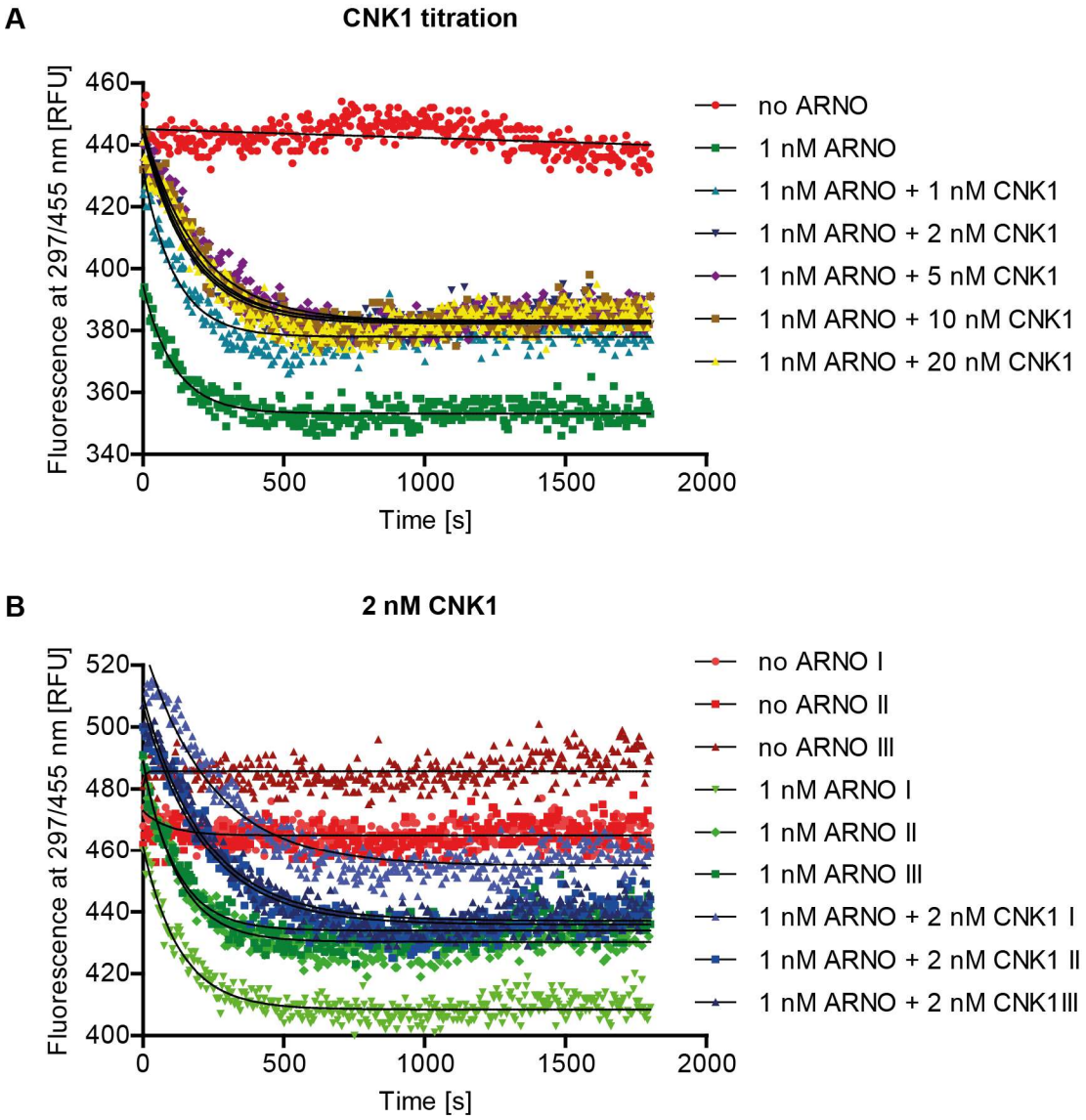

Fig. 3-20: CNK1 does not enhance ARNO exchange activity on myr-ARF1. 400 nM myr-ARF1 was pre-loaded with 1 µM Mant-GDP. The exchange reaction in presence of liposomes (2 % PIP_2, 200 µM total lipid concentration) and 100 µM GTP was initiated by the addition of 1 nM ARNO or mixtures of 1 nM ARNO and the indicated CNK1 concentrations. The reaction was performed at 37 °C and monitored by the decreasing Mant-FRET signal. The black lines show the mono-exponential fits of the data assuming pseudo-first order kinetics.

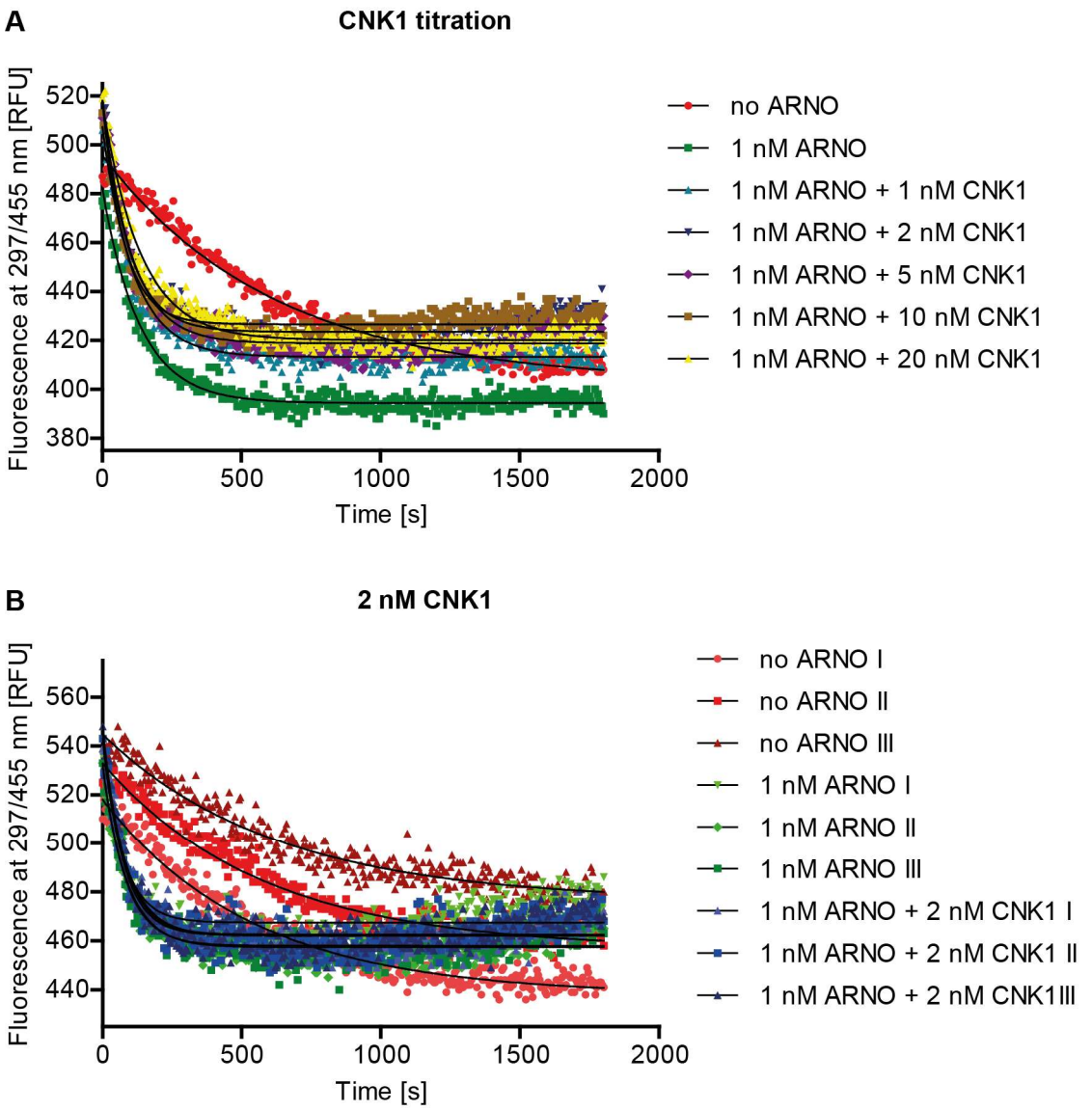

Fig. 3-21: CNK1 does not influence ARNO exchange activity on myr-ARF6. 400 nM myr-ARF6 was pre-loaded with 1 µM Mant-GDP. The exchange reaction in presence of liposomes (2 % PIP_2, 200 µM total lipid concentration) and 100 µM GTP was initiated by the addition of 1 nM ARNO or mixtures of 1 nM ARNO and the indicated CNK1 concentrations. The reaction was performed at 37 °C and monitored by the decreasing Mant-FRET signal. The black lines show the mono-exponential fits of the data assuming pseudo-first order kinetics.

The nucleotide exchange kinetics were analysed assuming pseudo-first order rate constants which were obtained by fitting the fluorescence traces using a mono-exponential fit (black curves in fig. 3-20 and fig. 3-21). Since the signal remains constant if no ARNO is added to myr-ARF1, no apparent initial rate constant can be deduced. In presence of 1 nM ARNO, the rate constant was 0.009 s^{-1}. When CNK1 was added, this dropped to around 0.005 s^{-1}, for concentrations higher than 2 nM CNK1, as confirmed via the triplicate measurement (fig. 3-20 B).

In contrast, CNK1 does not seem to influence the ARNO exchange on myr-ARF6 at all (fig. 3-21). While the initial rate constant was 0.002 s^{-1} in absence of ARNO due to the higher spontaneous exchange, this increased to around 0.013 s^{-1} when ARNO was added independent of the presence and concentration of CNK1.

Taken together, CNK1 did not enhance of the exchange activity of ARNO towards myr-ARF1 nor myr-ARF6.

3.6 The CNK1 membrane localisation

3.6.1 Membrane localisation of CNK1 wildtype

Using the Mant-GDP release assay, no enhancement of nucleotide exchange by CNK1 on the ARNO/ARF system was observed (chapter 3.5.4). One possible explanation is the localisation of the ARNO-CNK1-complex since the exchange activity of ARNO towards GTPases is dependent on its membrane targeting. In the cytosol, cytohesins reside in their autoinhibited form where the C-terminal polybasic region occludes the ARF binding site (DiNitto *et al.* 2007). Membrane binding contributes to the release of autoinhibition and was shown to be crucial for the activity of the Sec7-containing ARF-GEF Brag2 (Karandur *et al.* 2017).

Since GEF activity is linked to membrane localisation, it was investigated whether CNK1 wildtype localises to liposomes used in the exchange assays. It was hypothesised that CNK1 remained unbound to liposomes and therefore failed to enhance the amount of ARNO at the membrane via its tight interaction, leaving the exchange activity unaffected.

To address this question, liposome flotation assays were performed (Bigay and Antonny 2005). The assay is based on ultracentrifugation of a protein/liposome mixture in sucrose, which is overlaid with a sucrose cushion of lower concentration and a buffer layer. If the protein binds to the liposomes, it migrates to the top fraction alongside the lipids. If it does not interact with the liposomes, the protein stays in the bottom fraction. The result is shown in fig. 3-22.

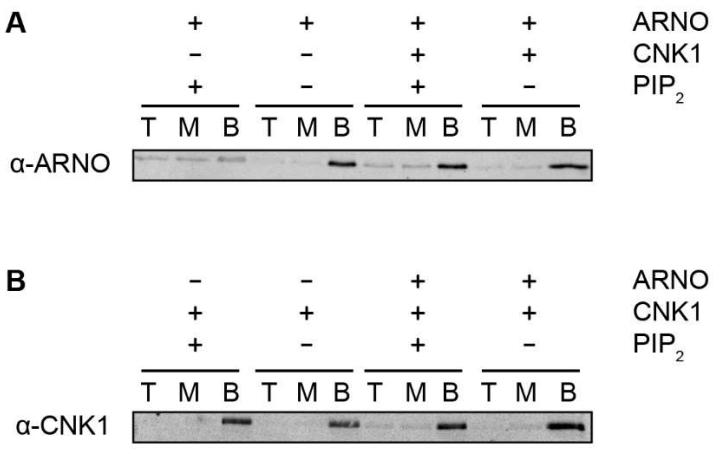

Fig. 3-22: CNK1 does not recruit ARNO to the liposome fraction. 30 nM ARNO and 30 nM CNK1 were prepared in a 30 % sucrose containing buffer and overlaid with two layers of 25 % sucrose and 0 % sucrose, respectively. After centrifugation at 240000 xg, top fraction (containing liposomes and bound proteins), middle fraction and bottom fraction (containing unbound protein) were analysed via 10 % SDS-PAGE and western blot. T = top fraction, M = middle fraction, B = bottom fraction. Note, that protein amounts of top, middle and bottom fraction cannot directly be compared due to the procedure of sample taking (chapter 5.2.21). **A** | ARNO bound to liposomes containing 2 % PIP_2 but not to liposomes without PIP_2. In presence of CNK1, the total ARNO amount was larger and the free ARNO proportion increased, probably due to reduced sticking. **B |** CNK1 was predominantly found in the bottom fraction, not bound to liposomes. When ARNO was present, a certain proportion of CNK1 was also recovered in the liposome containing layer.

While part of ARNO bound to the PIP_2 containing liposomes, it did not bind to liposomes without PIP_2, which was expected since the ARNO PH domain specifically binds PIP_2 and PIP_3 (Chardin *et al.* 1996, Klarlund *et al.* 2000). CNK1 in general remained in the bottom fraction indicating no interaction with the liposomes. When mixed with ARNO, some CNK1 shifts to the liposome-bound top fraction, but another phenomenon interferes with straight-forward data interpretation: The total protein amount of either protein increases, when they are mixed. This is probably due to reduced sticking of the complex to the polycarbonate centrifugation tubes. Taken together, CNK1 does not bind to liposomes and does not affect ARNO localisation to a large extent.

Recent data suggests that CNK1 is only localised to the plasma membrane if it is acetylated by CREB (cyclic adenosine 3',5'-monophosphate response element-binding protein)-binding protein (CBP) within its PH domain (Fischer *et al.* 2017). In the next step, it was therefore tested whether an acetylation-mimic mutant, $CNK1_{K414Q}$, localises to liposomes and can be used to investigate the activated form of CNK1.

3.6.2 Membrane localisation of the CNK1$_{K414Q}$ mutant

CNK1$_{K414Q}$ was shown to localise constitutively at the plasma membrane of HeLa cells and was used as an acetylation-mimic mutant in a recent study (Fischer *et al.* 2017). However, the authors did not identify the mechanism why acetylation of Lys414 and the abovementioned CNK1$_{K414Q}$ mutant led to plasma membrane localisation. It was therefore tested whether the binding can be reconstituted *in vitro* using the liposome flotation assay employed earlier. Fig. 3-23 shows that neither CNK1 nor CNK1$_{K414Q}$ bind to liposomes. Apparently, the reductionist liposome model is incapable of reconstructing the membrane recruitment of CNK1$_{K414Q}$ as observed in living cells. Similar to CNK1 wildtype, CNK1$_{K414Q}$ does not accelerate the exchange of ARNO on myr-ARF1 (supporting fig. A-2).

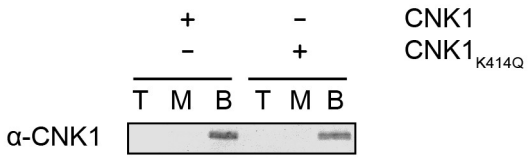

Fig. 3-23: CNK1$_{K414Q}$ does not bind to liposomes. 30 nM CNK1 and 30 nM CNK1$_{K414Q}$ were prepared in a 30 % sucrose containing buffer and overlaid with two layers of 25 % sucrose and 0 % sucrose, respectively. After centrifugation at 240000 xg, top fraction (containing liposomes and bound proteins), middle fraction and bottom fraction (containing unbound protein) were analysed via 10 % SDS-PAGE and western blot. T = top fraction, M = middle fraction, B = bottom fraction. Note, that protein amounts of top, middle and bottom fraction cannot directly be compared due to the procedure of sample taking (chapter 5.2.21). Both proteins can be found in the bottom fraction which indicates that they do not interact with the liposomes (2 % PIP_2).

3.6.3 Tethering His-tagged CNK1 to liposomes containing Ni-complexing lipids

Since the $CNK1_{K414Q}$ mutant did not bind to liposomes, I aimed to artificially tether the His-tagged CNK1 wildtype to liposomes containing the DGS-NTA(Ni) lipid. The headgroup of this lipid coordinates a nickel ion similar to Ni-NTA agarose beads and binds the hexahistidine-tag of recombinant proteins. Liposomes supplemented with 5 % DGS-NTA(Ni) have already been successfully used to tether His-tagged ARFs and exchange activity could be monitored (Peurois *et al.* 2017). Production of liposomes led to particles in the expected size range (supporting fig. A-3). In order to test if His-tagged CNK1 binds to liposomes containing DGS-NTA(Ni), concentrations of 5-25 % were tested (fig. 3-24). Unlike to the previously mentioned publication, where a concentration of 5 % DGS-NTA(Ni) was sufficient (Peurois *et al.* 2017), a concentration of 25 % needed to be used to tether the majority of CNK1 to the liposomes. When concentrations of 5 % and 10 % were used, almost the complete protein amount remained free in solution.

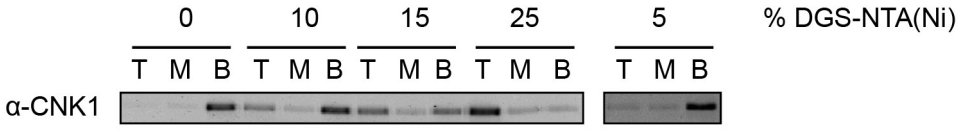

Fig. 3-24: Binding of His-tagged CNK1 to liposomes with increasing concentration of DGS-NTA(Ni). 60 nM His-tagged CNK1 was prepared in a 30 % sucrose containing buffer without reducing agent and overlaid with two layers of 25 % sucrose and 0 % sucrose, respectively. After centrifugation at 240000 xg, top fraction (containing liposomes and bound proteins), middle fraction and bottom fraction (containing unbound protein) were analysed via 10 % SDS-PAGE and western blot. T = top fraction, M = middle fraction, B = bottom fraction. Note, that protein amounts of top, middle and bottom fraction cannot directly be compared due to the procedure of sample taking (chapter 5.2.21). Increasing DGS-NTA(Ni) concentrations led to localisation of CNK1 to the liposome fraction (2 % PIP_2).

Subsequently, the effect of CNK1 on ARNO-mediated exchange on myr-ARF1 was tested using liposomes containing 5 % and 25 % DGS-NTA(Ni). The exchange with liposomes containing 5 % DGS-NTA(Ni) worked but expectedly CNK1 showed no effect (fig. 3-25 A). When the liposomes were supplemented with 25 % DGS-NTA(Ni), no exchange could be observed at all, even if the ARNO concentration was raised to 20 nM (fig. 3-25 B). Unfortunately, the effect of CNK1 on the ARNO exchange activity could thus not be further investigated by artificially tethering His-tagged CNK1 to the membrane. Liposomes with 10 % and 15 % DGS-NTA(Ni) also did not allow any exchange reaction to be monitored (data not shown).

Taken together, the exchange reaction of ARNO on myr-ARFs could be successfully reconstructed *in* vitro using PIP_2-containing liposomes, however the effect of membrane-localised CNK1 is still not completely understood.

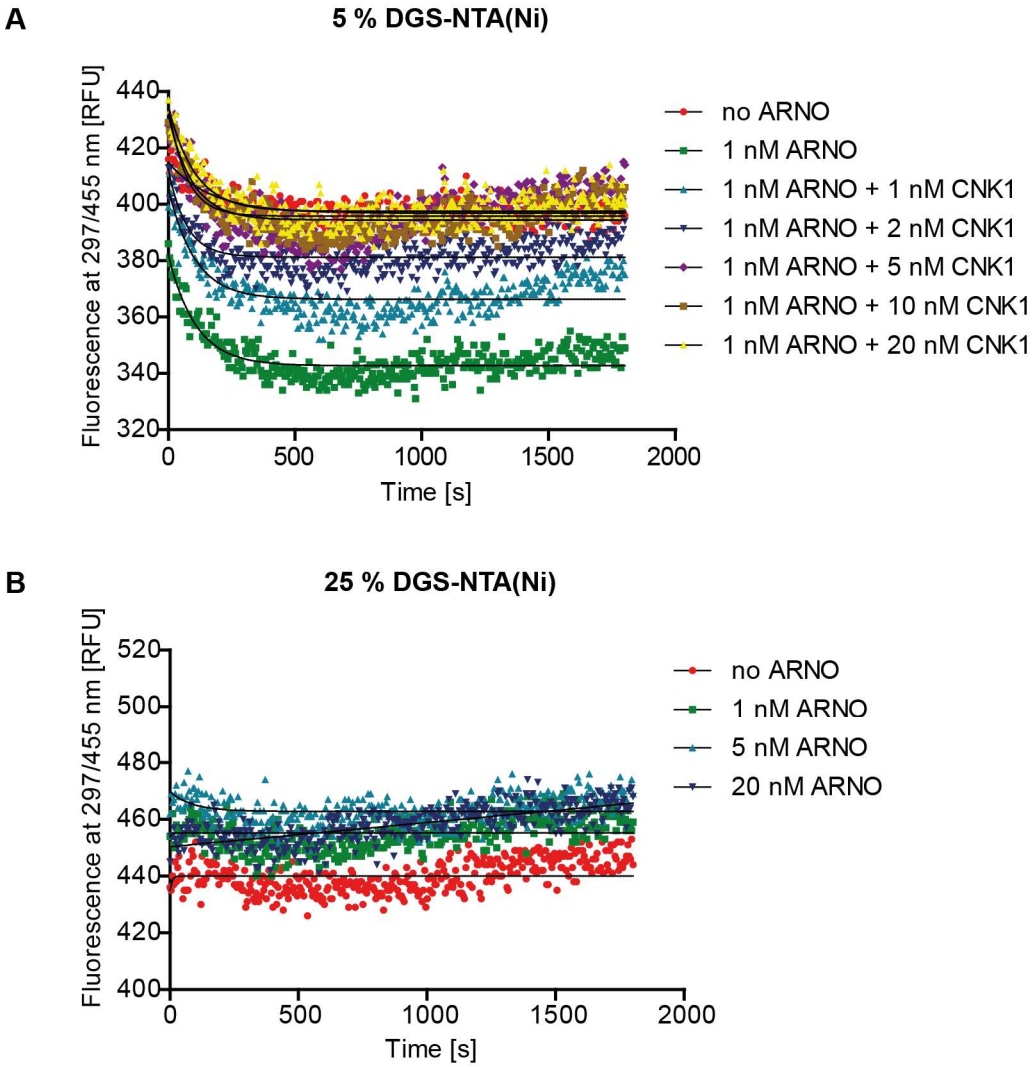

Fig. 3-25: Exchange assays using DGS-NTA(Ni) containing lipids failed to elucidate the effect of CNK1. 400 nM myr-ARF1 was pre-loaded with 1 µM Mant-GDP using a buffer without reducing agent. The exchange reaction in presence of liposomes (200 µM total lipid concentration, 5 % or 25 % DGS-NTA(Ni), 2 % PIP_2) and 100 µM GTP was initiated by the addition of 1 nM ARNO or mixtures of 1 nM ARNO and the indicated CNK1 concentrations (A). For 25 % DGS-NTA(Ni), ARNO concentrations of up to 20 nM were tested (B). The reaction was performed at 37 °C and monitored by the decreasing Mant-FRET signal. The black lines show the mono-exponential fits of the data assuming pseudo-first order kinetics.

4 Discussion

Insulin signalling is a key metabolic pathway in vertebrates and dysregulation in form of diabetes mellitus poses a major health risk to the ageing society (Navarro *et al.* 1999, WHO and IDF 2006). Thus, understanding the molecular mechanisms of how the insulin signal is processed within the cell is decisive for developing new strategies for pathway modification and hence treatment of diabetes. The signalling process is described in chapter 1.2.4 and consists of the activation of the IR, a receptor tyrosine kinase, and a downstream signalling cascade involving phosphoinositides and several other kinases. It has long been known that cytohesins, exchange factors for ARF GTPases, are also involved in this process (Venkateswarlu *et al.* 1998) and their role was further investigated during this work.

4.1 The influence of ARNO on IR activity

In the late 1990s it became apparent that cytohesins are involved in insulin signalling and that the cytohesin ARNO is translocated to the cell membrane upon insulin stimulation (Venkateswarlu *et al.* 1998). Two more recent studies then shed further light on the cytohesin involvement in insulin signalling and showed that chemical inhibition of cytohesins leads to insulin resistance phenotype (Hafner *et al.* 2006, Fuss *et al.* 2006).

Insulin-dependent localisation of cytohesins at the cell membrane raised the question of whether the influence of cytohesins on IR signalling could be rooted in enhanced receptor activity, which could be deduced from an increase in autophosphorylation. Therefore, *in vitro* autophosphorylation experiments were performed (fig. 3-2). Typically, *in vitro* autophosphorylation is induced by $MgCl_2$, which leads to augmented intermolecular interactions between the IR molecules and hence autophosphorylation (Herrera and Rosen 1986). Addition of a tenfold molar excess of ARNO and ARNOΔpbr did not alter IR autophosphorylation, arguing against a direct influence of ARNO on the receptor activity. This approach however comes with certain limitations: Autophosphorylation was monitored devoid of a membrane environment and was induced by an artificial stimulus, which relies on mild receptor aggregation (Herrera and Rosen 1986). Additionally, autophosphorylation proceeds very fast under these conditions and the experimental setup was unable to detect differences occurring during the first 15 sec after initiation of autophosphorylation. In order to monitor these early kinetics, a stopped-flow approach would have to be chosen.

However, the experiment supports earlier cellular approaches (Hafner *et al.* 2006). The study found that neither autophosphorylation nor the density of the IR was affected by

blocking cytohesins in HepG2 cells. Instead, the first hint at reduced pathway activity due to chemical cytohesin blockage was a decreased phosphorylation of IRS1 (Hafner *et al.* 2006).

4.2 Putative physical interaction between ARNO and IR

Due to the involvement in the early steps of IR signalling, a direct interaction between ARNO and the IR was proposed, even if the receptor autophosphorylation remains unaffected by cytohesins (Li *et al.* 2003a, Hafner *et al.* 2006).

In order to test the hypothesis of a direct protein-protein contact, several biochemical approaches using the purified proteins were employed (chapter 3.2). While the label transfer and microscale thermophoresis techniques suggested a physical interaction (fig. 3-3 and fig. 3-4), this finding could not be confirmed by pull-down, analytical SEC nor ITC experiments (fig. 3-5, fig. 3-6 and fig. 3-7).

The performed experiments deliver contradictory results. One explanation might be a difference in sensitivity. Especially transient interactions, which are a common feature of protein interaction networks, are challenging to detect (Perkins *et al.* 2010). Crosslinking experiments like the label transfer facilitate the detection of weak and transient interactions, however they increase the risk of detecting false positive interactions; the detectable label transfer from ARNO to MBP and IR-ICD to GST shows that unspecific interactions were also found. This underlines that the cross-linking approach is very sensitive to the concentrations of crosslinker and interaction partners used as well as the crosslinking duration.

The ITC method represents a well-established biochemical approach to investigate biomolecular interactions based on the detection of small temperature changes during the controlled mixing of interaction partners (Ladbury 2004). The range of detection is limited by the signal intensity in case for high affinity measurements, where low sample concentrations need to be used. For affinities in the millimolar to micromolar range on the other hand, the required high sample concentrations can be limiting. To obtain a complete measurement set, the concentration of the injected partner needs to be approximately one order of magnitude higher concentrated than the expected K_D. In the case of proteins, concentrations exceeding 500 µM to 1 mM are often very hard to achieve and lead to aggregation. Therefore, weak affinities cannot be elucidated under those circumstances. Due to solubility limitations and the consumed total protein amount, IR-ICD was injected at approximately 200 µM (fig. 3-7). Hence, weak binding ($K_D \geq 20$ µM) cannot be ruled out by the ITC approach.

Similarly, also for analytical SEC and pull-down approaches, the complex needs to be rather stable to be detected.

The phosphorylation status of the IR-ICD adds another level of complexity since the interaction with cytohesins could be phosphorylation-dependent. However, the MST and pull-down experiments were repeated with phosphorylated receptors and no change in interaction behaviour could be seen (data not shown).

Although co-immunoprecipitation studies indicated an insulin-dependent interaction of cytohesins with the IR-IRS1 complex in cells (Hafner *et al.* 2006), a direct interaction between ARNO and the IR could not be shown unambiguously using purified proteins. However, transient binding with low affinity is a possible mode of action.

4.3 Properties of the ARNO-CNK1 complex

Since the interaction between ARNO and the IR-ICD remains uncertain and a high-affinity interaction appears unlikely, another postulated interaction was investigated. Here, the interaction between ARNO and the scaffold protein CNK1 was followed up. Scaffold proteins mediate binding in signalling cascades and can lead to complex assembly, a specific subcellular localisation, coordination of feedback loops and protection of activated signalling molecules from inactivation (Shaw and Filbert 2009). The most prominent scaffold protein within the IR signalling pathway is certainly IRS1, which directly binds the phosphorylated IR, gets phosphorylated and relays the insulin signal further within the cell (White *et al.* 1985, Eck *et al.* 1996, Sun *et al.* 1993).

CNK1 is a multidomain scaffold protein and cytohesins were discovered to be a major interaction partner (Lim *et al.* 2010). In the same study, the authors showed that the CKN1-cytohesin complex is critical for the activation of the PI3K/PKB cascade downstream of the IR. CNK1 depletion in HeLa cells reduced the insulin-induced localisation of endogenous cytohesins to the cell membrane and ARF activity. The ARNO cc domain as well as the C-terminal domain of CNK1 were identified to be critical for the interaction and the involvement of CNK1 in insulin signalling. However, all experiments were performed in cell culture and hence a direct physical interaction without the need of cofactors remained to be proven (Lim *et al.* 2010).

4.3.1 ARNO and CNK1 interact via their coiled-coil domains

Pull-down experiments with GST-ARNO and CNK1 constructs lacking their respective coiled-coil domains showed that an interaction could only be detected when both cc domains were present (fig. 3-8). Subsequent pull-down experiments further confirmed the important role of the ARNO cc domain (fig. 3-9). Not only GST-ARNO was able to

pull-down CNK1, also the isolated ARNO cc domain fused to GST interacted with CNK1 and only slightly less CNK1, as compared to full-length ARNO, could be eluted indicating a somewhat reduced affinity. When the ARNO cc domain was deleted, no interaction with CNK1 was observed. Hence the ARNO cc domain is necessary and sufficient for the interaction with CNK1.

GST-ARNO and Halo-ARNO were used to confirm that also the CNK1 cc domain is sufficient for the ARNO interaction (fig. 3-10 and fig. 3-11). The CNK1 cc domain and the CNK1 cc domain fused to MBP both interacted with the ARNO fusions while control proteins remained in the supernatant fraction. The CNK1-cc band is visualised rather weakly due to its small size and lack of high resolution in the SDS-PAGE. This could be circumvented by using TRIS-Glycine PAGE or gradient PAGE. Taken together, the pull-down experiments successfully mapped the interaction sites of ARNO and CNK1 to their respective cc domains and were in line with the published cellular data (Lim *et al.* 2010).

4.3.2 The ARNO-CNK1 complex is stable and highly affine

Stoichiometry and affinity are two further questions which were addressed in this work. Analytical SEC confirmed the requirement of the ARNO cc domain (fig. 3-12) and the interaction between ARNO and CNK1. Furthermore, different protein ratios were tested. While a 1:1 molar ratio of ARNO and CNK1 led to one major peak consisting of both proteins and a second peak which predominantly consisted of ARNO, a 1:2 ratio led to one peak containing both proteins (fig. 3-12 A). It is noteworthy that the molecular weights of the single proteins as well as the complex only roughly match the theoretical elution volumes according to the calibration curve created using standard proteins. Critically, SEC separates proteins according to their hydrodynamic radius and not according to the actual molecular weight. For globular proteins such as thyroglobulin, γ-globulin, ovalbumin and myoglobin of the SEC standard, the hydrodynamic radius correlates very well with the molecular weight and the approximation of molecular weights of globular proteins is thus sufficiently exact. Since ARNO dimerises via its cc domain, it likely rather adopts an extended rod-like structure resulting in an elution volume corresponding to a higher molecular weight.

In order to investigate stoichiometry and especially affinity independently, ITC experiments were performed using ARNO and CNK1 or MBP-CNK1-cc (fig. 3-14). The ITC experiment using full-length proteins confirmed the 1:2 stoichiometry, which can be deduced clearly from the data since a steep increase from the unbound to bound state does not interfere with stoichiometry calculations. The affinity was determined as

2.6 nM ± 0.9 nM, however the low signal intensity and the steep transition zone limit the accuracy of the measurement. Since the signal intensity was already low, lowering the reactant's concentrations was no option. Also altering the temperature did not affect the affinity significantly. In order to circumvent this problem, the MBP-CNK1-cc construct was used, which interacted with ARNO with a K_D value in the double-digit nanomolar range. This supports the first finding of pull-down experiments, that the cc domain of either protein is sufficient for the interaction but has a slightly lower affinity compared to the full-length protein. Taken together, the data showed that ARNO and CNK1 interact in a 1:2 ratio with a very high affinity.

Apparently, CNK1 is able to disrupt the cc interaction of the ARNO dimer to form a heterotrimer consisting of two CNK1 molecules and one ARNO molecule. Theoretically also a complex of four CNK1 and two ARNO molecules is thinkable, although the elution volume in the SEC experiments clearly argues against this option. The biological consequences of this particular interaction mode are uncertain since the activity of cytohesins is independent from its oligomeric form (DiNitto *et al.* 2007). It can be speculated that this oligomeric form enables the proper integration within a larger signalling complex or influences membrane localisation. Dimers as well as trimers are frequent occurrences of cc interactions and single amino acids can determine the oligomeric state; also, a mixture of different states is possible (Mason and Arndt 2004). Hence, a regulatory mechanism dependent on the oligomeric state is conceivable, although the mechanism is uncertain at this point.

4.3.3 Crystallisation failed to provide deeper insight into the ARNO-CNK1 complex

In order to understand the molecular basis of the ARNO-CNK1 interaction, the three-dimensional structure should be solved by X-ray crystallography. One of the most difficult steps in structure determination is the generation of robust and diffracting protein crystals. Since flexible regions such as N- and C-termini can hamper proper crystal packaging, several truncated constructs of ARNO were used for co-crystallisation with CNK1 or the CNK1 cc domain. The proteins could be generated in sufficient amounts and a SEC step before crystallisation was performed to increase sample homogeneity. This approach led to several crystals which could be stained with IZIT dye, indicating that the crystals were most likely composed of protein. Even though crystal shape and size were optimised in the hanging-drop method, none of the crystals diffracted when tested at the synchrotron beamline. Unfortunately, crystallisation conditions are practically impossible to predict and a rational approach to increase the likelihood of a successful crystallisation is limited. Testing more initial conditions as well as further constructs enhances the chances of finding appropriate crystallisation conditions but can be a very time-consuming process.

However, shortening the constructs too much bears the risk of deviating from the cellular situation resulting in a misleading conclusion. Interestingly, the 1 ARNO:2 CNK1 ratio found for the full-length proteins was not resembled when the MBP-CNK1-cc construct was used (fig. 3-14 B). Therefore, constructs resembling the 1 ARNO:2 CNK1 ratio should primarily be considered for future crystallisation studies.

4.4 Monitoring ARNO activity on myr-ARFs *in vitro*: Approach and challenges

The catalytic activity of exchange factors on GTPases can be monitored using different approaches. Since assays based on intrinsic tryptophan fluorescence (Kahn and Gilman 1986, Antonny *et al.* 1997) and fluorescently labelled fluorophores (as in Stalder *et al.* 2011) exist, no radioactive assays were performed (Kahn and Gilman 1986, Franco *et al.* 1995).

Exchange reactions have been monitored using full-length myristoylated ARFs in presence of liposomes or by employing a more simplistic model in solution using ARFs devoid of the N-terminal myristoylated amphipathic helix (NΔ17ARF1 and NΔ13ARF6, Antonny *et al.* 1997). Notably, kinetics are significantly faster when myristoylated ARFs are used (Nawrotek *et al.* 2016). Since the membrane environment changes kinetics drastically and the reaction takes place at the membrane within the cell (Stalder *et al.* 2011, Padovani *et al.* 2014), a liposome model was chosen for the analyses in this work (Stalder *et al.* 2011).

4.4.1 Purification of myristoylated ARFs

Heterologously expressed ARFs can either be myristoylated during expression by co-expressing an NMT (Franco *et al.* 1995) or by expressing ARF and NMT separately and then performing the myristoylation *in vitro* (Padovani *et al.* 2013). Since myristoylated ARFs have a higher tendency to bind membranes, the purification is quite tedious and yields are comparatively low. Therefore, I pursued the *in vitro* myristoylation approach for ARF6 which led to a pure final protein with a very high degree of myristoylation (fig. 3-17). The process worked well, and hence this approach was also tested for ARF1, which has not been published. However, neither GDP nor GTP loaded ARF1 could be myristoylated, possibly since the N-terminus was inaccessible. A new attempt to circumvent the complex purification of myristoylated ARFs is the use of hexahistidine-tagged ARFs in combination with liposomes containing DGS-NTA(Ni) (Peurois *et al.* 2017). Although the exchange kinetics are slightly slowed down, this approach might replace the use of myristoylated ARFs for certain applications in the future.

4.4.2 Different ways to monitor exchange activity on ARFs

Intrinsic tryptophan fluorescence and fluorescently labelled GTP or GDP analogues are both used to monitor exchange activity on ARFs. Indeed, both techniques are frequently used complementary within one study (Stalder *et al.* 2011). Working with GDP and GTP can be beneficial since the kinetics with the natural nucleotides is studied, while fluorescent modifications such as a Mant moiety attached to the ribose can influence nucleotide binding. However, characteristics of fluorescently labelled nucleotides were found to generally resemble the non-modified versions and fluorescent nucleotide analogues have successfully been used in the past to study cytohesin/ARF nucleotide exchange kinetics (Hiratsuka 1983, Stalder *et al.* 2011, Malaby *et al.* 2013).

Also, the choice of whether Mant-GTP binding to ARF-GDP or Mant-GDP dissociation from ARF-Mant-GDP is monitored can be varied and both approaches were performed in the abovementioned publications. No specific experimental setup is particularly preferred in a certain situation. For the exchange reactions in presence of liposomes however, I found the use of a Mant-GDP release assay most reliable (fig. 3-19). Notably, a Tecan plate reader was used in the experiments, while most published data were generated in a fluorescence spectrophotometer equipped with a stirring device, probably accounting for a better signal-to-noise ratio. The assay worked best when myr-ARFs were pre-loaded with a rather small excess of Mant-GDP (1 µM) over the myr-ARF (400 nM). Additionally, myr-ARF1 was pre-incubated with GTP for temperature equilibration before ARNO addition which was impossible for myr-ARF6. The spontaneous exchange of Mant-GDP to GTP in absence of exchange factor was too high, probably due to the permanent localisation of myr-ARF6 to the membrane (Macia *et al.* 2004). Why this setup proved to be superior to intrinsic tryptophan fluorescence or a Mant-GTP binding assay remains elusive.

4.5 The mechanism of CNK1 involvement in insulin signalling

CNK1 depletion results in the same effect on insulin signalling (Lim *et al.* 2010) as inhibition of cytohesins (Hafner *et al.* 2006), namely the reduction of IRS and PKB phosphorylation. Since another member of the CNK family, CNK3B directly affects ARNO exchange activity (Venkateswarlu 2003), it was tested whether also CNK1 might enhance the exchange activity of cytohesins. Unlike for CNK3B, CNK1 did not accelerate the ARNO mediated exchange in solution (data not shown) nor in a lipid environment (fig. 3-20 and fig. 3-21). There are three possible explanations for this result: 1. ARNO and CNK1 do not interact under the tested exchange conditions, 2. the ARNO-CNK1 complex does not localise to the liposomes and 3. CNK1 exerts its action in the insulin signalling

pathway independent of the ARNO exchange rate. The possibility that ARNO and CNK1 do not interact at 1 nM to 20 nM cannot be ruled out, however that fact that already the CNK1 cc domain interacts with ARNO in the double-digit nanomolar range and that the full-length proteins show an even higher affinity argues against this option. Additionally, similar buffer conditions were used in the exchange assay as well as the interaction studies. All data have hinted at a very stable interaction and it is overall highly unlikely that ARNO and CNK1 do not interact in the tested exchange assay. The localisation of CNK1 is discussed in the next chapter.

4.5.1 The CNK1 localisation

Exchange factors exert their catalytic activity towards ARF GTPases at the cell membrane and are in their auto-inhibited state in the cytosol (DiNitto *et al.* 2007, Karandur *et al.* 2017). The co-localisation of exchange factor and GTPase at the membrane is therefore an important prerequisite for exchange activity and a higher concentration of membrane-bound cytohesins correlates with an increased level of activated GTPase. It was therefore investigated whether CNK1 localises to the liposomes used for exchange assays and in how far it influences ARNO localisation (fig. 3-22). The performed liposome flotation assay showed that CNK1 did not interact with liposomes and hence did not increase the amount of membrane-bound ARNO. Possibly, a certain amount of ARNO is even sequestered in solution via CNK1 (fig. 3-22), which might explain the reduced exchange kinetics on myr-ARF1 (fig. 3-20).

This result is in line with recent literature, where cellular experiments showed that CNK1 only localises to the plasma membrane after it has been acetylated within its PH domain (Fischer *et al.* 2017). It was therefore tested whether the acetylation-mimic mutant $CNK1_{K414Q}$ localised to the liposomes. However, also the acetylation-mimic mutant remained unbound to liposomes (fig. 3-23). Since Fischer and colleagues were unable to elucidate the exact mechanism of membrane targeting, it is unclear why the acetylation-mimic mutant localises to the plasma membrane but not to the prepared liposomes. Apparently, another factor is required for lipid binding, which is only present in the cell. A simplistic phosphoinositide binding mode can be excluded, since CNK1 only binds weakly and non-specifically to phosphoinositides (Jaffe *et al.* 2004) and masking the positive charge of lysine would rather decrease than increase phosphoinositide binding as shown for the lysine acetylation within the PH domain of PKB (Sundaresan *et al.* 2011).

Because CNK1 remained unbound to liposomes, it was next artificially tethered to liposomes. The method was adapted from Peurois, who was able to bind hexahistidine-tagged ARFs to liposomes complemented with DGS-NTA(Ni), a lipid with a nickel-

containing headgroup, which can chelate the affinity tag (Peurois *et al.* 2017). A titration experiment clearly showed that unlike to the publication, where 5 % DGS-NTA(Ni) was sufficient to bind histidine-tagged ARFs, a higher DGS-NTA(Ni) concentration needed to be used. Only when the concentration was raised to 15 % and 25 %, a substantial amount of histidine-tagged CNK1 bound to the liposomes (fig. 3-24). While the exact reason for this difference remains unclear, it can be speculated that the affinity tag of CNK1 is less well accessible and might be covered by parts of CNK1, a protein which is significantly larger than ARF GTPases. As the next step, the exchange reaction of ARNO on myr-ARF1 using liposomes with DGS-NTA(Ni) was tested (fig. 3-25). The exchange using 5 % DGS-NTA(Ni) works, but CNK1 does not affect the exchange rate. This was expected since CNK1 behaves the same way as in a setup using liposomes without DGS-NTA(Ni), remaining free in solution.

Unfortunately, the exchange could not be monitored on liposomes with higher DGS-NTA(Ni) concentration (fig. 3-25 B). Even when the ARNO concentration was increased, no exchange reaction, recognisable by a drop in fluorescence intensity, could be observed. The reason for this remains elusive but apparently the high DGS-NTA(Ni) concentration hampers the proper arrangement of ARNO and myr-ARF1 at the surface of the liposomes. Hence, the question of whether CNK1 can increase the local ARNO concentration at membranes and therefore contributes to an increased ARF signalling remains unclear.

4.5.2 A possible mode of action for the ARNO-CNK1 complex

This work could clearly demonstrate that ARNO and CNK1 directly interact with one another and form a stable complex (chapter 3.3). Previous research showed that CNK1 directs cytohesins to the cell membrane and established CNK1 “as a new positive regulator of insulin signalling” (Lim *et al.* 2010). All findings to this point indicate that the CNK1-ARNO interaction is highly stable and of permanent nature. So why is CNK1 required in IR signalling and how is it regulated? According to the model shown in fig. 1-11, it is likely that CNK1 helps localise cytohesins to the plasma membrane, resulting in a higher ARF activation with increased PIP_2 levels, which facilitates the recruitment of IRS1 and hence reinforces the insulin signal. It remains elusive, how CNK1 is directed to the cell membrane upon insulin stimulation. One possible mechanism is lysine acetylation within its PH domain as recently shown (Fischer *et al.* 2017). Stimulation with EGF as well as IGF enhanced CNK1 acetylation by CBP via RAS/RAF/MEK/ERK signalling which reinforces ERK signalling and in turn again increases the amount of acetylated CNK1 (Fischer *et al.* 2017).

5 Materials and Methods

5.1 Material

5.1.1 Equipment

Analytical balance CPA324S	Sartorius
Anion exchange column HiTrap DEAE FF	GE Healthcare
Autoclave VX-150	Systec
Balance BL1500S	Sartorius
Block heater	Stuart Scientific
Centrifuge 5427 R	Eppendorf
Centrifuge 5804 R	Eppendorf
Cooling cabinet Unichromat 1500 “Pro”	Uniequip
Desalting column HiPrep™ 26/10	GE Healthcare
DLS cuvette ZEN2112 ultra low volume	Malvern Instruments
DLS equipment Zetasizer Nano S	Malvern Instruments
FPLC, ÄKTA	GE Healthcare
French press and pressure cell FA-032	Thermo Scientific
Gastight syringes, 50 µL, 500 µL, 1000 µL	Hamilton
High-performance centrifuge J-26S XP with rotors JLA-8.1000 and JA-25.50	Beckman coulter
HPLC, Agilent 1100	Agilent Technologies
HPLC column MultoHigh®-Bio-200-C18 5 µ	CS-Chromatographie Service GmbH
Imaging System Odyssey	LI-COR Biotechnology
Incubator Heratherm	Thermo Scientific
Incubator Innova 40R	New Brunswick
Incubator Multitron Pro	Infors HT
ITC iTC200 MicroCalorimeter	Microcal
Liposome mini extruder	Avanti Polar Lipids
Magnetic stirrer IKAMAG® RCT	IKA
Mass spectrometer esquire HCT	Bruker
Microwave	Bosch
MST instrument Monolith NT.115	NanoTemper Technologies
Overhead tumbler DTR-30	Grant-bio
pH meter	Mettler Toledo
Pipette controller accu-jet® pro	Brand GmbH & Co KG
Pipettes Research (plus)	Eppendorf
Plate reader Infinite M1000 Pro	Tecan
Power supply for electrophoresis E802	Consort
Rotary evaporator Laborota 4000-efficient	Heidolph instruments
SDS-PAGE equipment and chambers	BioRad
SEC column HiLoad 16/600 Superdex 200 pg	GE Healthcare
SEC column HiLoad 16/600 Superdex 75 pg	GE Healthcare
SEC column Superdex 200 10/300 GL	GE Healthcare
Semi dry blotting chamber Pegasus	Phase GmbH
Spectrophotometer NanoDrop 2000c	Thermo Scientific
Thermomixer comfort	Eppendorf

Ultracentrifuge Optima™ MAX-XP with rotor TLA-100	Beckman coulter
Ultrasound bath Sonorex Super 10P	Bandelin
UV light source, MiniBIS	DNR Bio Imaging Systems
Vertical shaker KS 501 digital	IKA
Vortex 4 basic	IKA
Water bath	GFL
Water system MicroPure UV/UF	Thermo Scientific

5.1.2 Chemicals and reagents

4-(2-aminoethyl)benzenesulfonyl fluoride (AEBSF)	Serva
Acetic acid, p. a.	Roth
Acetone, p. a.	Roth
Acetonitrile, LC-MS grade	Roth
Acrylamide-Bisacrylamide solution (37.5:1)	Roth
Adenosine 5′-triphosphate (ATP)	AppliChem
Agar Agar	Roth
Ammonium persulphate (APS), p. a.	Roth
Ammoniumsulphate, p. a.	Roth
Ampicillin, ≥ 99 %	Roth
β-mercaptoethanol, p. a.	Roth
Bestatin	Serva
Bromophenol blue	Merck
BSA fraction V	PAN Biotech
BSA, fatty acid free	Roth
Chloramphenicol	Sigma
Chloroform, HPLC grade	Roth
Coomassie Blue G	Serva
Dimethylformamide (DMF), ≥ 99.5 %	Roth
Dimethylsulphoxide (DMSO), ACS	Acros organics
Dithiothreitol (DTT), p. a.	Roth
E-64	Serva
Ethanol, HPLC grade	Roth
Ethylendiaminetetraacetic acid (EDTA), p. a.	AppliChem
Ethylene glycol bis(β-aminoethyl)-ether) N,N,N',N' tetraacetic acid (EGTA), p. a.	Roth
Formic acid, LC-MS grade	Roth
Gel filtration standard	BioRad
Glycerol, Ph. Eur.	Roth
Glycine, p. a.	Roth
Guanosine 5′-diphosphate (GDP), ≥ 96 %	Sigma
Guanosine 5′-triphosphate (GTP), ≥ 95 %	Sigma
HEPES, p. a.	Roth
Hydrochloric acid, Ph. Eur.	VWR Chemicals
Imidazole, ≥ 99 %	Merck
Isopropyl β-D-1-thiogalactopyranoside (IPTG)	Carbolution

Isopropanol, p. a.	Roth
IZIT dye	Hampton Research
Kanamycin, > 750 I. U./mg	Roth
L-Glutathione, reduced (GSH)	AppliChem
LB medium Lennox	Roth
Magnesium chloride, p. a.	Fluka
Maltose, ≥ 99 %	Sigma
Mant-GDP, ≥ 95 %	Jena Bioscience
Mant-GTP, ≥ 95 %	Jena Bioscience
Methanol, LC-MS grade	Roth
Myristoyl-Coenzyme A (Myristoyl-CoA), ≥ 95 %	Sigma
Nalidixic acid, ≥ 99 %	Roth
N,N,N',N'-Tetramethylendiamine (TEMED)	Roth
NHS-Fluorescein	Thermo Scientific
PAGE Ruler Prestained Plus	Thermo Scientific
Phosphoramidon	Serva
Potassium acetate, p. a.	Roth
Potassium hydroxide, p. a.	Roth
Sodium acetate, p. a.	Roth
Sodium chloride, p. a.	Roth
Sodium dodecyl sulphate (SDS), p. a.	AppliChem
Sodium hydroxide, p. a.	Roth
Sodium myristate, ≥ 99 %	Sigma
Sucrose, ≥ 99.5 %	Sigma
Sulfo-SBED label transfer reagent	Thermo Scientific
Thimerosal	AppliChem
Tris(2-carboxyethyl)phosphine (TCEP), ≥ 98 %	Roth
Tris(hydroxymethyl)aminomethane (TRIS), ≥ 99.9 %	Roth
Triton X-100	AppliChem
Tween 20, Ph. Eur.	AppliChem

5.1.3 Consumables

Amylose resin #E8021L	New England Biolabs
Blotting paper	Macherey-Nagel
Capillaries for MST, standard treated	NanoTemper Technologies
Centrifugation tubes (15 mL and 50 mL)	Sarstedt
Columns for affinity purification, Protino®, 35 mL, Ø 21.7 mm	Macherey-Nagel
Concentrator Vivaspin Turbo 15	Sartorius
Concentrator Vivaspin 15 R 2000 MWCO HY	Sartorius
Desalting columns NAP-5	GE Healthcare
Dialysis units, Slide-A-Lyzer® MINI, 10K	Thermo Scientific
Dialysis membrane, 6-8 kDa	Spectra/Por
Disposable cuvettes	Roth
Gastight syringes	Hamilton
Glutathione agarose 4B, Protino ®	Macherey-Nagel

Glutathione sepharose 4B resin	GE Healthcare
HaloLink™ resin	Promega
Liposome membrane Nucleopore Track-Etch-Membrane 0.1 µm	Whatman
Liposome membrane filter support	Whatman
Membrane filters ME24	GE Healthcare
Multiwell assay plate 96 well half area non-binding surface 3993	Corning
Multiwell assy plate 96 well transparent round bottom REF 82.1582	Sarstedt
Ni-NTA agarose, Protino®	Macherey-Nagel
Nitrocellulose membranes	GE Healthcare
Petri dishes #391-0455	VWR
Pipette tips	Sarstedt
Reaction tubes (1.5 mL, 2 mL, 15 mL, 50 mL)	Sarstedt
Reaction tubes, protein LoBind	Eppendorf
Serological pipettes (5-50 mL)	Sarstedt
Sf-900 III SFM medium	ThermoFisher Scientific
Syringes Discardit™	BD
Syringe filters Rotilabo® 0.22 µm	Roth
Ultracentrifuge centifuge tubes 7 x 21 mm thickwall polycarbonate, 230 µL	Beckman coulter

5.1.4 Antibodies

Antibody	Species	Dilution	Manufacturer, number
Phospho-Tyr	Mouse	1:5000	Santa Cruz sc7020
Insulin receptor pY1162/1163	Rabbit	1:1000	CellSignaling #3024
ARNO	Mouse	1:1000	Abnova #H00009266-MO2
CNK1	Mouse	1:500	BD 611734
IR-Dye Streptavidin 800 CW (no antibody)	–	1:10000	LI-COR 926-32230
Goat-anti-mouse DyLight 800	Goat	1:15000	CellSignaling #5257
Donkey-anti-rabbit 800 CW	Donkey	1:20000	LI-COR 926-32213

5.1.5 Phospholipids

Phospholipid	Origin	Manufacturer, number
L-α-Phosphatidylethanolamine (PE)	Liver, bovine	Avanti 840026P
L-α-Phosphatidylserine (PS)	Brain, porcine	Avanti 840032P
L-α-Phosphatidylinositol-4,5-bisphosphate (PIP_2)	Brain, porcine	Avanti 840046P
L-α-Phosphatidylcholine (PC)	Egg, chicken	Sigma P2772-1G
1,2-dioleoyl-*sn*-glycero-3-[(N-(5-amino-1-carboxypentyl)iminodiacetic acid)succinyl] nickel salt (DGS-NTA(Ni))	Synthetic	Avanti 790404C

5.1.6 *E. coli* strains and Sf9 cells

Strain	Genotype	Supplier
Escherichia coli BL21 (DE3)	*E. coli* B F– *dcm ompT hsdS*(r_B–m_B–) *gal* λ(DE3)	Thermo Fisher
Escherichia coli BL21 (DE3) RIL	*E. coli* B F– *dcm ompT hsdS*(r_B–m_B–) *gal* λ(DE3) Hte [argU ileY leuW Cam^r]	Agilent
Spodoptera frugiperda Sf9	IPLB-Sf-21-AE derivative	Thermo Fisher

5.1.7 Plasmids and constructs

Construct	N-terminal Affinity tag	Vector manufacturer
pFastBac1-HT-IR-ICD	6 x His	Thermo Fisher
pFastBac1-HT-IR-KC	6 x His	Thermo Fisher
pASK-IBA101-HT-ARNO	6 x His	IBA GmbH
pASK-IBA101-HT-ARNOdpbr	6 x His	IBA GmbH
pET28-HT-ARNO-GS2-PH	6 x His	Novagen
pET28-HT-ARNO-Sec7	6 x His	Novagen
pASK-IBA101-HT-ARNO-cc-Sec7	6 x His	IBA GmbH
pACEBac1-HT-CNK1	6 x His	ATG biosynthetics
pACEBac1-HT-CNK1$_{K414Q}$	6 x His	ATG biosynthetics
pACEBac1-HT-CNK1dcc	6 x His	ATG biosynthetics
pET15-Nd17ARF1	6 x His	Novagen
pET52-ARF6	6 x His (C-terminal)	Novagen
pET28-HT-hNMT	6 x His	Novagen
pMON5840-ARF1wt	–	Prof Felix Wieland
pHV738 (hNMT, MetAP)	–	Prof Richard A. Kahn
pGEX6P-GST	GST	GE Healthcare
pACEBac1-GST-IR-ICD	GST	ATG biosynthetics/ GE Healthcare
pGEX6P-ARNO	GST	GE Healthcare
pGEX6P-ARNOdcc	GST	GE Healthcare
pGEX6P-ARNOcc	GST	GE Healthcare
pET28-HT-HaTh	Halo	Novagen/Promega
pET28-HT-HaTh-ARNO	Halo	Novagen/Promega
pET28-MBPT-IR-CT	MBP	Novagen
pET28-MBPT-CNK1-cc	MBP	Novagen

5.2 Methods

5.2.1 Protein concentration determination

Protein concentrations were determined by applying the Beer-Lambert law, which makes use of the absorbance of ultraviolet radiation (280 nm) by certain amino acids. The equation

$$A_{280} = \log\frac{I_0}{I} = \varepsilon_{280} \times l \times c$$

links the absorbance at 280 nm (A_{280}, dimensionless) with the molar extinction coefficient (ε_{280}, $M^{-1} \times cm^{-1}$), the path length (l, cm) and the concentration (c, M). This corresponds to the log of the initial light intensity (I_0) divided by the light intensity after sample penetration (I). The theoretical molar extinction coefficients were determined via the web tool ProtParam by ExPASy (http://web.expasy.org/protparam/) based on the number of tryptophans and tyrosines in the amino acid sequence, which absorb ultraviolet light by their delocalised π electron system (Walker 2005). The absorbance measurements were performed in triplicates on the NanoDrop spectrophotometer using 2 µL samples.

5.2.2 SDS-PAGE analysis

SDS polyacrylamide gel electrophoresis (SDS-PAGE) was used to evaluate the approximate protein molecular weight and purity due to the migration behaviour of the denatured protein in an electrical field (Laemmli 1970). The SDS molecules convey a uniform charge to the proteins leading to a separation according to the molecular weight. The denaturation is achieved by the detergent SDS, the reducing agent DTT and exposing the sample to 95 °C for 5 min prior to electrophoresis. In order to estimate the molecular weight, the PAGE Ruler Prestained Plus standard was used. Electrophoresis was performed in running buffer for 50 min at 200 V using a polyacrylamide gel containing 10 %, 12.5 % or 15 % acrylamide. The gels were stained for at least 30 min in Coomassie blue staining solution and subsequently destained with 10 % acetic acid, which was heated in the microwave (adapted from Merril 1990). The gels were imaged using the LI-COR Odyssey scanner, 700 nm channel. In case only specific proteins ought to be visualised, western blotting and immunodetection (chapter 5.2.3) were performed instead of the Coomassie staining procedure. The required buffers for gel preparation, sample preparation and staining/destaining are listed below.

4 x Stacking gel buffer	4 x Separating gel buffer
0.5 M TRIS	1.5 M TRIS
14 mM SDS	14 mM SDS
pH 6.8	pH 8.8

5 x Running buffer

125 mM TRIS
960 mM glycine
17 mM SDS
pH 8.2 (do not titrate)

6 x SDS loading buffer

1 M TRIS, pH 6.8
30 % (v/v) glycerol
15 % (w/v) SDS
600 mM DTT
0.01 % (w/v) bromophenol blue

Staining solution

30 % (v/v) methanol
10 % (v/v) acetic acid
0.1 % (w/v) Coomassie blue G

Destaining solution

10 % (v/v) acetic acid

Tab. 5-1: Preparation of one polyacrylamide gel.

	Separating Gel			Stacking Gel
Percentage	10 %	12.5 %	15 %	4 %
30 % Acrylamide	1667 µL	2083 µL	2500 µL	213 µL
Water	2045 µL	1629 µL	1212 µL	975 µL
4 x Separating buffer	1250 µL			-
4 x Stacking buffer	-			400 µL
TEMED	8 µL			2 µL
APS	30 µL			10.4 µL

5.2.3 Western blotting and immunodetection

Visualisation of specific proteins was achieved by first resolving proteins via SDS-PAGE (chapter 5.2.2), transferring them onto a nitrocellulose membrane and subsequent detection with specific antibodies. For the transfer, the semi dry approach adapted from Kyhse-Andersen was performed (Kyhse-Andersen 1984). The gel and the nitrocellulose membrane were shortly equilibrated in cathode buffer and anode buffer II respectively. Gel and membrane were then assembled between three pieces of Whatman paper soaked in cathode buffer facing the cathode side and two pieces of Whatman paper soaked in anode buffer II plus one piece of Whatman paper soaked in anode buffer I facing the anode side. In order to transfer the proteins to the membrane, a current of 2 mA/cm^2 of gel was applied for 45 min.

After the transfer, unspecific binding sites on the membrane were blocked for 1 h using TBST + 5 % (w/v) BSA while shaking. The primary antibody was incubated in the required dilution (chapter 5.1.4) for 2 h at room temperature (RT) or overnight at 4 °C. The blot was

rinsed three times with TBST for 5 min and then incubated with the fluorescently labelled secondary antibody for 1 h at RT. All antibodies were diluted in TBST + 5 % (w/v) BSA. The blot was rinsed again three times for 5 min with TBST and imaged using the LI-COR Odyssey scanner. Since the streptavidin was directly labelled with a fluorescence tag, the blot was incubated for 1 h with the streptavidin dilution after blocking, washed three times with TBST and subsequently imaged.

Anode buffer I
- 300 mM TRIS
- pH 10.4

Anode buffer II
- 25 mM TRIS
- pH 10.4

Cathode buffer
- 25 mM TRIS
- 40 mM glycine
- pH 9.4

TBST
- 20 mM TRIS
- 136 mM NaCl
- 0.1 % (v/v) Tween 20
- pH 7.6

5.2.4 Protein production

E. coli BL21 (DE3) cells or *E. coli* BL21 (DE3) RIL cells conveying additional tRNAs for arginine, isoleucine and leucine (chapter 5.1.6) were transformed with the respective expression vector providing kanamycin or ampicillin resistance by heat shock transformation (adapted from Hanahan 1983). Therefore, 25 µL of the competent cells were mixed with 10-100 ng of the construct and incubated on ice for 15 min. A 45 sec heat shock at 42 °C was applied and the cells were chilled on ice for another 2 min. 500 µL of LB medium was added and the cells were allowed to grow for 60 min at 37 °C with 350 rpm shaking. The cells were pelleted by centrifugation at 2700 xg for 2 min, resuspended in 100 µL LB and then spread on a selective plate containing 50 µg/mL kanamycin or 100 µg/mL ampicillin and incubated overnight at 37 °C. In case BL21 (DE3) RIL cells were used (see tab. 5-2), the selective plate as well as the starter culture were additionally supplemented with 50 µg/mL chloramphenicol. To set up a starter culture, one colony from the selective plate was transferred into a 250 mL baffled flask filled with 50 mL LB medium containing the required antibiotics in the same concentration as previously stated and incubated overnight in an incubation shaker at 37 °C and 160 rpm.

For protein production, 2 L LB cultures containing the abovementioned antibiotics but no chloramphenicol were inoculated in 5 L baffled flasks with 50 mL of the overnight culture. The overnight cultures were also used to prepare glycerol stocks for easier re-expression. Therefore, 500 µL of the bacterial culture was mixed with 500 µL 50 % glycerol and stored at -80 °C. The cells were grown at 37 °C with 110 rpm shaking until OD_{600} reached ~0.5

and gene expression was induced by addition of 0.5 mM isopropyl β-D-1-thiogalacto-pyranoside (IPTG). Cells were either allowed to grow at 37 °C for 5 h or at 20 °C overnight (tab 5-2), in which case the cells were cooled down for 30 min at 4 °C prior to induction. After expression, the cells were centrifuged at 4000 xg (rotor JLA-8.100) for 20 min, the supernatant was discarded and the cell pellet was stored at -80 °C until further processing.

Proteins unsuited for production in *E. coli* were produced in Sf9 cells using the Bac-to-Bac vector system by Thermo Scientific (tab. 5-3). Expression was performed by Yvonne Aschenbach. Approximately 2.5 L Sf-900 III SFM culture medium with 2 million cells/mL were infected 1:1000 with the V1 virus stock and incubated for 3 days at 27 °C with 80 rpm shaking. The cells were harvested at 1200 xg (rotor JLA-8.100) for 12 min, the supernatant was discarded and the cell pellet was stored at -80 °C until further processing.

Tab. 5-2: Bacterial strains and expression conditions used for different constructs. ARNO-Sec7 and NΔ17ARF1 were expressed and purified by Max Yin and Volkmar Fieberg, respectively.

Construct	*E. coli* strain	Temperature, Duration	Antibiotic
pASK-IBA101-HT-ARNO	BL21 (DE3) RIL	20 °C, o/n	Ampicillin
pASK-IBA101-HT-ARNOdpbr	BL21 (DE3) RIL	20 °C, o/n	Ampicillin
pET28-HT-ARNO-GS2-PH	BL21 (DE3)	20 °C, o/n	Kanamycin
pET28-HT-ARNO-Sec7	BL21 (DE3)	37 °C, 5 h	Kanamycin
pASK-IBA101-HT-ARNO-cc-Sec7	BL21 (DE3)	20 °C, o/n	Ampicillin
pET15-Nd17ARF1	BL21 (DE3)	37 °C, 5 h	Ampicillin
pET52-ARF6	BL21 (DE3)	37 °C, 5 h	Ampicillin
pET28-HT-hNMT	BL21 (DE3)	20 °C, o/n	Kanamycin
pGEX6P-GST	BL21 (DE3)	20 °C, o/n	Ampicillin
pGEX6P-ARNO	BL21 (DE3)	20 °C, o/n	Ampicillin
pGEX6P-ARNOdcc	BL21 (DE3)	20 °C, o/n	Ampicillin
pGEX6P-ARNOcc	BL21 (DE3)	20 °C, o/n	Ampicillin
pET28-HT-HaTh	BL21 (DE3)	20 °C, o/n	Kanamycin
pET28-HT-HaTh-ARNO	BL21 (DE3)	20 °C, o/n	Kanamycin
pET28-MBPT-IR-CT	BL21 (DE3) RIL	20 °C, o/n	Kanamycin
pET28-MBPT-CNK1-cc	BL21 (DE3) RIL	20 °C, o/n	Kanamycin

Tab. 5-3: Constructs expressed in Sf9 cells. Expression performed by Yvonne Aschenbach.

Construct	*Expression host*	Expression conditions
pFastBac1-HT-IR-ICD	Sf9 cells	3 days, 27 °C
pFastBac1-HT-IR-KC	Sf9 cells	3 days, 27 °C
pACEBac1-HT-CNK1	Sf9 cells	3 days, 27 °C
pACEBac1-HT-CNK1$_{K414Q}$	Sf9 cells	3 days, 27 °C
pACEBac1-HT-CNK1dcc	Sf9 cells	3 days, 27 °C
pACEBac1-GST-IR-ICD	Sf9 cells	3 days, 27 °C

5.2.5 Protein purification

After heterologous expression (chapter 5.2.4), the majority of proteins used in this study were prepared by affinity purification followed by polishing steps such as SEC. Since the purification procedure of myr-ARF1 as well as myr-ARF6 deviated significantly from the other proteins, their purification is described separately in chapter 5.2.6 and chapter 5.2.7. For the remaining proteins, the purification is presented grouped after the respective affinity tag.

Purification of hexahistidine-tagged proteins

Fusing a hexahistidine-tag to proteins is one of the most widely applied techniques to obtain proteins for biomedical research. The histidine-tag forms a complex with immobilised nickel ions which can be competed with the histidine analogue imidazole to elute the target protein (Hochuli *et al.* 1987, Hochuli *et al.* 1988). This form of chromatography is also referred to as immobilised metal ion affinity chromatography (IMAC).

All purification steps were performed with cooled buffers at 4 °C or on ice. The cells obtained from 2 L LB medium expression (chapter 5.2.4) were resuspended in 20 mL lysis buffer + 1 x protease inhibitor mix. For proteins expressed in Sf9 cells, 30 mL lysis buffer + 1 x protease inhibitor mix were used per 2 L of cell culture. The completely resuspended cells were disrupted by passing them through a French press for two cycles with a maximum pressure of 18000 PSI (1240 bar). The lysate was cleared by centrifugation at 48000 xg for 30 min, added to 2.5 mL nickel nitrilotriacetic acid (Ni-NTA) beads previously equilibrated in lysis buffer and incubated for 1 h while shaking slightly. The suspension was then applied to Protino® columns equipped with a polymeric frit. The beads were washed with 15 mL lysis buffer and the target proteins were eluted with 12.5 mL lysis buffer + 230 mM imidazole.

In cases where the affinity tag was fused to the protein with a tobacco etch virus (TEV) protease-cleavable linker and should be removed, TEV protease, prepared by Volkmar Fieberg, was added in a 1:50 molar ratio (tab. 5-4). The protein was then transferred into dialysis tubing with a cut-off of 6-8 kDa and the protein was dialysed against 2 L dialysis buffer overnight while slowly stirring in order to remove the imidazole. To separate the tag and Ni-NTA-binding impurities from the digested target proteins, a re-binding affinity chromatography step was performed. Therefore, the sample was centrifuged at 3200 xg to remove aggregates and then mixed with 2.5 mL Ni-NTA beads, which were equilibrated in dialysis buffer, for 1 h. The samples were then applied to Protino® columns. The flow through fraction (sample + 5 mL wash with dialysis buffer), a 10 mL wash fraction with dialysis buffer + 20 mM imidazole and a 10 mL eluate fraction with dialysis buffer + 250 mM imidazole were collected and the target protein was recovered either from the flow through or the wash fraction, while the impurities were found in the eluate fraction.

The eluate fraction of the IMAC or the flow through/wash fraction of the reverse IMAC, respectively, were concentrated using Vivaspin turbo spin concentrators with appropriate molecular weight cut-off. 2-5 mL of the concentrated samples were then filtered through a 0.22 µm filter and applied to either a HiLoad™ 16/600 Superdex 200 pg or a HiLoad™ 16/600 Superdex 75 pg SEC column depending on the protein size. The column was previously equilibrated in storage buffer. Peak fractions were collected, concentrated with spin concentrators, flash frozen in liquid nitrogen and stored at -80 °C.

Tab. 5-4: Purification of hexahistidine-tagged proteins. ARNO-Sec7 and NΔ17ARF1 were purified by Max Yin and Volkmar Fieberg, respectively.

Protein	Tag cleaved?	Cleavage site	SEC column	Concentrator
ARNO	yes	TEV	S200	10 kDa
ARNOΔpbr	yes	TEV	S200	10 kDa
ARNO-PH	yes	TEV	S75	5 kDa
ARNO-Sec7	yes	TEV	S75	5 kDa
ARNO-cc-Sec7	yes	TEV	S200	10 kDa
NΔ17ARF1	no	Thrombin	No SEC	10 kDa
ARF6	no	None	S75	10 kDa
NMT	no	TEV	S200	10 kDa
IR-ICD	yes	TEV	S200	10 kDa
IR-KC	yes	TEV	S200	10 kDa
CNK1	no	TEV	S200	10 kDa
$CNK1_{K414Q}$	no	TEV	S200	10 kDa
CNK1Δcc	no	TEV	S200	10 kDa

Lysis buffer

50 mM HEPES
300 mM NaCl
3 mM $MgCl_2$
20 mM imidazole
0.5 mM TCEP
pH 7.5 (pH 8.0 for ARF6)

Dialysis buffer

20 mM HEPES
100 mM NaCl
3 mM $MgCl_2$
0.5 mM TCEP
pH 7.2

Storage buffer

20 mM HEPES
100 mM NaCl
3 mM $MgCl_2$
pH 7.2 (pH 8.0 for ARF6)

100 x protease inhibitor

1 mM AEBSF
5 µM E-64
5 µM Bestatin
5 µM Phosphoramidon

Purification of GST-tagged proteins

Another commonly used affinity tag, which is significantly larger than the hexahistidine-tag, is the GST tag (Smith and Johnson 1988). In this study, it was usually not cleaved, since it was subsequently exploited for pull-down assays (chapter 5.2.12). However, ARNOΔcc was purified in its GST-fusion form and enzymatically cleaved.

All purification steps were performed with cooled buffers at 4 °C or on ice. The cells obtained by expression in 2 L LB medium (chapter 5.2.4) were resuspended in 20 mL lysis buffer + 1 x protease inhibitor mix. For GST-IR-ICD expressed in Sf9 cells, 30 mL lysis buffer + 1 x protease inhibitor mix were used per 2 L of cell culture. The completely resuspended cells were disrupted by passing them through a French press for two cycles with a maximum pressure of 18000 PSI (1240 bar). The lysate was subsequently cleared by centrifugation at 48000 xg for 30 min and then added to 6 mL Protino® glutathione agarose 4B beads, which were previously equilibrated in lysis buffer and incubated for 1 h while shaking slightly. The suspension was then applied to Protino® columns equipped with a polymeric frit. The beads were washed with 100 mL lysis buffer and the target proteins were eluted with 20 mL lysis buffer + 20 mM GSH, pH readjusted to 7.2.

For ARNOΔcc, PreScission protease provided by Prof Matthias Geyer was added in a 1:50 molar ratio to half of the sample (tab. 5-5). The protein was then transferred into dialysis tubing with a cut-off of 6-8 kDa and the protein was dialysed against 2 L dialysis buffer over night while slowly stirring in order to reduce the GSH concentration. To separate the tag and impurities from the digested ARNOΔcc, a re-binding affinity chromatography step was performed. Therefore, the sample was centrifuged at 3200 xg to remove aggregates and then mixed with 3 mL Protino® glutathione agarose 4B beads, which were equilibrated in dialysis buffer, for 1 h. The samples were then applied to Protino® columns. The flow through fraction (sample + 5 mL wash with dialysis buffer), a 10 mL wash fraction with storage buffer and a 10 mL eluate fraction with storage buffer + 20 mM GSH were collected and the protein was recovered from the flow through fraction, while the impurities and GST were found in the eluate fraction.

The eluate fraction of the affinity purification or the flow through of the reverse affinity purification in case for ARNOΔcc, respectively, were concentrated using Vivaspin turbo spin concentrators with appropriate molecular weight cut-off. 2-5 mL of the concentrated samples were then filtered through a 0.22 µm filter and applied to a HiLoad™ 16/600 Superdex 200 pg SEC column previously equilibrated in storage buffer. Peak fractions were collected, concentrated with spin concentrators, flash frozen in liquid nitrogen and stored at -80 °C.

Tab. 5-5: Purification of GST-tagged proteins. ARNOΔcc was purified as GST-fusion and without affinity tag.

Protein	Tag cleaved?	Cleavage site	SEC column	Concentrator
GST	no	PreScission	S200	10 kDa
GST-IR-ICD	no	PreScission	S200	10 kDa
GST-ARNO	no	PreScission	S200	30 kDa
GST-ARNOΔcc	no + yes	PreScission	S200	10 kDa
GST-ARNO-cc	no	PreScission	S200	10 kDa

Lysis buffer

50 mM HEPES
300 mM NaCl
3 mM $MgCl_2$
0.5 mM TCEP
pH 7.5

Dialysis buffer

20 mM HEPES
100 mM NaCl
3 mM $MgCl_2$
0.5 mM TCEP
pH 7.2

Storage buffer

20 mM HEPES
100 mM NaCl
3 mM $MgCl_2$
pH 7.2

100 x protease inhibitor

1 mM AEBSF
5 µM E-64
5 µM Bestatin
5 µM Phosphoramidon

Purification of Halo-tagged proteins

Since the HaloTag® binds covalently to its ligand, it cannot be used for multiple interaction cycles. Therefore, the Halo-tagged proteins were furthermore fused to an N-terminal hexahistidine-tag, which could be cleaved by TEV protease. The Halo-tagged proteins were hence purified as described for hexahistidine-tagged proteins.

Tab. 5-6: Purification of hexahistidine-tagged proteins which also possess a HaloTag®.

Protein	His Tag cleaved?	Cleavage site	SEC column	Concentrator
Halo-ARNO	yes	TEV	S200	30 kDa
Halo	yes	TEV	S75	10 kDa

Purification of MBP-tagged proteins

The maltose-binding protein (MBP) can be used as an affinity tag since it binds to (cross-linked) amylose and enhances gene expression as well as solubility (Bedouelle and Duplay 1988, Di Guana *et al.* 1988, Nallamsetty and Waugh 2006).

Like the previously described purifications, all steps were performed with cooled buffers at 4 °C or on ice. The cells obtained by expression in 2 L LB medium (chapter 5.2.4) were resuspended in 20 mL lysis buffer + 1 x protease inhibitor mix. The completely resuspended cells were disrupted by passing them through a French press for two cycles with a maximum pressure of 18000 PSI (1240 bar). The lysate was subsequently cleared by centrifugation at 48000 xg for 30 min, added to 7.5 mL amylose beads, which were previously equilibrated in lysis buffer and incubated for 1 h while shaking slightly. The suspension was then applied to Protino® columns equipped with a polymeric frit. The beads were washed with 25 mL lysis buffer and the target proteins were eluted with 25 mL lysis buffer + 20 mM maltose.

All MBP fusion proteins also possessed a TEV protease cleavage site. CNK1-cc was purified as MBP-fusion and as the isolated domain. MBP-IR-CT was cleaved and the resulting MBP as well as the IR-CT fragment were used for subsequent experiments.

In case the construct was cleaved, TEV protease, prepared by Volkmar Fieberg, was added in a 1:50 molar ratio (tab. 5-7) and the samples were incubated with rotation overnight without the need of dialysis. No re-binding steps were performed since the molecular weight difference between MBP on the one hand and CNK1-cc and IR-CT on the other hand were large enough to separate the proteins via SEC.

The concentrated amylose purification eluate fraction or the digested sample (previously concentrated to reduce the volume for column application) was centrifuged at 3200 xg for 10 min. A maximum of 5 mL of the concentrated samples was then filtered through a 0.22 µm filter and applied to a HiLoad™ 16/600 Superdex 75 pg SEC column previously equilibrated in storage buffer. Peak fractions were collected, concentrated with spin concentrators, flash frozen in liquid nitrogen and stored at -80 °C. For the cleaved IR-CT sample however, an additional purification step was introduced to enhance purity. The SEC peak was applied to a 10 kDa spin concentrator but in contrast to a conventional concentration, the flow through was recovered, which was then devoid of any MBP contamination. The flow through was then further concentrated using a 2 kDa concentrator.

Tab. 5-7: Purification of MBP-tagged proteins.

Protein	Tag cleaved?	Cleavage site	SEC column	Concentrator
MBP-CNK1-cc	no + yes	TEV	S75	10 kDa/no concentration for cleaved protein
MBP-IR-CT	yes	TEV	S75	2 kDa
MBP	yes (MBP was recovered from MBP-IR-CT cleavage)	TEV	S75	10 kDa

Lysis buffer

50 mM HEPES
300 mM NaCl
3 mM $MgCl_2$
0.5 mM TCEP
pH 7.5

Storage buffer

20 mM HEPES
100 mM NaCl
3 mM $MgCl_2$
pH 7.2

100 x protease inhibitor

1 mM AEBSF
5 µM E-64
5 µM Bestatin
5 µM Phosphoramidon

5.2.6 Purification of myr-ARF1

Myr-ARF1 was prepared following the general protocols of Franco *et al.* 1995 and Ha *et al.* 2005, where ARFs are co-expressed with an N-myristoyltransferase (NMT) in *E. coli* in presence of sodium myristate.

E. coli BL21 (DE3) cells were transformed with the pMON5840-ARF1wt (non-tagged ARF1) and the pHV738 plasmid, which encodes the sequences of the human NMT1 under control of the IPTG inducible tac promotor as well as the *E. coli* methionine aminopeptidase (MetAP) under control of its endogenous promotor (Van Valkenburgh and Kahn 2002).

Starter and main culture contained 50 µg/mL kanamycin and 100 µg/mL ampicillin. 2 L LB was inoculated in 5 L baffled flasks with 50 mL of the overnight culture. The cells were grown at 37 °C with 110 rpm shaking until OD_{600} reached ~0.6. Then, 50 µM myristate bound to 6 µM fatty acid free BSA was added from a 100 x stock and the temperature was

reduced to 27 °C. After 10 min, NMT expression was induced with 0.5 mM IPTG. After additional 60 min, expression of ARF1 was induced with 30 µg/mL nalidixic acid, which was dissolved as a 30 mg/mL stock in 300 mM NaOH. The cells were grown for 4 h and then harvested at 4000 xg using the Beckman centrifuge. The supernatant was discarded and the cell pellet was stored at -80 °C until further processing.

All subsequent purification steps were performed with cooled buffers at 4 °C or on ice. The cells were resuspended in 20 mL lysis buffer + 1 x protease inhibitor mix + 1 mM GDP. The completely resuspended cells were disrupted by passing them through a French press for two cycles with a maximum pressure of 18000 PSI (1240 bar). The lysate was subsequently cleared by centrifugation at 48000 xg for 30 min.

In order to enrich myristoylated ARF1, the cleared and filtered cell lysate was precipitated at 35 % ammonium sulphate over 45 min using a saturated ammonium sulphate solution while stirring in an ice bath. The solution was left stirring for another 60 min and the precipitate was pelleted for 20 min at 20000 xg. The supernatant was discarded and the precipitated myr-ARF1 was resolubilised in 3 mL rebuffering buffer. The lysate was desalted using the HiPrep™ 26/10 desalting column equilibrated in rebuffering buffer. After centrifugation at 3200 xg for 10 min, the desalted lysate was applied to a 5 mL DEAE FF anion exchange column at 0.5 mL/min, which was previously equilibrated in rebuffering buffer. Myr-ARF1 was eluted with a linear gradient to 100 % elution buffer in 10 column volumes (i.e. 50 mL/100 min). The elution profile shows two major and two minor peaks and myr-ARF1 can be recovered from the first peak.

This peak was pooled, filtered through a 0.22 µm filter and applied to a HiLoad™ 16/600 Superdex 200 pg SEC column previously equilibrated in storage buffer. Peak fractions were collected, concentrated with 10 kDa spin concentrators, flash frozen in liquid nitrogen and stored at -80 °C.

Lysis buffer	Rebuffering buffer
50 mM TRIS	10 mM TRIS
1 mM $MgCl_2$	1 mM $MgCl_2$
1 mM DTT	1 mM DTT
pH 8.0	pH 8.0

Elution buffer

10 mM TRIS
1 M KCl
1 mM $MgCl_2$
1 mM DTT
pH 8.0

Storage buffer

20 mM HEPES
100 mM NaCl
1 mM $MgCl_2$
pH 8.0

100 x protease inhibitor

1 mM AEBSF
5 µM E-64
5 µM Bestatin
5 µM Phosphoramidon

5.2.7 *In vitro* myristoylation of ARF6

The *in vivo* myristoylation approach described for myr-ARF1 (chapter 5.2.6) proves even more difficult for ARF6 since GTP- and GDP-bound ARF6 localise to membranes (Macia *et al.* 2004). Therefore, myr-ARF6 was prepared *in vitro* as described recently (Padovani *et al.* 2013). The non-myristoylated ARF6 and NMT were expressed separately as hexahistidine-tagged fusion proteins (chapter 5.2.5 and chapter 3.5.1).

100 µM ARF6 was mixed with 1 µM NMT in myristoylation buffer. Myristoyl-CoA was added to a final concentration of 160 µM from a 420 µM stock dissolved in 20 mM sodium acetate, 1 % Triton X-100, pH 5.6. The total reaction volume was 1 mL. The myristoylation reaction was allowed to take place at room temperature for 4.5 h. To separate myr-ARF6 from non-myristoylated ARF6, myr-ARF6 was precipitated at 30 % ammonium sulphate, which was added over 30 min while stirring in an ice bath. After another 15 min incubation, the samples were centrifuged for 15 min at 20800 xg and the pellet was resolubilised in 200 µL HKM buffer. The sample was subsequently rebuffered by overnight dialysis against 400 mL HKM buffer and stored in liquid nitrogen. To confirm the myristoylation, the final sample was analysed via LC-MS (chapter 5.2.9).

Myristoylation buffer

20 mM HEPES
100 mM NaCl
1 mM $MgCl_2$
pH 8.0

HKM buffer

50 mM HEPES
120 mM potassium acetate
1 mM $MgCl_2$
2 mM β-mercaptoethanol
pH 7.4

5.2.8 Protein modification with fluorescein and SBED

For MST measurements (chapter 5.2.15) as well as label transfer studies (chapter 5.2.13), the heterologously expressed and purified proteins needed to be covalently modified with fluorescein and Sulfosuccinimidyl-2-[6-(biotinamido)-2-(*p*-azidobenzamido) hexanoamido]ethyl-1,3´-dithiopropionate (Sulfo-SBED), respectively. To couple the molecules to the proteins, both compounds possess groups reactive towards primary amines such as the N-terminus and lysine side chains of the protein.

N-Hydroxysuccinimide-fluorescein (NHS-fluorescein) was dissolved freshly at 10 mM in dimethylformamide (DMF). 50 µM ARNO and 750 µM NHS-fluorescein were mixed in labelling buffer and incubated on ice in the dark for 1.5 h. Unreacted dye was removed by NAP-5 chromatography yielding a protein with approximately 3 fluorescein molecules attached per protein in labelling buffer + 5 % glycerol.

Sulfo-SBED consists of a biotin moiety, a sulfonated N-hydroxysuccinimide (Sulfo-NHS) active ester and a photoactivatable aryl azide (chapter 5.2.13). Sulfo-SBED was freshly dissolved at 50 mM in DMF. 100 µM ARNO and 25 µM IR-ICD were incubated with a three times molar excess of Sulfo-SBED on ice in the dark for 2 h in labelling buffer. The reaction was stopped by the addition of 100 mM TRIS, pH 7.5. To remove unreacted dye as well as TRIS buffer, the labelled proteins were rebuffered in labelling buffer + 5 % glycerol using NAP-5 columns.

Labelling buffer

50 mM HEPES
150 mM NaCl
1 mM $MgCl_2$
0.05 % Triton X-100
pH 8.0

5.2.9 LC-MS analysis

To confirm the myristoylation of ARFs, the intact mass of the modified proteins was determined using an electron spray ionization ion trap mass spectrometer after reversed-phase chromatography (LC-MS). Therefore, the protein of interest was diluted to 2.5 µM in 0.1 % formic acid (buffer A) and a 20 µL sample (50 pmol) was injected onto a MultoHigh®-Bio-200-C18 5 µ column run with the Agilent 1100 HPLC. Chromatography was performed for 3 min in buffer A followed by a 20 min gradient to 100 % buffer B (acetonitrile) which was continued for another 3 min at a flow rate of 0.4 mL/min. The sample was measured with the BRUKER esquire HCT in positive mode. Charge deconvolution allowed for a maximum charge of 50.

5.2.10 Dynamic light scattering

The dynamic light scattering (DLS) technology was employed to determine the size of the prepared liposomes. DLS allows the deduction of the hydrodynamic radius and thus estimation of the particle size by measuring the diffusion velocity due to Brownian motion. Therefore, monochromatic light is shone through a sample and the rate at which the intensity of scattered light fluctuates is measured (Stetefeld *et al.* 2016). For small and hence fast diffusing particles, the detector records different light intensities already after a short time interval. If the molecules are larger however, there is a good correlation for the intensity at a given time and the following situation which is analysed by a digital autocorrelator.

The prepared liposomes (chapter 5.2.18) were diluted 1:100 in storage buffer and measured in the DLS Zetasizer nano Series S. The intensity representation was chosen to show the average of 3 measurements, each consisting of 15 10-sec runs of the same sample.

Storage buffer

50 mM HEPES
120 mM potassium acetate
pH 7.2

5.2.11 Autophosphorylation assay

Activation of the insulin receptor is accompanied by autophosphorylation of three tyrosine residues within the activation loop (Hubbard 1997). Addition of 30 mM $MgCl_2$ leads to receptor aggregation followed by autophosphorylation mimicking the cellular activation (Herrera and Rosen 1986).

For the assay, 525 nM IR-ICD or 525 nM IR-ICD mixed with a tenfold ARNO excess was incubated with 30 mM $MgCl_2$ and the phosphorylation reaction was started by addition of 1 mM ATP. SDS-PAGE samples were taken in a time course and applied to 10 % SDS-PAGE (chapter 5.2.2), transferred to a nitrocellulose membrane via western blot and detected with α-pY or α-pY1162/1163 antibodies (chapter 5.2.3).

Autophosphorylation buffer

50 mM TRIS
150 mM NaCl
0.5 mM TCEP
pH 7.5

5.2.12 Pull-down assay

Pull-down experiments, especially in combination with mass spectrometric analysis, are a powerful tool and enable screening for new or confirmation of putative protein-protein interactions (Brymora *et al.* 2004). A “bait” protein is immobilised on a solid support like functionalised polymeric beads and bound partners are analysed after incubation and washing steps (Einarson *et al.* 2007). Two different types of pull-down assays were performed using either GST- or Halo-fusion proteins to ascertain independence from the used tag.

In the first system, GST-fusion proteins were pulled down using glutathione sepharose beads. Within cells, GST plays a central role in detoxification by catalysing the conjunction of reduced glutathione to xenobiotic substances (Mannervik *et al.* 2005, Combes and Stakelum 1961). GST hence binds to glutathione which can be exploited for protein purification and further biotechnological applications (Smith and Johnson 1988, Perperopoulou *et al.* 2017).

As indicated in the results section, 1 µM or 5 µM GST and GST-fusion proteins and 1 µM, 5 µM or 25 µM interaction partner (total volume 200 µL) were incubated in pull-down buffer with 10 µL glutathione sepharose 4 B beads for 30 min at RT or 3 h at 4 °C. After constant mixing in the overhead tumbler, the beads were washed three times with 500 µL pull-down buffer and pelleted at 500 xg. The proteins were eluted using 200 µL pull-down buffer supplemented with 50 mM reduced GSH to compete the protein-bead interaction. Eppendorf 1.5 mL protein LoBind tubes were used to reduce sticking to the plastic surface. Samples of the input before beads incubation, the supernatant after beads incubation and the eluate were mixed with sample buffer and analysed via SDS-PAGE and stained using Coomassie blue (see chapter 5.2.2).

The HaloTag® is a 34 kDa mutated haloalkane dehalogenase, which covalently binds to a chloroalkane ligand (Zhang *et al.* 2006). In contrast to the reversible GST-GSH interaction, the His272 to Phe mutation within the catalytic triad renders the formed ester bond between the HaloTag® and its ligand unhydrolysable.

5 µM Halo-ARNO or 5 µM Halo protein were mixed with equimolar amounts of interaction partner and 10 µL of HaloLink™ resin in a total volume of 200 µL in pull-down buffer. The samples were incubated for 4 h at 4 °C while mixing in the overhead tumbler. After incubation, the beads were washed three times with 500 µL pull-down buffer and pelleted at 500 xg. The bound proteins were eluted using 50 µL pull-down buffer plus 10 µL 6 x SDS loading buffer (chapter 5.2.2). The Halo fusion protein itself cannot be eluted since it is covalently attached to the beads. Eppendorf 1.5 mL LoBind tubes were used to reduce

sticking to the plastic surface. Samples of the input before beads incubation and the supernatant after beads incubation were mixed with 6 x SDS loading buffer and, together with the eluate sample, analysed via SDS-PAGE/Coomassie stain (see chapter 5.2.2).

Pull-down buffer

20 mM HEPES
100 mM NaCl
3 mM $MgCl_2$
0.15 % Triton X-100
pH 7.2

5.2.13 SBED label transfer

Transient protein-protein interactions can be stabilised by covalent chemical crosslinking which facilitates the characterisation of their interplay (Das and Fox 1979, Arora *et al.* 2017). The trifunctional crosslinking reagent Sulfo-SBED was used to analyse the interaction between ARNO and the IR-ICD (Alley *et al.* 2000). The crosslinker consists of a biotin moiety, a sulfonated N-hydroxysuccinimide (Sulfo-NHS) active ester and a photoactivatable aryl azide (fig. 5-1).

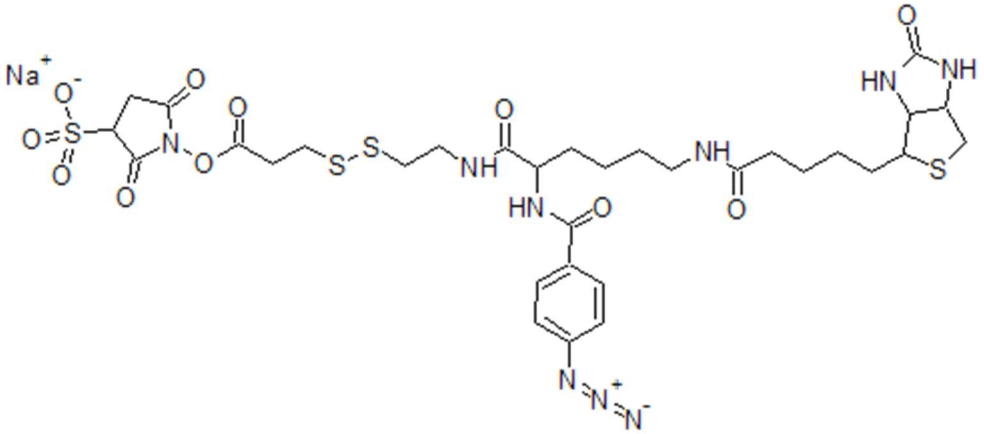

Fig. 5-1: Chemical structure of the trifunctional crosslinking reagent Sulfo-SBED. First, the compound is coupled via its NHS group to primary amines of the first interaction partner. Upon UV irradiation, the aryl azide is activated and reacts with the target protein. Reduction of the disulphide bridge separates the proteins and transfers the biotin moiety to the interaction partner.

As described in chapter 5.2.8, the compound is coupled to primary amines of one of the interacting proteins (here ARNO and IR-ICD) via its NHS group to form a covalent amide bond. For the crosslinking experiment, 250 nM of the SBED-modified proteins were incubated with 1 µM of the interaction partners and irradiated at RT for 3 min with UV light in a transparent 96 well plate in label transfer buffer. The UV light activates the aryl azide group which in turn interacts with diverse functional groups in vicinity. The disulphide bridge was reduced by addition of 6 x SDS loading buffer containing 100 mM DTT as a

final concentration for 15 min, splitting the previously crosslinked partners. Samples pre and post irradiation were separated via SDS-PAGE (chapter 5.2.2), transferred to a nitrocellulose membrane by western blot and detected via fluorescently labelled streptavidin (chapter 5.2.3).

Label transfer buffer

20 mM HEPES
150 mM NaCl
3 mM $MgCl_2$
pH 7.4

5.2.14 Analytical size-exclusion chromatography

Molecular complex formation can be addressed by analytical size-exclusion chromatography (SEC). SEC separates molecules due to their hydrodynamic radius, which is in good accordance with the molecular weight for globular proteins (Hong *et al.* 2012). Small molecules pass through all cavities of the porous beads and possess a correspondingly long retention time while larger molecules do not enter the matrix and elute earlier.

All samples were diluted in SEC buffer which was also used for the SEC runs. 100 µL samples ranging from 7.5 µM to 50 µM (see results) were incubated for 5 min on ice, centrifuged at 20800 xg for 10 min and subjected to a Superdex 200 10/300 GL gel filtration column at a flow rate of 0.4 mL/min. The ÄKTA FPLC chromatography system was used. 500 µL peak fractions were collected and analysed via SDS-PAGE and Coomassie blue staining (chapter 5.2.2).

In order to estimate the molecular weight of the analysed proteins and protein complexes, the BioRad gel filtration standard was run under the same conditions as the samples and the elution profile was recorded. The calibration was performed and evaluated according to Appendix 10 of the GE Size Exclusion Chromatography Principles and Methods handbook (GE 2014). In short, the K_{av} values for all elution maxima of the molecular weight standard within the separation range of the column were determined as:

$$K_{av} = \frac{V_e - V_0}{V_t - V_0}$$

with V_e = elution volume of the standard protein, V_0 = column void volume (approximately 6.7 mL), V_t = total bed volume (24 mL). The K_{av} values were then plotted against the molecular weight of the standard proteins on a logarithmic scale and a calibration curve

was generated by linear regression. The regression curve in turn serves to calculate the molecular weight of test proteins and complexes.

SEC buffer

20 mM HEPES
100 mM NaCl
3 mM $MgCl_2$
pH 7.2

5.2.15 Microscale thermophoresis

One means of quantifying biomolecular interactions is microscale thermophoresis (MST). Two comprehensive review articles summarise the theoretical background as well as applications and served as the basis for this chapter (Jerabek-Willemsen *et al.* 2011, Seidel *et al.* 2013). Thermophoresis refers to the movement of particles in a temperature gradient, which is counterbalanced by mass diffusion. In the standard experimental setup, a fluorescently labelled molecule situated in a glass capillary is heated using an infrared laser at a precise location. Upon heating, the migration of molecules is monitored via a simultaneous fluorescence measurement. The movement is dependent on the size, charge and hydration shell of the molecule (Duhr and Braun 2006). Mathematically, the concentration change can be described as:

$$\frac{c_1}{c_0} = e^{(-S_T \Delta T)}$$

with c_0 = initial concentration, c_1 = hot equilibrium concentration, S_T = Soret coefficient and ΔT = temperature change. It is the Soret coefficient, the thermodiffusion constant divided by the diffusion coefficient, which encompasses the contribution of size, charge and hydration shell of the molecule as delineated in the following formula (Duhr and Braun 2006):

$$S_T = \frac{\overbrace{A}^{\text{size}}}{k\,T}\left(-\underbrace{s_{hyd}}_{\text{hydration shell}} + \frac{\beta \overbrace{\sigma_{eff}^2}^{\text{charge}^2}}{4\varepsilon\varepsilon_0 T} \times \lambda_{DH}\right)$$

with A = particle surface, k = Boltzmann constant, T = temperature, s_{hyd} = hydration entropy, β = factor resulting from temperature derivatives, σ_{eff} = effective surface charge density, ε = dielectric constant, ε_0 = vacuum permittivity and λ_{DH} = Debye length.

To obtain binding data, the fluorescent molecule is mixed with increasing amounts of the interactor in up to 16 capillaries and the fluorescence is monitored before and during infrared laser irradiation (fig. 5-2). Since binding will at least influence one of the factors which determine the thermophoretic behaviour, the affinity can be inferred. Therefore, the ratio F_{norm} of the normalised florescence of the hot equilibrium state F_1 and the normalised initial fluorescence F_0 is calculated and plotted against the logarithmic ligand concentration. The curve is then fitted by using a model derived from the law of mass action:

$$F_{norm} = (1 - x) \times F_{norm}(unbound) + x\, F_{norm}\,(bound)$$

with x = the fraction of labelled molecules bound to their targets.

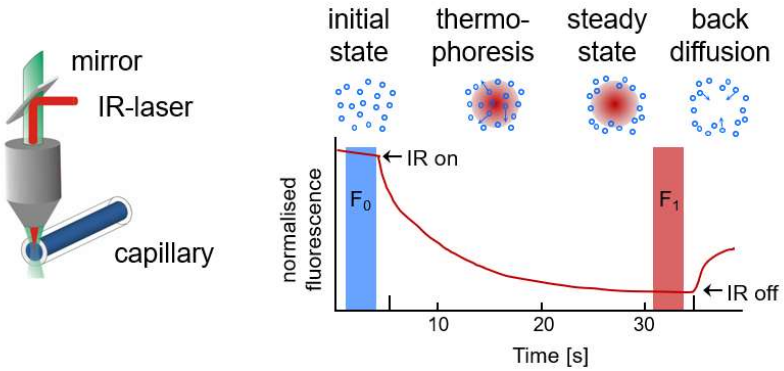

Fig. 5-2: Principle of microscale thermophoresis. The samples in up to 16 capillaries are heated by irradiation with an infrared laser and the fluorescence is measured through a mirror. The fluorescence is recorded, normalised and $F_{norm} = F_1/F_0$ is plotted against the ligand concentration in a logarithmic scale. Adapted from Seidel *et al.* 2013.

For the performed measurements, ARNO was labelled with fluorescein (chapter 5.2.8) and used at 100 nM final concentration. IR-ICD and IR-KC were titrated in 1:2 dilutions ranging from 5 nM to 100 µM. All proteins were prepared and diluted in MST buffer and the measurements were performed using standard treated capillaries from NanoTemper Technologies. Thermophoresis was measured using a Monolith NT.115 instrument at room temperature with 5 s/30 s/5 s laser off/on/off times, respectively. The instrument parameters were set to 40 % LED power and 10 % MST power. Data of two independent measurements were analysed using the signal from thermophoresis + t-jump (initial fluorescence change caused by temperature increase independent of particle flow).

MST buffer

20 mM HEPES
100 mM NaCl
3 mM $MgCl_2$
0.05 % Triton X-100
pH 7.2

5.2.16 Isothermal titration calorimetry

Isothermal titration calorimetry (ITC) measurements enable the complete thermodynamic characterisation of (biomolecular) interactions including determination of the K_D value, enthalpy and entropy. The underlying principle is a very accurate measurement of the required energy to adapt the temperature of a reference and a reaction chamber after repeated addition of a defined amount of a ligand to the molecule in the reaction chamber (Ladbury 2004).

The heat development or consumption is subsequently integrated over time and plotted against the molar ratio of the reactants. Application of the appropriate non-linear least squares fit binding model enables the determination of the enthalpy, K_D and reaction stoichiometry. These parameters are linked by the equation

$$\Delta G = \Delta H - T \times \Delta S = -R \times T \times lnK_B$$

where ΔG = change in Gibb's free energy, ΔH = change in enthalpy, T = temperature (in Kelvin), ΔS = change in entropy, R = gas constant and lnK_B = natural logarithm of the binding constant = $1/K_D$ (Ladbury 2004).

Prior to the experiment, the purified proteins were dialysed overnight against 2 L of ITC buffer using Slide-A-Lyzer® MINI dialysis units, 10000 MWCO. The iTC200 MicroCalorimeter cell contained 200 µL of the diluted interaction partner and the respective partner was injected via the 40 µL microsyringe at an approximately 10 times higher concentration (see results for exact concentrations). The 18 ligand injections were performed at 15 °C or 25 °C with a reference power of 5 µCal/sec and feedback mode gain high. The first 0.2 µL injection was omitted in the data analysis; the following injections were 2 µL each in volume with 120 sec intervals at a stirring speed 750 rpm with a twisted paddle syringe. The data was analysed with Microcal's ITC software for ORIGIN and the control injections of protein into buffer were subtracted if necessary. A single binding site model was employed for all experiments. For the ARNO to CNK1Δcc experiment, the buffer contained 500 mM NaCl.

ITC buffer

20 mM HEPES
100 mM NaCl
3 mM $MgCl_2$
pH 7.2

5.2.17 Protein crystallisation

Protein crystallography addresses the conversion of a highly pure soluble protein into a protein crystal where all molecules are positioned in an ordered manner. This ordered arrangement in so called unit cells is the prerequisite to determine the three-dimensional structure of the biomolecule via X-ray diffraction analysis. For a comprehensive introduction to protein crystallography and subsequent X-ray structure determination one may refer to Bernhard Rupp's textbook Biomolecular Crystallography (Rupp 2009).

The crystallisation complexes were obtained by mixing the respective proteins and applying them to the HiLoad 16/600 Superdex 200 pg or HiLoad 16/600 Superdex 75 pg (for ARNO-cc-Sec7/CNK1-cc) in SEC buffer at a flow rate of 1 mL/min and refreezing them in liquid nitrogen.

The subsequent work of protein crystallisation and crystal testing at a synchrotron beamline was essentially performed by Dr Kanchan Anand at the Karlsruhe Institute of Technology. In short, the vapour diffusion sitting drop method was used. 100 nL of the concentrated protein complexes (10.3 mg/mL ARNO:CNK1, 7.4 mg/mL ARNO:CNK1-cc, 6.7 mg/mL ARNO-cc-Sec7:CNK1-cc, 12.6 mg/mL ARNOΔpbr:CNK1-cc) were mixed 1:1 with several different precipitants. The mix of protein and crystallisation screen solutions was kept at different temperatures ranging from 10 °C to 20 °C in an atmosphere containing the crystallisation buffer for several days to weeks. Since the precipitant concentration is higher in the reservoir solution than in the drop, water vapour diffuses out of the drop, so both the protein as well as the precipitant concentration increase, which can allow for crystal formation. Since the crystallisation conditions for the complexes were unknown, several commercial screens (such as Wizard 1+2, Wizard 3+4, JCSG+, Morpheus and Proplex, all by Molecular Dimensions) and home-made screens were used. Initial conditions were optimised using the hanging drop method.

SEC buffer

20 mM HEPES
100 mM NaCl
3 mM $MgCl_2$
pH 7.2

5.2.18 Liposome preparation

Liposomes are spherical membrane systems which consist of at least one lipid bilayer. They can be prepared in a multitude of ways including sonication and extrusion methods leading to liposomes of different sizes and numbers of bilayers (Akbarzadeh *et al.* 2013). For the present study, liposomes were prepared following the general manufacturer's advice as well as the described procedures for liposome preparation in the study of ARFs (Avanti Polar Lipids 2017, Robbe and Antonny 2003, Stalder *et al.* 2011).

Adapted from Stalder *et al.* 2011, 20 % L-α-phosphatidylethanolamine (PE), 30 % L-α-phosphatidylserine (PS), 48 % (or 50 %) L-α-phosphatidylcholine (PC) and 2 % (or no) L-α-phosphatidylinositol-4,5-bisphosphate (PIP_2) (chapter 5.1.5) were mixed. The composition of liposomes containing DGS-NTA(Ni) is listed in tab. 5-8 where concentrations of PE and PS were slightly lowered accordingly.

Tab. 5-8: Composition of DGS-NTA(Ni) containing liposomes.

% DGS-NTA (Ni)	Composition
5	20 % PE, 30 % PS, 2 % PIP_2, 43 % PC
10	15 % PE, 25 % PS, 2 % PIP_2, 48 % PC
15	15 % PE, 25 % PS, 2 % PIP_2, 43 % PC
25	15 % PE, 25 % PS, 2 % PIP_2, 33 % PC

The lipids were prepared in a volume of 2 mL at 2 mM total lipid concentration in a 10 mL pointed hand vice. PE, PS and PC were dissolved in chloroform, PIP_2 in a 20:9:1 mix of chloroform, methanol and ddH_2O. To keep the polar PIP_2 in solution, the final methanol concentration was adjusted to around 35 % (v/v) while the remaining solvent was chloroform.

The lipids were equilibrated to 34 °C in a rotary evaporator for 5 min, rotating at 60 rpm without vacuum. Most of the solvent was then evaporated within one minute without boiling and full vacuum was applied for 1-2 h to evaporate the remaining solvent at RT without rotation. After drying, the lipids were hydrated for 25 min in 1 mL liposome buffer at a total lipid concentration of 4 mM leading to the formation of large multilamellar vesicles. The liposomes were transferred to a microcentrifuge tube and subjected to five freeze-thaw cycles using dry ice and a 37 °C heat block, which reduces the liposome size (Traïkia *et al.* 2000). As a last step, the liposomes were extruded through a 100 nm polycarbonate membrane using the Avanti mini extruder and two 1 mL gastight syringes. The liposomes were analysed via DLS (chapter 5.2.10), stored at RT and used within four days after production.

Liposome buffer

50 mM HEPES
120 mM potassium acetate
pH 7.2

5.2.19 Guanine nucleotide exchange assay for soluble ARFs

In order to test the enzymatic activity of different ARNO constructs, guanine nucleotide exchange assays on the soluble NΔ17ARF1 GTPase were performed.

Apart from radioactive assays, either the intrinsic tryptophan fluorescence of ARFs or binding/release of a fluorescently labelled nucleotide analogue can be utilised (Kahn and Gilman 1986, Antonny *et al.* 1997, Remmers 1998, Stalder *et al.* 2011). For this assay, binding of the fluorescent nucleotide analogue Mant-GTP was monitored adapted from Stalder *et al.* 2011. When Mant-GTP is bound to the GTPase, excited tryptophan residues transfer energy to the Mant moiety via FRET. The radiationless energy transfer results in an increased emission fluorescence signal at around 450 nm when the tryptophans are exited at approximately 280 nm.

The bound nucleotide of 1 µM NΔ17ARF1 was displaced by incubation with 2 mM EDTA and 5 µM GDP for 15 min at 37 °C in exchange buffer. GDP was allowed to bind by the addition of 3 mM $MgCl_2$ and incubation for 5 min at 37 °C. For the actual exchange reaction, 400 nM NΔ17ARF1-GDP was mixed with 5 µM Mant-GTP and the reaction was initiated by addition of 20 nM or 200 nM ARNO in exchange buffer + 1 mM $MgCl_2$. The exchange reaction was monitored in a Corning black 96 well non-binding surface half area plate with the Tecan infinite M1000 reader by Mant-FRET at 297/455 nm at 37 °C.

Exchange buffer

50 mM HEPES
120 mM potassium acetate
5 µM $CaCl_2$
100 µM EGTA
1 mM DTT
pH 7.2

5.2.20 Guanine nucleotide exchange assay for myr-ARFs

A Mant-FRET assay similar to the one described for soluble ARFs (chapter 5.2.19) was also used to assess GEF activity on liposome-bound, myr-ARFs. In contrast to the assay for soluble ARFs however, the myr-ARFs were pre-loaded with Mant-GDP instead of GDP and hence a fluorescence decrease upon exchange of Mant-GDP for GTP was monitored.

The bound nucleotide of 1 µM myr-ARF1 or myr-ARF6 was displaced by incubation with 2 mM EDTA and 2.5 µM Mant-GDP for 15 min at 37 °C in exchange buffer. Mant-GDP was allowed to bind by the addition of 3 mM $MgCl_2$ and incubation for 5 min at 37 °C. For the actual exchange reaction, 400 nM myr-ARF and liposomes (for composition see chapter 5.2.18, 200 µM total lipid concentration) were mixed with 100 µM GTP and the reaction was initiated by addition of 1 nM ARNO in exchange buffer + 1 mM $MgCl_2$. For the initial assays, 0.25-10 nM ARNO were tested. To assess the effect of CNK1, 1-20 nM CNK1 were added to the reaction simultaneously with ARNO. The exchange reaction was monitored in a Corning black 96 well non-binding surface half area plate with the Tecan infinite M1000 reader by Mant-FRET at 297/455 nm at 37 °C. For myr-ARF1, the reaction was incubated at 37 °C for 20 min prior to the addition of ARNO to allow for complete temperature equilibration. Since the intrinsic exchange for myr-ARF6 is higher than for myr-ARF1, the reaction could not be pre-incubated but was started immediately.

In case the exchange assay was performed using liposomes containing the DGS-NTA(Ni) lipid, a non-reducing exchange buffer omitting DTT was used to avoid reduction of the coordinated nickel.

The nucleotide exchange kinetics were analysed assuming pseudo-first order rate constants which were obtained by fitting the fluorescence traces using a mono-exponential fit with GraphPad PRISM (Stalder *et al.* 2011).

Exchange buffer

50 mM HEPES
120 mM potassium acetate
5 µM $CaCl_2$
100 µM EGTA
1 mM DTT
pH 7.2

5.2.21 Liposome flotation assay

In order to assess protein binding to PIP_2-containing liposomes or liposomes without PIP_2 (chapter 5.2.18), a previously described ultracentrifugation approach was applied (Bigay and Antonny 2005). Therefore, proteins and liposomes were mixed in a 30 % sucrose-containing buffer, which was overlaid with a cushion of 25 % sucrose and a buffer layer. In case a protein binds to the liposomes, it migrates to the top fraction alongside the lipids. If the protein remains free in solution, it can be recovered from the bottom fraction (fig. 5-3).

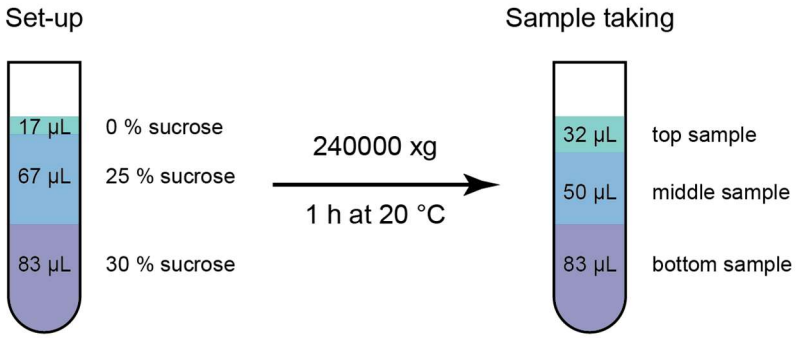

Fig. 5-3: Experimental setup of the liposome flotation assay. The protein-lipid mixtures were prepared in a buffer containing 30 % sucrose and added to the tube first with two layers of 25 % sucrose and 0 % sucrose on top. The samples were taken using a 50 µL gastight syringe according to the depicted scheme. Adapted from Bigay and Antonny 2005.

30 nM ARNO, 30 nM CNK1, 30 nM $CNK1_{K414Q}$ or 60 nM CNK1 and liposomes (200 µM total lipid concentration) were prepared in liposome flotation buffer + 30 % sucrose, incubated for 10 min and overlaid with two layers of 25 % sucrose and 0 % sucrose, respectively. After centrifugation with the Beckman ultracentrifuge at 240000 xg for 1 h at 20°C, the liposome-containing top fraction, the middle fraction and the bottom fraction with unbound protein were recovered with a gastight syringe. The samples were mixed with SDS loading buffer and analysed via SDS-PAGE (chapter 5.2.2) and western blot (chapter 5.2.3) as depicted in fig. 5-3. In case the flotation assay was performed using liposomes containing the DGS-NTA(Ni) lipid, a non-reducing exchange buffer without DTT was used to avoid reduction of the coordinated nickel.

Liposome flotation buffer

50 mM HEPES
120 mM potassium acetate
1 mM $MgCl_2$
1 mM DTT
pH 7.2

6 References

Achstetter, T.; Franzusoff, A.; Field, C.; Schekman, R. (1988): SEC7 encodes an unusual, high molecular weight protein required for membrane traffic from the yeast Golgi apparatus. *The Journal of biological chemistry* 263 (24), pp. 11711–11717.

Adams, M. J.; Blundell, T. L.; Dodson, E. J.; Dodson, G. G.; Viljayan, M.; Baker, E. N. et al. (1969): Structure of Rhombohedral 2 Zinc Insulin Crystals. *Nature* 224 (5218), pp. 491–495.

Ahmad, F.; Lindh, R.; Tang, Y.; Ruishalme, I.; Ost, A.; Sahachartsiri, B. et al. (2009): Differential regulation of adipocyte PDE3B in distinct membrane compartments by insulin and the beta3-adrenergic receptor agonist CL316243: effects of caveolin-1 knockdown on formation/maintenance of macromolecular signalling complexes. *The Biochemical journal* 424 (3), pp. 399–410.

Akbarzadeh, A.; Rezaei-Sadabady, R.; Davaran, S.; Joo, S. W.; Zarghami, N.; Hanifehpour, Y. et al. (2013): Liposome: classification, preparation, and applications. *Nanoscale research letters* 8 (1), pp. 102.

Alessi, D. R.; James, S. R.; Downes, C. P.; Holmes, A. B.; Gaffney, P. R.; Reese, C. B.; Cohen, P. (1997): Characterization of a 3-phosphoinositide-dependent protein kinase which phosphorylates and activates protein kinase Balpha. *Current biology: CB* 7 (4), pp. 261–269.

Alley, S. C.; Ishmael, F. T.; Jones, A. Daniel; Benkovic, S. J. (2000): Mapping Protein−Protein Interactions in the Bacteriophage T4 DNA Polymerase Holoenzyme Using a Novel Trifunctional Photo-cross-linking and Affinity Reagent. *J. Am. Chem. Soc.* 122 (25), pp. 6126–6127.

Amor, J. C.; Harrison, D. H.; Kahn, R. A.; Ringe, D. (1994): Structure of the human ADP-ribosylation factor 1 complexed with GDP. *Nature* 372 (6507), pp. 704–708.

Anthonsen, M. W.; Rönnstrand, L.; Wernstedt, C.; Degerman, E.; Holm, C. (1998): Identification of novel phosphorylation sites in hormone-sensitive lipase that are phosphorylated in response to isoproterenol and govern activation properties in vitro. *The Journal of biological chemistry* 273 (1), pp. 215–221.

Antonny, B.; Beraud-Dufour, S.; Chardin, P.; Chabre, M. (1997): N-terminal hydrophobic residues of the G-protein ADP-ribosylation factor-1 insert into membrane phospholipids upon GDP to GTP exchange. *Biochemistry* 36 (15), pp. 4675–4684.

Arora, B.; Tandon, R.; Attri, P.; Bhatia, R. (2017): Chemical Crosslinking: Role in Protein and Peptide Science. *Current protein & peptide science* 18 (9), pp. 946–955.

Austin, C.; Hinners, I.; Tooze, S. A. (2000): Direct and GTP-dependent interaction of ADP-ribosylation factor 1 with clathrin adaptor protein AP-1 on immature secretory granules. *The Journal of biological chemistry* 275 (29), pp. 21862–21869.

Avanti Polar Lipids (2017): Preparing Large, Unilamellar Vesicles by Extrusion (LUVET). Available online at https://avantilipids.com/tech-support/liposome-preparation/luvet/, checked on 6/10/2017.

Avruch, J. (1998): Insulin signal transduction through protein kinase cascades. *Molecular and cellular biochemistry* 182 (1-2), pp. 31–48.

Baker, E. N.; Blundell, T. L.; Cutfield, J. F.; Cutfield, S. M.; Dodson, E. J.; Dodson, G. G. et al. (1988): The structure of 2Zn pig insulin crystals at 1.5 A resolution. *Philosophical transactions of the Royal Society of London. Series B, Biological sciences* 319 (1195), pp. 369–456.

Bayburt, T. H.; Sligar, S. G. (2003): Self-assembly of single integral membrane proteins into soluble nanoscale phospholipid bilayers. *Protein science: a publication of the Protein Society* 12 (11), pp. 2476–2481.

Bedouelle, H.; Duplay, P. (1988): Production in Escherichia coli and one-step purification of bifunctional hybrid proteins which bind maltose. Export of the Klenow polymerase into the periplasmic space. *European journal of biochemistry* 171 (3), pp. 541–549.

Ben-Tekaya, H.; Kahn, R. A.; Hauri, H.-P. (2010): ADP ribosylation factors 1 and 4 and group VIA phospholipase A_2 regulate morphology and intraorganellar traffic in the endoplasmic reticulum-Golgi intermediate compartment. *Molecular biology of the cell* 21 (23), pp. 4130–4140.

Béraud-Dufour, S.; Robineau, S.; Chardin, P.; Paris, S.; Chabre, M.; Cherfils, J.; Antonny, B. (1998): A glutamic finger in the guanine nucleotide exchange factor ARNO displaces Mg2+ and the beta-phosphate to destabilize GDP on ARF1. *The EMBO journal* 17 (13), pp. 3651–3659.

Bigay, J.; Antonny, B. (2005): Real-time assays for the assembly-disassembly cycle of COP coats on liposomes of defined size. *Methods in enzymology* 404, pp. 95–107.

Booker, G. W.; Breeze, A. L.; Downing, A. K.; Panayotou, G.; Gout, I.; Waterfield, M. D.; Campbell, I. D. (1992): Structure of an SH2 domain of the p85 alpha subunit of phosphatidylinositol-3-OH kinase. *Nature* 358 (6388), pp. 684–687.

Brymora, A.; Valova, V. A.; Robinson, P. J. (2004): Protein-protein interactions identified by pull-down experiments and mass spectrometry. *Current protocols in cell biology* Chapter 17, pp. Unit 17.5.

Burack, W. R.; Shaw, A. S. (2000): Signal transduction: hanging on a scaffold. *Current opinion in cell biology* 12 (2), pp. 211–216.

Casanova, J. E. (2007): Regulation of Arf activation: the Sec7 family of guanine nucleotide exchange factors. *Traffic (Copenhagen, Denmark)* 8 (11), pp. 1476–1485.

Chardin, P.; Paris, S.; Antonny, B.; Robineau, S.; Béraud-Dufour, S.; Jackson, C. L.; Chabre, M. (1996): A human exchange factor for ARF contains Sec7- and pleckstrin-homology domains. *Nature* 384 (6608), pp. 481–484.

Chawla, B.; Hedman, A. C.; Sayedyahossein, S.; Erdemir, H. H.; Li, Z.; Sacks, D. B. (2017): Absence of IQGAP1 leads to insulin resistance. *The Journal of biological chemistry*.

Cherfils, J.; Ménétrey, J.; Mathieu, M.; Le Bras, G.; Robineau, S.; Béraud-Dufour, S. et al. (1998): Structure of the Sec7 domain of the Arf exchange factor ARNO. *Nature* 392 (6671), pp. 101–105.

Chun, J.; Shapovalova, Z.; Dejgaard, S. Y.; Presley, J. F.; Melançon, P. (2008): Characterization of class I and II ADP-ribosylation factors (Arfs) in live cells: GDP-bound class II Arfs associate with the ER-Golgi intermediate compartment independently of GBF1. *Molecular biology of the cell* 19 (8), pp. 3488–3500.

Ciszak, E.; Smith, G. D. (1994): Crystallographic evidence for dual coordination around zinc in the T3R3 human insulin hexamer. *Biochemistry* 33 (6), pp. 1512–1517.

Cohen, L. A.; Honda, A.; Varnai, P.; Brown, F. D.; Balla, T.; Donaldson, J. G. (2007): Active Arf6 recruits ARNO/cytohesin GEFs to the PM by binding their PH domains. *Molecular biology of the cell* 18 (6), pp. 2244–2253.

Cohen, P. (2006): The twentieth century struggle to decipher insulin signalling. *Nature reviews. Molecular cell biology* 7 (11), pp. 867–873.

Combes, B.; Stakelum, G. S. (1961): A liver enzyme that conjugates sulfobromophthalein sodium with glutathione. *The Journal of clinical investigation* 40, pp. 981–988.

Cosgrove, L.; Lovrecz, G. O.; Verkuylen, A.; Cavaleri, L.; Black, L. A.; Bentley, J. D. et al. (1995): Purification and properties of insulin receptor ectodomain from large-scale mammalian cell culture. *Protein expression and purification* 6 (6), pp. 789–798.

Craparo, A.; Freund, R.; Gustafson, T. A. (1997): 14-3-3 (epsilon) interacts with the insulin-like growth factor I receptor and insulin receptor substrate I in a phosphoserine-dependent manner. *The Journal of biological chemistry* 272 (17), pp. 11663–11669.

Crick, F. H. C. (1953): The packing of α-helices: simple coiled-coils. *Acta Crystallographica* 6 (8-9), pp. 689–697.

Croll, T. I.; Smith, B. J.; Margetts, M. B.; Whittaker, J.; Weiss, M. A.; Ward, C. W.; Lawrence, M. C. (2016): Higher-Resolution Structure of the Human Insulin Receptor Ectodomain: Multi-Modal Inclusion of the Insert Domain. *Structure (London, England: 1993)* 24 (3), pp. 469–476.

Cross, D. A.; Alessi, D. R.; Cohen, P.; Andjelkovich, M.; Hemmings, B. A. (1995): Inhibition of glycogen synthase kinase-3 by insulin mediated by protein kinase B. *Nature* 378 (6559), pp. 785–789.

Cryer, P. E. (2007): Hypoglycemia, functional brain failure, and brain death. *The Journal of clinical investigation* 117 (4), pp. 868–870.

Cukierman, E.; Huber, I.; Rotman, M.; Cassel, D. (1995): The ARF1 GTPase-activating protein: zinc finger motif and Golgi complex localization. *Science (New York, N.Y.)* 270 (5244), pp. 1999–2002.

Das, M.; Fox, C. F. (1979): Chemical cross-linking in biology. *Annual review of biophysics and bioengineering* 8, pp. 165–193.

Depetris, R. S.; Hu, J.; Gimpelevich, I.; Holt, L. J.; Daly, R. J.; Hubbard, S. R. (2005): Structural basis for inhibition of the insulin receptor by the adaptor protein Grb14. *Molecular cell* 20 (2), pp. 325–333.

Depetris, R. S.; Wu, J.; Hubbard, S. R. (2009): Structural and functional studies of the Ras-associating and pleckstrin-homology domains of Grb10 and Grb14. *Nature structural & molecular biology* 16 (8), pp. 833–839.

Derewenda, U.; Derewenda, Z.; Dodson, E. J.; Dodson, G. G.; Bing, X.; Markussen, J. (1991): X-ray analysis of the single chain B29-A1 peptide-linked insulin molecule. A completely inactive analogue. *Journal of molecular biology* 220 (2), pp. 425–433.

Di Guana, C.; Lib, P.; Riggsa, P. D.; Inouyeb, H. (1988): Vectors that facilitate the expression and purification of foreign peptides in Escherichia coli by fusion to maltose-binding protein. *Gene* 67 (1), pp. 21–30.

DiNitto, J. P.; Delprato, A.; Gabe Lee, M.-T.; Cronin, T. C.; Huang, S.; Guilherme, A. et al. (2007): Structural basis and mechanism of autoregulation in 3-phosphoinositide-dependent Grp1 family Arf GTPase exchange factors. *Molecular cell* 28 (4), pp. 569–583.

Donaldson, J. G.; Jackson, C. L. (2011): ARF family G proteins and their regulators: roles in membrane transport, development and disease. *Nature reviews. Molecular cell biology* 12 (6), pp. 362–375.

D'Souza-Schorey, C.; Chavrier, P. (2006): ARF proteins: roles in membrane traffic and beyond. *Nature reviews. Molecular cell biology* 7 (5), pp. 347–358.

Duhr, S.; Braun, D. (2006): Why molecules move along a temperature gradient. *Proceedings of the National Academy of Sciences of the United States of America* 103 (52), pp. 19678–19682.

Duijsings, D.; Lanke, Kjerstin H W; van Dooren, Sander H J; van Dommelen, Michiel M T; Wetzels, R.; Mattia, F. de et al. (2009): Differential membrane association properties and regulation of class I and class II Arfs. *Traffic (Copenhagen, Denmark)* 10 (3), pp. 316–323.

Ebina, Y.; Ellis, L.; Jarnagin, K.; Edery, M.; Graf, L.; Clauser, E. et al. (1985): The human insulin receptor cDNA: the structural basis for hormone-activated transmembrane signalling. *Cell* 40 (4), pp. 747–758.

Eck, M. J.; Dhe-Paganon, S.; Trüb, T.; Nolte, R. T.; Shoelson, S. E. (1996): Structure of the IRS-1 PTB domain bound to the juxtamembrane region of the insulin receptor. *Cell* 85 (5), pp. 695–705.

Einarson, M. B.; Pugacheva, E. N.; Orlinick, J. R. (2007): Identification of Protein-Protein Interactions with Glutathione-S-Transferase (GST) Fusion Proteins. *CSH protocols* 2007, pp. pdb.top11.

Ezkurdia, I.; Juan, D.; Rodriguez, J. M.; Frankish, A.; Diekhans, M.; Harrow, J. et al. (2014): Multiple evidence strands suggest that there may be as few as 19,000 human protein-coding genes. *Human molecular genetics* 23 (22), pp. 5866–5878.

Farrar, C. T.; Halkides, C. J.; Singel, D. J. (1997): The frozen solution structure of p21 ras determined by ESEEM spectroscopy reveals weak coordination of Thr35 to the active site metal ion. *Structure (London, England: 1993)* 5 (8), pp. 1055–1066.

Fischer, A.; Mühlhäuser, Wignand W D; Warscheid, B.; Radziwill, G. (2017): Membrane localization of acetylated CNK1 mediates a positive feedback on RAF/ERK signaling. *Science advances* 3 (8), pp. e1700475.

Franco, M.; Chardin, P.; Chabre, M.; Paris, S. (1995): Myristoylation of ADP-ribosylation factor 1 facilitates nucleotide exchange at physiological Mg2+ levels. *The Journal of biological chemistry* 270 (3), pp. 1337–1341.

Fritz, R. D.; Radziwill, G. (2011): CNK1 and other scaffolds for Akt/FoxO signaling. *Biochimica et biophysica acta* 1813 (11), pp. 1971–1977.

Fritz, R. D.; Varga, Z.; Radziwill, G. (2010): CNK1 is a novel Akt interaction partner that promotes cell proliferation through the Akt-FoxO signalling axis. *Oncogene* 29 (24), pp. 3575–3582.

Fuss, B.; Becker, T.; Zinke, I.; Hoch, M. (2006): The cytohesin Steppke is essential for insulin signalling in Drosophila. *Nature* 444 (7121), pp. 945–948.

Garriga, P.; Manyosa, J. (2002): The eye photoreceptor protein rhodopsin. Structural implications for retinal disease. *FEBS letters* 528 (1-3), pp. 17–22.

GE (2014): Size Exclusion Chromatography. Principles and Methods. Available online at http://www.gelifesciences.com/file_source/GELS/Service%20and%20Support/Documents%20and%20Downloads/Handbooks/pdfs/Size%20Exclusion%20Chromatography.pdf, checked on 5/10/2017.

Germain, P.; Staels, B.; Dacquet, C.; Spedding, M.; Laudet, V. (2006): Overview of nomenclature of nuclear receptors. *Pharmacological reviews* 58 (4), pp. 685–704.

Gillingham, A. K.; Munro, S. (2007): The small G proteins of the Arf family and their regulators. *Annual review of cell and developmental biology* 23, pp. 579–611.

Goldberg, J. (1999): Structural and functional analysis of the ARF1-ARFGAP complex reveals a role for coatomer in GTP hydrolysis. *Cell* 96 (6), pp. 893–902.

Gonzalez, L.; Woolfson, D. N.; Alber, T. (1996): Buried polar residues and structural specificity in the GCN4 leucine zipper. *Nature structural biology* 3 (12), pp. 1011–1018.

Goody, R. S.; Müller, M. P.; Wu, Y.-W. (2017): Mechanisms of action of Rab proteins, key regulators of intracellular vesicular transport. *Biological chemistry* 398 (5-6), pp. 565–575.

Gross, D. N.; Wan, M.; Birnbaum, M. J. (2009): The role of FOXO in the regulation of metabolism. *Current diabetes reports* 9 (3), pp. 208–214.

Gustafson, T. A.; He, W.; Craparo, A.; Schaub, C. D.; O'Neill, T. J. (1995): Phosphotyrosine-dependent interaction of SHC and insulin receptor substrate 1 with the NPEY motif of the insulin receptor via a novel non-SH2 domain. *Molecular and cellular biology* 15 (5), pp. 2500–2508.

Ha, V. L.; Thomas, Geraint M H; Stauffer, S.; Randazzo, P. A. (2005): Preparation of myristoylated Arf1 and Arf6. *Methods in enzymology* 404, pp. 164–174.

Hafner, M.; Schmitz, A.; Grüne, I.; Srivatsan, S. G.; Paul, B.; Kolanus, W. et al. (2006): Inhibition of cytohesins by SecinH3 leads to hepatic insulin resistance. *Nature* 444 (7121), pp. 941–944.

Hanahan, D. (1983): Studies on transformation of Escherichia coli with plasmids. *Journal of molecular biology* 166 (4), pp. 557–580.

Harlan, J. E.; Hajduk, P. J.; Yoon, H. S.; Fesik, S. W. (1994): Pleckstrin homology domains bind to phosphatidylinositol-4,5-bisphosphate. *Nature* 371 (6493), pp. 168–170.

Haslam, R. J.; Koide, H. B.; Hemmings, B. A. (1993): Pleckstrin domain homology. *Nature* 363 (6427), pp. 309–310.

Herrera, R.; Rosen, O. M. (1986): Autophosphorylation of the insulin receptor in vitro. Designation of phosphorylation sites and correlation with receptor kinase activation. *The Journal of biological chemistry* 261 (26), pp. 11980–11985.

Hiratsuka, T. (1983): New ribose-modified fluorescent analogs of adenine and guanine nucleotides available as substrates for various enzymes. *Biochimica et biophysica acta* 742 (3), pp. 496–508.

Hirsch, A. H.; Glantz, S. B.; Li, Y.; You, Y.; Rubin, C. S. (1992): Cloning and expression of an intron-less gene for AKAP 75, an anchor protein for the regulatory subunit of cAMP-dependent protein kinase II beta. *The Journal of biological chemistry* 267 (4), pp. 2131–2134.

Hochuli, E.; Bannwarth, W.; Dobeli, H.; Gentz, R.; Stuber, D. (1988): Genetic Approach to Facilitate Purification of Recombinant Proteins with a Novel Metal Chelate Adsorbent. *Nat Biotech* 6 (11), pp. 1321–1325.

Hochuli, E.; Döbeli, H.; Schacher, A. (1987): New metal chelate adsorbent selective for proteins and peptides containing neighbouring histidine residues. *Journal of chromatography* 411, pp. 177–184.

Hong, P.; Koza, S.; Bouvier, Edouard S P (2012): Size-Exclusion Chromatography for the Analysis of Protein Biotherapeutics and their Aggregates. *Journal of liquid chromatography & related technologies* 35 (20), pp. 2923–2950.

Hu, J.; Liu, J.; Ghirlando, R.; Saltiel, A. R.; Hubbard, S. R. (2003): Structural basis for recruitment of the adaptor protein APS to the activated insulin receptor. *Molecular cell* 12 (6), pp. 1379–1389.

Hubbard, S. R. (1997): Crystal structure of the activated insulin receptor tyrosine kinase in complex with peptide substrate and ATP analog. *The EMBO journal* 16 (18), pp. 5572–5581.

Hubbard, S. R. (2004): Juxtamembrane autoinhibition in receptor tyrosine kinases. *Nature reviews. Molecular cell biology* 5 (6), pp. 464–471.

Hubbard, S. R. (2013): The insulin receptor: both a prototypical and atypical receptor tyrosine kinase. *Cold Spring Harbor perspectives in biology* 5 (3), pp. a008946.

Hubbard, S. R.; Wei, L.; Ellis, L.; Hendrickson, W. A. (1994): Crystal structure of the tyrosine kinase domain of the human insulin receptor. *Nature* 372 (6508), pp. 746–754.

International Diabetes Federation (2015): IDF diabetes atlas. Seventh edition. Brussels: International Diabetes Federation.

Jaffe, A. B.; Aspenström, P.; Hall, A. (2004): Human CNK1 acts as a scaffold protein, linking Rho and Ras signal transduction pathways. *Molecular and cellular biology* 24 (4), pp. 1736–1746.

Jaffe, A. B.; Hall, A.; Schmidt, A. (2005): Association of CNK1 with Rho guanine nucleotide exchange factors controls signaling specificity downstream of Rho. *Current biology: CB* 15 (5), pp. 405–412.

James, S. R.; Downes, C. P.; Gigg, R.; Grove, S. J.; Holmes, A. B.; Alessi, D. R. (1996): Specific binding of the Akt-1 protein kinase to phosphatidylinositol 3,4,5-trisphosphate without subsequent activation. *The Biochemical journal* 315 (Pt 3), pp. 709–713.

Jerabek-Willemsen, M.; Wienken, C. J.; Braun, D.; Baaske, P.; Duhr, S. (2011): Molecular interaction studies using microscale thermophoresis. *Assay and drug development technologies* 9 (4), pp. 342–353.

Kahn, R. A.; Cherfils, J.; Elias, M.; Lovering, R. C.; Munro, S.; Schurmann, A. (2006): Nomenclature for the human Arf family of GTP-binding proteins: ARF, ARL, and SAR proteins. *The Journal of cell biology* 172 (5), pp. 645–650.

Kahn, R. A.; Gilman, A. G. (1986): The protein cofactor necessary for ADP-ribosylation of Gs by cholera toxin is itself a GTP binding protein. *The Journal of biological chemistry* 261 (17), pp. 7906–7911.

Kahn, R. A.; Goddard, C.; Newkirk, M. (1988): Chemical and immunological characterization of the 21-kDa ADP-ribosylation factor of adenylate cyclase. *The Journal of biological chemistry* 263 (17), pp. 8282–8287.

Karandur, D.; Nawrotek, A.; Kuriyan, J.; Cherfils, J. (2017): Multiple interactions between an Arf/GEF complex and charged lipids determine activation kinetics on the membrane. *Proceedings of the National Academy of Sciences of the United States of America*.

Karlin, A. (2002): Emerging structure of the nicotinic acetylcholine receptors. *Nature reviews. Neuroscience* 3 (2), pp. 102–114.

Kasuga, M.; Zick, Y.; Blithe, D. L.; Crettaz, M.; Kahn, C. R. (1982): Insulin stimulates tyrosine phosphorylation of the insulin receptor in a cell-free system. *Nature* 298 (5875), pp. 667–669.

Kavanaugh, W. M.; Williams, L. T. (1994): An alternative to SH2 domains for binding tyrosine-phosphorylated proteins. *Science (New York, N.Y.)* 266 (5192), pp. 1862–1865.

Kitamura, T.; Kitamura, Y.; Kuroda, S.; Hino, Y.; Ando, M.; Kotani, K. et al. (1999): Insulin-induced phosphorylation and activation of cyclic nucleotide phosphodiesterase 3B by the serine-threonine kinase Akt. *Molecular and cellular biology* 19 (9), pp. 6286–6296.

Klarlund, J. K.; Tsiaras, W.; Holik, J. J.; Chawla, A.; Czech, M. P. (2000): Distinct polyphosphoinositide binding selectivities for pleckstrin homology domains of GRP1-like proteins based on diglycine versus triglycine motifs. *The Journal of biological chemistry* 275 (42), pp. 32816–32821.

Kolanus, W. (2007): Guanine nucleotide exchange factors of the cytohesin family and their roles in signal transduction. *Immunological reviews* 218, pp. 102–113.

Kolanus, W.; Nagel, W.; Schiller, B.; Zeitlmann, L.; Godar, S.; Stockinger, H.; Seed, B. (1996): Alpha L beta 2 integrin/LFA-1 binding to ICAM-1 induced by cytohesin-1, a cytoplasmic regulatory molecule. *Cell* 86 (2), pp. 233–242.

Komander, D.; Fairservice, A.; Deak, M.; Kular, G. S.; Prescott, A. R.; Peter Downes, C. et al. (2004): Structural insights into the regulation of PDK1 by phosphoinositides and inositol phosphates. *The EMBO journal* 23 (20), pp. 3918–3928.

Koyama, S.; Yu, H.; Dalgarno, D. C.; Shin, T. B.; Zydowsky, L. D.; Schreiber, S. L. (1993): Structure of the PI3K SH3 domain and analysis of the SH3 family. *Cell* 72 (6), pp. 945–952.

Kyhse-Andersen, J. (1984): Electroblotting of multiple gels: a simple apparatus without buffer tank for rapid transfer of proteins from polyacrylamide to nitrocellulose. *Journal of biochemical and biophysical methods* 10 (3-4), pp. 203–209.

Ladbury, J. E. (2004): Application of isothermal titration calorimetry in the biological sciences: things are heating up! *BioTechniques* 37 (6), pp. 885–887.

Laemmli, U. K. (1970): Cleavage of structural proteins during the assembly of the head of bacteriophage T4. *Nature* 227 (5259), pp. 680–685.

Langille, S. E.; Patki, V.; Klarlund, J. K.; Buxton, J. M.; Holik, J. J.; Chawla, A. et al. (1999): ADP-ribosylation factor 6 as a target of guanine nucleotide exchange factor GRP1. *The Journal of biological chemistry* 274 (38), pp. 27099–27104.

Laouini, A.; Jaafar-Maalej, C.; Limayem-Blouza, I.; Sfar, S.; Charcosset, C.; Fessi, H. (2012): Preparation, Characterization and Applications of Liposomes: State of the Art. *Journal of Colloid Science and Biotechnology* 1 (2), pp. 147–168.

Lenzen, C.; Cool, R. H.; Prinz, H.; Kuhlmann, J.; Wittinghofer, A. (1998): Kinetic analysis by fluorescence of the interaction between Ras and the catalytic domain of the guanine nucleotide exchange factor Cdc25Mm. *Biochemistry* 37 (20), pp. 7420–7430.

Levine, R.; Goldstein, M. (1949): The action of insulin on the distribution of galactose in eviscerated nephrectomized dogs. *The Journal of biological chemistry* 179 (2), pp. 985.

Li, H.-S.; Shome, K.; Rojas, R.; Rizzo, M. A.; Vasudevan, C.; Fluharty, E. et al. (2003a): The guanine nucleotide exchange factor ARNO mediates the activation of ARF and phospholipase D by insulin. *BMC cell biology* 4, pp. 13.

Li, J.; Malaby, A. W.; Famulok, M.; Sabe, H.; Lambright, D. G.; Hsu, V. W. (2012): Grp1 plays a key role in linking insulin signaling to glut4 recycling. *Developmental cell* 22 (6), pp. 1286–1298.

Li, Q.; Wong, Y. L.; Kang, C. (2014): Solution structure of the transmembrane domain of the insulin receptor in detergent micelles. *Biochimica et biophysica acta* 1838 (5), pp. 1313–1321.

Li, S.; Covino, N. D.; Stein, E. G.; Till, J. H.; Hubbard, S. R. (2003b): Structural and biochemical evidence for an autoinhibitory role for tyrosine 984 in the juxtamembrane region of the insulin receptor. *The Journal of biological chemistry* 278 (28), pp. 26007–26014.

Lim, J.; Zhou, M.; Veenstra, T. D.; Morrison, D. K. (2010): The CNK1 scaffold binds cytohesins and promotes insulin pathway signaling. *Genes & development* 24 (14), pp. 1496–1506.

Liu, Y.; Kahn, R. A.; Prestegard, J. H. (2009): Structure and membrane interaction of myristoylated ARF1. *Structure (London, England : 1993)* 17 (1), pp. 79–87.

Locasale, J. W.; Shaw, A. S.; Chakraborty, A. K. (2007): Scaffold proteins confer diverse regulatory properties to protein kinase cascades. *Proceedings of the National Academy of Sciences of the United States of America* 104 (33), pp. 13307–13312.

Macia, E.; Luton, F.; Partisani, M.; Cherfils, J.; Chardin, P.; Franco, M. (2004): The GDP-bound form of Arf6 is located at the plasma membrane. *Journal of cell science* 117 (Pt 11), pp. 2389–2398.

Macia, E.; Paris, S.; Chabre, M. (2000): Binding of the PH and polybasic C-terminal domains of ARNO to phosphoinositides and to acidic lipids. *Biochemistry* 39 (19), pp. 5893–5901.

Macleod, J. J. (1922): Insulin and diabetes: A general statement of the physiological and therapeutic effects of insulin. *British medical journal* 2 (3227), pp. 833–835.

Malaby, A. W.; van den Berg, Bert; Lambright, D. G. (2013): Structural basis for membrane recruitment and allosteric activation of cytohesin family Arf GTPase exchange factors. *Proceedings of the National Academy of Sciences of the United States of America* 110 (35), pp. 14213–14218.

Mandiyan, V.; Andreev, J.; Schlessinger, J.; Hubbard, S. R. (1999): Crystal structure of the ARF-GAP domain and ankyrin repeats of PYK2-associated protein beta. *The EMBO journal* 18 (24), pp. 6890–6898.

Mannervik, B.; Board, P. G.; Hayes, J. D.; Listowsky, I.; Pearson, W. R. (2005): Nomenclature for mammalian soluble glutathione transferases. *Methods in enzymology* 401, pp. 1–8.

Mason, J. M.; Arndt, K. M. (2004): Coiled coil domains: stability, specificity, and biological implications. *Chembiochem : a European journal of chemical biology* 5 (2), pp. 170–176.

Massague, J.; Pilch, P. F.; Czech, M. P. (1980): Electrophoretic resolution of three major insulin receptor structures with unique subunit stoichiometries. *Proceedings of the National Academy of Sciences of the United States of America* 77 (12), pp. 7137–7141.

McKern, N. M.; Lawrence, M. C.; Streltsov, V. A.; Lou, M.-Z.; Adams, T. E.; Lovrecz, G. O. et al. (2006): Structure of the insulin receptor ectodomain reveals a folded-over conformation. *Nature* 443 (7108), pp. 218–221.

Menting, J. G.; Whittaker, J.; Margetts, M. B.; Whittaker, L. J.; Kong, G. K.-W.; Smith, B. J. et al. (2013): How insulin engages its primary binding site on the insulin receptor. *Nature* 493 (7431), pp. 241–245.

Mergenthaler, P.; Lindauer, U.; Dienel, G. A.; Meisel, A. (2013): Sugar for the brain: the role of glucose in physiological and pathological brain function. *Trends in neurosciences* 36 (10), pp. 587–597.

Merril, C. R. (1990): Gel-staining techniques. *Methods in enzymology* 182, pp. 477–488.

Meyts, P. de (2015): Insulin/receptor binding: the last piece of the puzzle? What recent progress on the structure of the insulin/receptor complex tells us (or not) about negative cooperativity and activation. *BioEssays: news and reviews in molecular, cellular and developmental biology* 37 (4), pp. 389–397.

Milburn, M. V.; Tong, L.; deVos, A. M.; Brünger, A.; Yamaizumi, Z.; Nishimura, S.; Kim, S. H. (1990): Molecular switch for signal transduction: structural differences between active and inactive forms of protooncogenic ras proteins. *Science (New York, N.Y.)* 247 (4945), pp. 939–945.

Moore, C. X.; Cooper, G. J. (1991): Co-secretion of amylin and insulin from cultured islet beta-cells: modulation by nutrient secretagogues, islet hormones and hypoglycemic agents. *Biochemical and biophysical research communications* 179 (1), pp. 1–9.

Musacchio, A.; Noble, M.; Pauptit, R.; Wierenga, R.; Saraste, M. (1992): Crystal structure of a Src-homology 3 (SH3) domain. *Nature* 359 (6398), pp. 851–855.

Nagai, M.; Yoneda, Y. (2012): Small GTPase Ran and Ran-binding proteins. *Biomolecular concepts* 3 (4), pp. 307–318.

Nakai, W.; Kondo, Y.; Saitoh, A.; Naito, T.; Nakayama, K.; Shin, H.-W. (2013): ARF1 and ARF4 regulate recycling endosomal morphology and retrograde transport from endosomes to the Golgi apparatus. *Molecular biology of the cell* 24 (16), pp. 2570–2581.

Nallamsetty, S.; Waugh, D. S. (2006): Solubility-enhancing proteins MBP and NusA play a passive role in the folding of their fusion partners. *Protein expression and purification* 45 (1), pp. 175–182.

Nauck, M. A.; Heimesaat, M. M.; Orskov, C.; Holst, J. J.; Ebert, R.; Creutzfeldt, W. (1993): Preserved incretin activity of glucagon-like peptide 1 [7-36 amide] but not of synthetic human gastric inhibitory polypeptide in patients with type-2 diabetes mellitus. *The Journal of clinical investigation* 91 (1), pp. 301–307.

Navarro, I.; Leibush, B.; Moon, T. W.; Plisetskaya, E. M.; Baños, N.; Méndez, E. et al. (1999): Insulin, insulin-like growth factor-I (IGF-I) and glucagon: the evolution of their receptors. *Comparative biochemistry and physiology. Part B, Biochemistry & molecular biology* 122 (2), pp. 137–153.

Nawrotek, A.; Zeghouf, M.; Cherfils, J. (2016): Allosteric regulation of Arf GTPases and their GEFs at the membrane interface. *Small GTPases* 7 (4), pp. 283–296.

Newton, A. C.; Bootman, M. D.; Scott, J. D. (2016): Second Messengers. *Cold Spring Harbor perspectives in biology* 8 (8).

Oldham, W. M.; Hamm, H. E. (2008): Heterotrimeric G protein activation by G-protein-coupled receptors. *Nature reviews. Molecular cell biology* 9 (1), pp. 60–71.

O'Neal, C. J.; Jobling, M. G.; Holmes, R. K.; Hol, Wim G J (2005): Structural basis for the activation of cholera toxin by human ARF6-GTP. *Science (New York, N.Y.)* 309 (5737), pp. 1093–1096.

Padovani, D.; Folly-Klan, M.; Labarde, A.; Boulakirba, S.; Campanacci, V.; Franco, M. et al. (2014): EFA6 controls Arf1 and Arf6 activation through a negative feedback loop. *Proceedings of the National Academy of Sciences of the United States of America* 111 (34), pp. 12378–12383.

Padovani, D.; Zeghouf, M.; Traverso, J. A.; Giglione, C.; Cherfils, J. (2013): High yield production of myristoylated Arf6 small GTPase by recombinant N-myristoyl transferase. *Small GTPases* 4 (1), pp. 3–8.

PDB (2016): Insulin and Diabetes. Available online at https://cdn.rcsb.org/pdb101/learn/resources/insulin-and-diabetes/insulin-and-diabetes-poster.pdf, checked on 6/10/2017.

Perkins, J. R.; Diboun, I.; Dessailly, B. H.; Lees, J. G.; Orengo, C. (2010): Transient protein-protein interactions: structural, functional, and network properties. *Structure (London, England: 1993)* 18 (10), pp. 1233–1243.

Perperopoulou, F.; Pouliou, F.; Labrou, N. E. (2017): Recent advances in protein engineering and biotechnological applications of glutathione transferases. *Critical reviews in biotechnology*, pp. 1–18.

Peurois, F.; Veyron, S.; Ferrandez, Y.; Ladid, I.; Benabdi, S.; Zeghouf, M. et al. (2017): Characterization of the activation of small GTPases by their GEFs on membranes using artificial membrane tethering. *The Biochemical journal*.

Pierce, M. M.; Raman, C. S.; Nall, B. T. (1999): Isothermal titration calorimetry of protein-protein interactions. *Methods (San Diego, Calif.)* 19 (2), pp. 213–221.

Ponting, C. P.; Phillips, C.; Davies, K. E.; Blake, D. J. (1997): PDZ domains: targeting signalling molecules to sub-membranous sites. *BioEssays: news and reviews in molecular, cellular and developmental biology* 19 (6), pp. 469–479.

Pronk, G. J.; McGlade, J.; Pelicci, G.; Pawson, T.; Bos, J. L. (1993): Insulin-induced phosphorylation of the 46- and 52-kDa Shc proteins. *The Journal of biological chemistry* 268 (8), pp. 5748–5753.

Ramm, G.; Larance, M.; Guilhaus, M.; James, D. E. (2006): A role for 14-3-3 in insulin-stimulated GLUT4 translocation through its interaction with the RabGAP AS160. *The Journal of biological chemistry* 281 (39), pp. 29174–29180.

Randazzo, P. A.; Kahn, R. A. (1994): GTP hydrolysis by ADP-ribosylation factor is dependent on both an ADP-ribosylation factor GTPase-activating protein and acid phospholipids. *The Journal of biological chemistry* 269 (14), pp. 10758–10763.

Remmers, A. E. (1998): Detection and quantitation of heterotrimeric G proteins by fluorescence resonance energy transfer. *Analytical biochemistry* 257 (1), pp. 89–94.

Ren, X.; Farías, G. G.; Canagarajah, B. J.; Bonifacino, J. S.; Hurley, J. H. (2013): Structural basis for recruitment and activation of the AP-1 clathrin adaptor complex by Arf1. *Cell* 152 (4), pp. 755–767.

Renault, L.; Guibert, B.; Cherfils, J. (2003): Structural snapshots of the mechanism and inhibition of a guanine nucleotide exchange factor. *Nature* 426 (6966), pp. 525–530.

Robbe, K.; Antonny, B. (2003): Liposomes in the study of GDP/GTP cycle of Arf and related small G proteins. *Methods in enzymology* 372, pp. 151–166.

Ruderman, N. B.; Kapeller, R.; White, M. F.; Cantley, L. C. (1990): Activation of phosphatidylinositol 3-kinase by insulin. *Proceedings of the National Academy of Sciences of the United States of America* 87 (4), pp. 1411–1415.

Rupp, B. (2009): Biomolecular Crystallography: Principles, Practice, and Application to Structural Biology. 1st. New York: Garland Science.

Russell, R. B.; Breed, J.; Barton, G. J. (1992): Conservation analysis and structure prediction of the SH2 family of phosphotyrosine binding domains. *FEBS letters* 304 (1), pp. 15–20.

Sadowski, I.; Stone, J. C.; Pawson, T. (1986): A noncatalytic domain conserved among cytoplasmic protein-tyrosine kinases modifies the kinase function and transforming activity of Fujinami sarcoma virus P130gag-fps. *Molecular and cellular biology* 6 (12), pp. 4396–4408.

Saltiel, A. R. (2016): Insulin Signaling in the Control of Glucose and Lipid Homeostasis. *Handbook of experimental pharmacology*.

Sanders, C. R.; Landis, G. C. (1995): Reconstitution of membrane proteins into lipid-rich bilayered mixed micelles for NMR studies. *Biochemistry* 34 (12), pp. 4030–4040.

Sanger, F.; Thompson, E. O. P. (1953a): The amino-acid sequence in the glycyl chain of insulin. 1. The identification of lower peptides from partial hydrolysates. *Biochem J* 53 (3), pp. 353–366.

Sanger, F.; Thompson, E. O. P. (1953b): The amino-acid sequence in the glycyl chain of insulin. 2. The investigation of peptides from enzymic hydrolysates. *Biochem J* 53 (3), pp. 366–374.

Sanger, F.; Tuppy, H. (1951a): The amino-acid sequence in the phenylalanyl chain of insulin. 1. The identification of lower peptides from partial hydrolysates. *Biochem J* 49 (4), pp. 463–481.

Sanger, F.; Tuppy, H. (1951b): The amino-acid sequence in the phenylalanyl chain of insulin. 2. The investigation of peptides from enzymic hydrolysates. *Biochem J* 49 (4), pp. 481–490.

Sano, H.; Kane, S.; Sano, E.; Mîinea, C. P.; Asara, J. M.; Lane, W. S. et al. (2003): Insulin-stimulated phosphorylation of a Rab GTPase-activating protein regulates GLUT4 translocation. *The Journal of biological chemistry* 278 (17), pp. 14599–14602.

Saraste, M.; Sibbald, P. R.; Wittinghofer, A. (1990): The P-loop--a common motif in ATP- and GTP-binding proteins. *Trends in biochemical sciences* 15 (11), pp. 430–434.

Sarbassov, D. D.; Guertin, D. A.; Ali, S. M.; Sabatini, D. M. (2005): Phosphorylation and regulation of Akt/PKB by the rictor-mTOR complex. *Science (New York, N.Y.)* 307 (5712), pp. 1098–1101.

Schlessinger, J. (1994): SH2/SH3 signaling proteins. *Current opinion in genetics & development* 4 (1), pp. 25–30.

Seidel, Susanne A I; Dijkman, P. M.; Lea, W. A.; van den Bogaart, Geert; Jerabek-Willemsen, M.; Lazic, A. et al. (2013): Microscale thermophoresis quantifies biomolecular interactions under previously challenging conditions. *Methods (San Diego, Calif.)* 59 (3), pp. 301–315.

Serafini, T.; Orci, L.; Amherdt, M.; Brunner, M.; Kahn, R. A.; Rothman, J. E. (1991): ADP-ribosylation factor is a subunit of the coat of Golgi-derived COP-coated vesicles: a novel role for a GTP-binding protein. *Cell* 67 (2), pp. 239–253.

Shaw, A. S.; Filbert, E. L. (2009): Scaffold proteins and immune-cell signalling. *Nature reviews. Immunology* 9 (1), pp. 47–56.

Shiba, T.; Kawasaki, M.; Takatsu, H.; Nogi, T.; Matsugaki, N.; Igarashi, N. et al. (2003): Molecular mechanism of membrane recruitment of GGA by ARF in lysosomal protein transport. *Nature structural biology* 10 (5), pp. 386–393.

Shome, K.; Vasudevan, C.; Romero, G. (1997): ARF proteins mediate insulin-dependent activation of phospholipase D. *Current biology: CB* 7 (6), pp. 387–396.

Simanshu, D. K.; Nissley, D. V.; McCormick, F. (2017): RAS Proteins and Their Regulators in Human Disease. *Cell* 170 (1), pp. 17–33.

Smith, D. B.; Johnson, K. S. (1988): Single-step purification of polypeptides expressed in Escherichia coli as fusions with glutathione S-transferase. *Gene* 67 (1), pp. 31–40.

Sparrow, L. G.; McKern, N. M.; Gorman, J. J.; Strike, P. M.; Robinson, C. P.; Bentley, J. D.; Ward, C. W. (1997): The disulfide bonds in the C-terminal domains of the human insulin receptor ectodomain. *The Journal of biological chemistry* 272 (47), pp. 29460–29467.

Sprang, S. R. (1997): G protein mechanisms: insights from structural analysis. *Annual review of biochemistry* 66, pp. 639–678.

Stalder, D.; Antonny, B. (2013): Arf GTPase regulation through cascade mechanisms and positive feedback loops. *FEBS letters* 587 (13), pp. 2028–2035.

Stalder, D.; Barelli, H.; Gautier, R.; Macia, E.; Jackson, C. L.; Antonny, B. (2011): Kinetic studies of the Arf activator Arno on model membranes in the presence of Arf effectors suggest control by a positive feedback loop. *The Journal of biological chemistry* 286 (5), pp. 3873–3883.

Stapleton, D.; Balan, I.; Pawson, T.; Sicheri, F. (1999): The crystal structure of an Eph receptor SAM domain reveals a mechanism for modular dimerization. *Nature structural biology* 6 (1), pp. 44–49.

Stetefeld, J.; McKenna, S. A.; Patel, T. R. (2016): Dynamic light scattering: a practical guide and applications in biomedical sciences. *Biophysical reviews* 8 (4), pp. 409–427.

Strålfors, P.; Björgell, P.; Belfrage, P. (1984): Hormonal regulation of hormone-sensitive lipase in intact adipocytes: identification of phosphorylated sites and effects on the phosphorylation by lipolytic hormones and insulin. *Proceedings of the National Academy of Sciences of the United States of America* 81 (11), pp. 3317–3321.

Sugimoto, S.; Wandless, T. J.; Shoelson, S. E.; Neel, B. G.; Walsh, C. T. (1994): Activation of the SH2-containing protein tyrosine phosphatase, SH-PTP2, by phosphotyrosine-containing peptides derived from insulin receptor substrate-1. *The Journal of biological chemistry* 269 (18), pp. 13614–13622.

Sun, X. J.; Crimmins, D. L.; Myers, M. G.; Miralpeix, M.; White, M. F. (1993): Pleiotropic insulin signals are engaged by multisite phosphorylation of IRS-1. *Molecular and cellular biology* 13 (12), pp. 7418–7428.

Sundaresan, N. R.; Pillai, V. B.; Wolfgeher, D.; Samant, S.; Vasudevan, P.; Parekh, V. et al. (2011): The deacetylase SIRT1 promotes membrane localization and activation of Akt and PDK1 during tumorigenesis and cardiac hypertrophy. *Science signaling* 4 (182), pp. ra46.

Tanford, C.; Reynolds, J. A. (1976): Characterization of membrane proteins in detergent solutions. *Biochimica et biophysica acta* 457 (2), pp. 133–170.

Traïkia, M.; Warschawski, D. E.; Recouvreur, M.; Cartaud, J.; Devaux, P. F. (2000): Formation of unilamellar vesicles by repetitive freeze-thaw cycles: characterization by electron microscopy and 31P-nuclear magnetic resonance. *European biophysics journal: EBJ* 29 (3), pp. 184–195.

Traut, T. W. (1994): Physiological concentrations of purines and pyrimidines. *Molecular and cellular biochemistry* 140 (1), pp. 1–22.

Van Valkenburgh, H. A.; Kahn, R. A. (2002): Coexpression of proteins with methionine aminopeptidase and/or N-myristoyltransferase in Escherichia coli to increase acylation and homogeneity of protein preparations. *Methods in enzymology* 344, pp. 186–193.

Vega, F. M.; Ridley, A. J. (2016): The RhoB small GTPase in physiology and disease. *Small GTPases*, pp. 1–10.

Venkateswarlu, K. (2003): Interaction protein for cytohesin exchange factors 1 (IPCEF1) binds cytohesin 2 and modifies its activity. *The Journal of biological chemistry* 278 (44), pp. 43460–43469.

Venkateswarlu, K.; Oatey, P. B.; Tavaré, J. M.; Cullen, P. J. (1998): Insulin-dependent translocation of ARNO to the plasma membrane of adipocytes requires phosphatidylinositol 3-kinase. *Current biology: CB* 8 (8), pp. 463–466.

Vetter, I. R.; Wittinghofer, A. (2001): The guanine nucleotide-binding switch in three dimensions. *Science (New York, N.Y.)* 294 (5545), pp. 1299–1304.

Villar-Palasi, C.; Larner, J. (1960): Insulin-mediated effect on the activity of UDPG-glycogen transglucosylase of muscle. *Biochimica et biophysica acta* 39, pp. 171–173.

Walker, John M. (2005): The proteomics protocols handbook. Totowa, N.J: Humana Press.

Wang, D. S.; Shaw, R.; Winkelmann, J. C.; Shaw, G. (1994): Binding of PH domains of beta-adrenergic receptor kinase and beta-spectrin to WD40/beta-transducin repeat containing regions of the beta-subunit of trimeric G-proteins. *Biochemical and biophysical research communications* 203 (1), pp. 29–35.

Wang, H.-W.; Wang, J.-W. (2017): How cryo-electron microscopy and X-ray crystallography complement each other. *Protein science: a publication of the Protein Society* 26 (1), pp. 32–39.

Ward, C. W.; Lawrence, M. C. (2011): Landmarks in insulin research. *Frontiers in endocrinology* 2, pp. 76.

Ward, C. W.; Menting, J. G.; Lawrence, M. C. (2013): The insulin receptor changes conformation in unforeseen ways on ligand binding: sharpening the picture of insulin receptor activation. *BioEssays: news and reviews in molecular, cellular and developmental biology* 35 (11), pp. 945-54.

Weizhong, Z.; Shuohui, G.; Hanjiao, Q.; Yuhong, M.; Xiaohua, Y.; Jian, C.; Lisen, L. (2011): Inhibition of cytohesin-1 by siRNA leads to reduced IGFR signaling in prostate cancer. *Brazilian journal of medical and biological research = Revista brasileira de pesquisas médicas e biológicas / Sociedade Brasileira de Biofísica … [et al.]* 44 (7), pp. 642–646.

Wennerberg, K.; Rossman, K. L.; Der, C. J. (2005): The Ras superfamily at a glance. *Journal of cell science* 118 (Pt 5), pp. 843–846.

White, M. F.; Maron, R.; Kahn, C. R. (1985): Insulin rapidly stimulates tyrosine phosphorylation of a Mr-185,000 protein in intact cells. *Nature* 318 (6042), pp. 183–186.

WHO; IDF (2006): Definition and diagnosis of diabetes mellitus and intermediate hyperglycaemia. Report of a WHO/IDF consultation.

Wilcox, G. (2005): Insulin and insulin resistance. *The Clinical biochemist. Reviews* 26 (2), pp. 19–39.

Wolf, E.; Kim, P. S.; Berger, B. (1997): MultiCoil: a program for predicting two- and three-stranded coiled coils. *Protein science: a publication of the Protein Society* 6 (6), pp. 1179–1189.

Wong, W.; Scott, J. D. (2004): AKAP signalling complexes: focal points in space and time. *Nature reviews. Molecular cell biology* 5 (12), pp. 959–970.

Wright, M. H.; Heal, W. P.; Mann, D. J.; Tate, E. W. (2010): Protein myristoylation in health and disease. *Journal of chemical biology* 3 (1), pp. 19–35.

Yamaoka, M.; Ishizaki, T.; Kimura, T. (2015): GTP- and GDP-Dependent Rab27a Effectors in Pancreatic Beta-Cells. *Biological & pharmaceutical bulletin* 38 (5), pp. 663–668.

Yu, H.; Rosen, M. K.; Shin, T. B.; Seidel-Dugan, C.; Brugge, J. S.; Schreiber, S. L. (1992): Solution structure of the SH3 domain of Src and identification of its ligand-binding site. *Science (New York, N.Y.)* 258 (5088), pp. 1665–1668.

Zeigerer, A.; McBrayer, M. K.; McGraw, T. E. (2004): Insulin stimulation of GLUT4 exocytosis, but not its inhibition of endocytosis, is dependent on RabGAP AS160. *Molecular biology of the cell* 15 (10), pp. 4406–4415.

Zhang, Y.; So, M.-K.; Loening, A. M.; Yao, H.; Gambhir, S. S.; Rao, J. (2006): HaloTag protein-mediated site-specific conjugation of bioluminescent proteins to quantum dots. *Angewandte Chemie (International ed. in English)* 45 (30), pp. 4936–4940.

Ziogas, A.; Moelling, K.; Radziwill, G. (2005): CNK1 is a scaffold protein that regulates Src-mediated Raf-1 activation. *The Journal of biological chemistry* 280 (25), pp. 24205–24211.

Appendix

Protein sequences

IR-ICD (aa 953-1355, IR-B numbering w/o signal sequence)

```
MSHHHHHHEN LYFQGARKRQ PDGPLGPLYA SSNPEYLSAS DVFPCSVYVP DEWEVSREKI TLLRELGQGS
FGMVYEGNAR DIIKGEAETR VAVKTVNESA SLRERIEFLN EASVMKGFTC HHVVRLLGVV SKGQPTLVVM
ELMAHGDLKS YLRSLRPEAE NNPGRPPPTL QEMIQMAAEI ADGMAYLNAK KFVHRDLAAR NCMVAHDFTV
KIGDFGMTRD IYETDYYRKG GKGLLPVRWM APESLKDGVF TTSSDMWSFG VVLWEITSLA EQPYQGLSNE
QVLKFVMDGG YLDQPDNCPE RVTDLMRMCW QFNPKMRPTF LEIVNLLKDD LHPSFPEVSF FHSEENKAPE
SEELEMEFED MENVPLDRSS HCQREEAGGR DGGSSLGFKR SYEEHIPYTH MNGGKKNGRI LTLPRSNPS
```

IR-KC (aa 978-1283, IR-B numbering w/o signal sequence)

```
MSHHHHHHEN LYFQGAVFPS SVYVPDEWEV SREKITLLRE LGQGSFGMVY EGNARDIIKG EAETRVAVKT
VNESASLRER IEFLNEASVM KGFTCHHVVR LLGVVSKGQP TLVVMELMAH GDLKSYLRSL RPEAENNPGR
PPPTLQEMIQ MAAEIADGMA YLNAKKFVHR DLAARNCMVA HDFTVKIGDF GMTRDIYETD YYRKGGKGLL
PVRWMAPESL KDGVFTTSSD MWSFGVVLWE ITSLAEQPYQ GLSNEQVLKF VMDGGYLDQP DNCPERVTDL
MRMCWQFNPK MRPTFLEIVN LLKDDLHPSF PEVSFFHSEE NK
```

ARNO

```
MASRGSHHHH HHGAGDRGPE FENLYFQSET EDGVYEPPDL TPEERMELEN IRRRKQELLV EIQRLREELS
EAMSEVEGLE ANEGSKTLQR NRKMAMGRKK FNMDPKKGIQ FLVENELLQN TPEEIARFLY KGEGLNKTAI
GDYLGEREEL NLAVLHAFVD LHEFTDLNLV QALRQFLWSF RLPGEAQKID RMMEAFAQRY CLCNPGVFQS
TDTCYVLSFA VIMLNTSLHN PNVRDKPGLE RFVAMNRGIN EGGDLPEELL RNLYDSIRNE PFKIPEDDGN
DLTHTFFNPD REGWLLKLGG GRVKTWKRRW FILTDNCLYY FEYTTDKEPR GIIPLENLSI REVDDPRKPN
CFELYIPNNK GQLIKACKTE ADGRVVEGNH MVYRISAPTQ EEKDEWIKSI QAAVSVDPFY EMLAARKKRI
SVKKKQEQP
```

ARNOΔpbr (aa 2-378)

```
MASRGSHHHH HHGAGDRGPE FENLYFQSET EDGVYEPPDL TPEERMELEN IRRRKQELLV EIQRLREELS
EAMSEVEGLE ANEGSKTLQR NRKMAMGRKK FNMDPKKGIQ FLVENELLQN TPEEIARFLY KGEGLNKTAI
GDYLGEREEL NLAVLHAFVD LHEFTDLNLV QALRQFLWSF RLPGEAQKID RMMEAFAQRY CLCNPGVFQS
TDTCYVLSFA VIMLNTSLHN PNVRDKPGLE RFVAMNRGIN EGGDLPEELL RNLYDSIRNE PFKIPEDDGN
DLTHTFFNPD REGWLLKLGG GRVKTWKRRW FILTDNCLYY FEYTTDKEPR GIIPLENLSI REVDDPRKPN
CFELYIPNNK GQLIKACKTE ADGRVVEGNH MVYRISAPTQ EEKDEWIKSI QAAVSVD
```

ARNO-PH (aa 261-378)

```
MGSHHHHHHE NLYFQGSGSD REGWLLKLGG GRVKTWKRRW FILTDNCLYY FEYTTDKEPR GIIPLENLSI
REVDDPRKPN CFELYIPNNK GQLIKACKTE ADGRVVEGNH MVYRISAPTQ EEKDEWIKSI QAAVSVD
```

ARNO-Sec7 (aa 61-246)

```
MGSHHHHHHE NLYFQGSRNR KMAMGRKKFN MDPKKGIQFL VENELLQNTP EEIARFLYKG EGLNKTAIGD
YLGEREELNL AVLHAFVDLH EFTDLNLVQA LRQFLWSFRL PGEAQKIDRM MEAFAQRYCL CNPGVFQSTD
TCYVLSFAVI MLNTSLHNPN VRDKPGLERF VAMNRGINEG GDLPEELLRN LYDSIRNEPF KIP
```

ARNO-cc-Sec7 (aa 2-246)

```
MASRGSHHHH HHGAGDRGPE FENLYFQSET EDGVYEPPDL TPEERMELEN IRRRKQELLV EIQRLREELS
EAMSEVEGLE ANEGSKTLQR NRKMAMGRKK FNMDPKKGIQ FLVENELLQN TPEEIARFLY KGEGLNKTAI
GDYLGEREEL NLAVLHAFVD LHEFTDLNLV QALRQFLWSF RLPGEAQKID RMMEAFAQRY CLCNPGVFQS
TDTCYVLSFA VIMLNTSLHN PNVRDKPGLE RFVAMNRGIN EGGDLPEELL RNLYDSIRNE PFKIP
```

CNK1

```
MSHHHHHHEN LYFQGSMEPV ETWTPGKVAT WLRGLDDSLQ DYPFEDWQLP GKNLLQLCPQ SLEALAVRSL
GHQELILGGV EQLQALSSRL QTENLQSLTE GLLGATHDFQ SIVQGCLGDC AKTPIDVLCA AVELLHEADA
LLFWLSRYLF SHLNDFSACQ EIRDLLEELS QVLHEDGPAA EKEGTVLRIC SHVAGICHNI LVCCPKELLE
QKAVLEQVQL DSPLGLEIHT TSNCQHFVSQ VDTQVPTDSR LQIQPGDEVV QINEQVVVGW PRKNMVRELL
REPAGLSLVL KKIPIPETPP QTPPQVLDSP HQRSPSLSLA PLSPRAPSED VFAFDLSSNP SPGPSPAWTD
SASLGPEPLP IPPEPPAILP AGVAGTPGLP ESPDKSPVGR KKSKGLATRL SRRRVSCREL GRPDCDGWLL
LRKAPGGFMG PRWRRRWFVL KGHTLYWYRQ PQDEKAEGLI NVSNYSLESG HDQKKKYVFQ LTHDVYKPFI
FAADTLTDLS MWVRHLITCI SKYQSPGRAP PPREEDCYSE TEAEDPDDEA GSHSASPSPA QAGSPLHGDT
SPAATPTQRS PRTSFGSLTD SSEEALEGMV RGLRQGGVSL LGQPQPLTQE QWRSSFMRCN RDPQLNERVH
RVRALQSTLK AKLQELQVLE EVLGDPELTG EKFRQWKEQN RELYSEGLGA WGVAQAEGSS HILTSDSTEQ
SPNSLPSDPE EHSHLCPLTS ESSLRPPDL
```

CNK1$_{K414Q}$

```
MSHHHHHHEN LYFQGSMEPV ETWTPGKVAT WLRGLDDSLQ DYPFEDWQLP GKNLLQLCPQ SLEALAVRSL
GHQELILGGV EQLQALSSRL QTENLQSLTE GLLGATHDFQ SIVQGCLGDC AKTPIDVLCA AVELLHEADA
LLFWLSRYLF SHLNDFSACQ EIRDLLEELS QVLHEDGPAA EKEGTVLRIC SHVAGICHNI LVCCPKELLE
QKAVLEQVQL DSPLGLEIHT TSNCQHFVSQ VDTQVPTDSR LQIQPGDEVV QINEQVVVGW PRKNMVRELL
REPAGLSLVL KKIPIPETPP QTPPQVLDSP HQRSPSLSLA PLSPRAPSED VFAFDLSSNP SPGPSPAWTD
SASLGPEPLP IPPEPPAILP AGVAGTPGLP ESPDKSPVGR KKSKGLATRL SRRRVSCREL GRPDCDGWLL
LRQAPGGFMG PRWRRRWFVL KGHTLYWYRQ PQDEKAEGLI NVSNYSLESG HDQKKKYVFQ LTHDVYKPFI
FAADTLTDLS MWVRHLITCI SKYQSPGRAP PPREEDCYSE TEAEDPDDEA GSHSASPSPA QAGSPLHGDT
SPAATPTQRS PRTSFGSLTD SSEEALEGMV RGLRQGGVSL LGQPQPLTQE QWRSSFMRCN RDPQLNERVH
RVRALQSTLK AKLQELQVLE EVLGDPELTG EKFRQWKEQN RELYSEGLGA WGVAQAEGSS HILTSDSTEQ
SPNSLPSDPE EHSHLCPLTS ESSLRPPDL
```

CNK1Δcc (aa 615-646 deleted)

```
MSHHHHHHEN LYFQGSMEPV ETWTPGKVAT WLRGLDDSLQ DYPFEDWQLP GKNLLQLCPQ SLEALAVRSL
GHQELILGGV EQLQALSSRL QTENLQSLTE GLLGATHDFQ SIVQGCLGDC AKTPIDVLCA AVELLHEADA
LLFWLSRYLF SHLNDFSACQ EIRDLLEELS QVLHEDGPAA EKEGTVLRIC SHVAGICHNI LVCCPKELLE
QKAVLEQVQL DSPLGLEIHT TSNCQHFVSQ VDTQVPTDSR LQIQPGDEVV QINEQVVVGW PRKNMVRELL
REPAGLSLVL KKIPIPETPP QTPPQVLDSP HQRSPSLSLA PLSPRAPSED VFAFDLSSNP SPGPSPAWTD
SASLGPEPLP IPPEPPAILP AGVAGTPGLP ESPDKSPVGR KKSKGLATRL SRRRVSCREL GRPDCDGWLL
LRKAPGGFMG PRWRRRWFVL KGHTLYWYRQ PQDEKAEGLI NVSNYSLESG HDQKKKYVFQ LTHDVYKPFI
FAADTLTDLS MWVRHLITCI SKYQSPGRAP PPREEDCYSE TEAEDPDDEA GSHSASPSPA QAGSPLHGDT
SPAATPTQRS PRTSFGSLTD SSEEALEGMV RGLRQGGVSL LGQPQPLTQE QWRSSFMRCN RDPPELTGEK
FRQWKEQNRE LYSEGLGAWG VAQAEGSSHI LTSDSTEQSP NSLPSDPEEH SHLCPLTSES SLRPPDL
```

NΔ17ARF1 (aa 18-181)

```
MGSSHHHHHH SSGLVPRGSH MCMRILMVGL DAAGKTTILY KLKLGEIVTT IPTIGFNVET VEYKNISFTV
WDVGGQDKIR PLWRHYFQNT QGLIFVVDSN DRERVNEARE ELMRMLAEDE LRDAVLLVFA NKQDLPNAMN
AAEITDKLGL HSLRHRNWYI QATCATSGDG LYEGLDWLSN QLRNQK
```

ARF6 (*in vitro* myristoylated)

```
MGKVLSKIFG NKEMRILMLG LDAAGKTTIL YKLKLGQSVT TIPTVGFNVE TVTYKNVKFN VWDVGGQDKI
RPLWRHYYTG TQGLIFVVDC ADRDRIDEAR QELHRIINDR EMRDAIILIF ANKQDLPDAM KPHEIQEKLG
LTRIRDRNWY VQPSCATSGD GLYEGLTWLT SNYKHHHHHH
```

N-myristoyltransferase (NMT)

```
MGSHHHHHHE NLYFQGSMNS LPAERIQEIQ KAIELFSVGQ GPAKTMEEAS KRSYQFWDTQ PVPKLGEVVN
THGPVEPDKD NIRQEPYTLP QGFTWDALDL GDRGVLKELY TLLNENYVED DDNMFRFDYS PEFLLWALRP
PGWLPQWHCG VRVVSSRKLV GFISAIPANI HIYDTEKKMV EINFLCVHKK LRSKRVAPVL IREITRRVHL
EGIFQAVYTA GVVLPKPVGT CRYWHRSLNP RKLIEVKFSH LSRNMTMQRT MKLYRLPETP KTAGLRPMET
KDIPVVHQLL TRYLKQFHLT PVMSQEEVEH WFYPQENIID TFVVENANGE VTDFLSFYTL PSTIMNHPTH
KSLKAAYSFY NVHTQTPLLD LMSDALVLAK MKGFDVFNAL DLMENKTFLE KLKFGIGDGN LQYYLYNWKC
PSMGAEKVGL VLQ
```

ARF1 (*in vivo* myristoylated)

```
MGNIFANLFK GLFGKKEMRI LMVGLDAAGK TTILYKLKLG EIVTTIPTIG FNVETVEYKN ISFTVWDVGG
QDKIRPLWRH YFQNTQGLIF VVDSNDRERV NEAREELMRM LAEDELRDAV LLVFANKQDL PNAMNAAEIT
DKLGLHSLRH RNWYIQATCA TSGDGLYEGL DWLSNQLRNQ K
```

GST

```
MSPILGYWKI KGLVQPTRLL LEYLEEKYEE HLYERDEGDK WRNKKFELGL EFPNLPYYID GDVKLTQSMA
IIRYIADKHN MLGGCPKERA EISMLEGAVL DIRYGVSRIA YSKDFETLKV DFLSKLPEML KMFEDRLCHK
TYLNGDHVTH PDFMLYDALD VVLYMDPMCL DAFPKLVCFK KRIEAIPQID KYLKSSKYIA WPLQGWQATF
GGGDHPPKSD LEVLFQGPLG S
```

GST-IR-ICD (aa 953-1355, IR-B numbering w/o signal sequence)

```
MSPILGYWKI KGLVQPTRLL LEYLEEKYEE HLYERDEGDK WRNKKFELGL EFPNLPYYID GDVKLTQSMA
IIRYIADKHN MLGGSPKERA EISMLEGAVL DIRYGVSRIA YSKDFETLKV DFLSKLPEML KMFEDRLSHK
TYLNGDHVTH PDFMLYDALD VVLYMDPMSL DAFPKLVSFK KRIEAIPQID KYLKSSKYIA WPLQGWQATF
GGGDHPPKSG GGSGGGSGGG LEVLFQGPGS RKRQPDGPLG PLYASSNPEY LSASDVFPCS VYVPDEWEVS
REKITLLREL GQGSFGMVYE GNARDIIKGE AETRVAVKTV NESASLRERI EFLNEASVMK GFTCHHVVRL
LGVVSKGQPT LVVMELMAHG DLKSYLRSLR PEAENNPGRP PPTLQEMIQM AAEIADGMAY LNAKKFVHRD
LAARNCMVAH DFTVKIGDFG MTRDIYETDY YRKGGKGLLP VRWMAPESLK DGVFTTSSDM WSFGVVLWEI
TSLAEQPYQG LSNEQVLKFV MDGGYLDQPD NCPERVTDLM RMCWQFNPKM RPTFLEIVNL LKDDLHPSFP
EVSFFHSEEN KAPESEELEM EFEDMENVPL DRSSHCQREE AGGRDGGSSL GFKRSYEEHI PYTHMNGGKK
NGRILTLPRS NPS
```

GST-ARNO

```
MSPILGYWKI KGLVQPTRLL LEYLEEKYEE HLYERDEGDK WRNKKFELGL EFPNLPYYID GDVKLTQSMA
IIRYIADKHN MLGGCPKERA EISMLEGAVL DIRYGVSRIA YSKDFETLKV DFLSKLPEML KMFEDRLCHK
TYLNGDHVTH PDFMLYDALD VVLYMDPMCL DAFPKLVCFK KRIEAIPQID KYLKSSKYIA WPLQGWQATF
GGGDHPPKSD LEVLFQGPLG SMEDGVYEPP DLTPEERMEL ENIRRRKQEL LVEIQRLREE LSEAMSEVEG
LEANEGSKTL QRNRKMAMGR KKFNMDPKKG IQFLVENELL QNTPEEIARF LYKGEGLNKT AIGDYLGERE
ELNLAVLHAF VDLHEFTDLN LVQALRQFLW SFRLPGEAQK IDRMMEAFAQ RYCLCNPGVF QSTDTCYVLS
FAVIMLNTSL HNPNVRDKPG LERFVAMNRG INEGGDLPEE LLRNLYDSIR NEPFKIPEDD GNDLTHTFFN
PDREGWLLKL GGGRVKTWKR RWFILTDNCL YYFEYTTDKE PRGIIPLENL SIREVDDPRK PNCFELYIPN
NKGQLIKACK TEADGRVVEG NHMVYRISAP TQEEKDEWIK SIQAAVSVDP FYEMLAARKK RISVKKKQEQ
P
```

GST-ARNOΔcc (aa 61-400)

```
MSPILGYWKI KGLVQPTRLL LEYLEEKYEE HLYERDEGDK WRNKKFELGL EFPNLPYYID GDVKLTQSMA
IIRYIADKHN MLGGCPKERA EISMLEGAVL DIRYGVSRIA YSKDFETLKV DFLSKLPEML KMFEDRLCHK
TYLNGDHVTH PDFMLYDALD VVLYMDPMCL DAFPKLVCFK KRIEAIPQID KYLKSSKYIA WPLQGWQATF
GGGDHPPKSD LEVLFQGPLG SRNRKMAMGR KKFNMDPKKG IQFLVENELL QNTPEEIARF LYKGEGLNKT
AIGDYLGERE ELNLAVLHAF VDLHEFTDLN LVQALRQFLW SFRLPGEAQK IDRMMEAFAQ RYCLCNPGVF
QSTDTCYVLS FAVIMLNTSL HNPNVRDKPG LERFVAMNRG INEGGDLPEE LLRNLYDSIR NEPFKIPEDD
GNDLTHTFFN PDREGWLLKL GGGRVKTWKR RWFILTDNCL YYFEYTTDKE PRGIIPLENL SIREVDDPRK
PNCFELYIPN NKGQLIKACK TEADGRVVEG NHMVYRISAP TQEEKDEWIK SIQAAVSVDP FYEMLAARKK
RISVKKKQEQ P
```

GST-ARNO-cc (aa 1-60)

```
MSPILGYWKI KGLVQPTRLL LEYLEEKYEE HLYERDEGDK WRNKKFELGL EFPNLPYYID GDVKLTQSMA
IIRYIADKHN MLGGCPKERA EISMLEGAVL DIRYGVSRIA YSKDFETLKV DFLSKLPEML KMFEDRLCHK
TYLNGDHVTH PDFMLYDALD VVLYMDPMCL DAFPKLVCFK KRIEAIPQID KYLKSSKYIA WPLQGWQATF
GGGDHPPKSD LEVLFQGPLG SMEDGVYEPP DLTPEERMEL ENIRRRKQEL LVEIQRLREE LSEAMSEVEG
LEANEGSKTL Q
```

Halo

```
MGSHHHHHHE NLYFQSELMA EIGTGFPFDP HYVEVLGERM HYVDVGPRDG TPVLFLHGNP TSSYVWRNII
PHVAPTHRCI APDLIGMGKS DKPDLGYFFD DHVRFMDAFI EALGLEEVVL VIHDWGSALG FHWAKRNPER
VKGIAFMEFI RPIPTWDEWP EFARETFQAF RTTDVGRKLI IDQNVFIEGT LPMGVVRPLT EVEMDHYREP
FLNPVDREPL WRFPNELPIA GEPANIVALV EEYMDWLHQS PVPKLLFWGT PGVLIPPAEA ARLAKSLPNC
KAVDIGPGLN LLQEDNPDLI GSEIARWLST LEISGEPTTL VPRGSG
```

Halo-ARNO

```
MGSHHHHHHE NLYFQSELMA EIGTGFPFDP HYVEVLGERM HYVDVGPRDG TPVLFLHGNP TSSYVWRNII
PHVAPTHRCI APDLIGMGKS DKPDLGYFFD DHVRFMDAFI EALGLEEVVL VIHDWGSALG FHWAKRNPER
VKGIAFMEFI RPIPTWDEWP EFARETFQAF RTTDVGRKLI IDQNVFIEGT LPMGVVRPLT EVEMDHYREP
FLNPVDREPL WRFPNELPIA GEPANIVALV EEYMDWLHQS PVPKLLFWGT PGVLIPPAEA ARLAKSLPNC
KAVDIGPGLN LLQEDNPDLI GSEIARWLST LEISGEPTTL VPRGSMEDGV YEPPDLTPEE RMELENIRRR
KQELLVEIQR LREELSEAMS EVEGLEANEG SKTLQRNRKM AMGRKKFNMD PKKGIQFLVE NELLQNTPEE
IARFLYKGEG LNKTAIGDYL GEREELNLAV LHAFVDLHEF TDLNLVQALR QFLWSFRLPG EAQKIDRMME
AFAQRYCLCN PGVFQSTDTC YVLSFAVIML NTSLHNPNVR DKPGLERFVA MNRGINEGGD LPEELLRNLY
DSIRNEPFKI PEDDGNDLTH TFFNPDREGW LLKLGGGRVK TWKRRWFILT DNCLYYFEYT TDKEPRGIIP
LENLSIREVD DPRKPNCFEL YIPNNKGQLI KACKTEADGR VVEGNHMVYR ISAPTQEEKD EWIKSIQAAV
SVDPFYEMLA ARKKRISVKK KQEQP
```

MBP-IR-CT (aa 1278-1355, IR-B numbering w/o signal sequence)

```
MAMKIEEGKL VIWINGDKGY NGLAEVGKKF EKDTGIKVTV EHPDKLEEKF PQVAATGDGP DIIFWAHDRF
GGYAQSGLLA EITPDKAFQD KLYPFTWDAV RYNGKLIAYP IAVEALSLIY NKDLLPNPPK TWEEIPALDK
ELKAKGKSAL MFNLQEPYFT WPLIAADGGY AFKYENGKYD IKDVGVDNAG AKAGLTFLVD LIKNKHMNAD
TDYSIAEAAF NKGETAMTIN GPWAWSNIDT SKVNYGVTVL PTFKGQPSKP FVGVLSAGIN AASPNKELAK
EFLENYLLTD EGLEAVNKDK PLGAVALKSY EEELAKDPRI AATMENAQKG EIMPNIPQMS AFWYAVRTAV
INAASGRQTV DEALKDAQTS SGENLYFQGS HSEENKAPES EELEMEFEDM ENVPLDRSSH CQREEAGGRD
GGSSLGFKRS YEEHIPYTHM NGGKKNGRIL TLPRSNPS
```

MBP-CNK1-cc (aa 601-660)

```
MAMKIEEGKL VIWINGDKGY NGLAEVGKKF EKDTGIKVTV EHPDKLEEKF PQVAATGDGP DIIFWAHDRF
GGYAQSGLLA EITPDKAFQD KLYPFTWDAV RYNGKLIAYP IAVEALSLIY NKDLLPNPPK TWEEIPALDK
ELKAKGKSAL MFNLQEPYFT WPLIAADGGY AFKYENGKYD IKDVGVDNAG AKAGLTFLVD LIKNKHMNAD
TDYSIAEAAF NKGETAMTIN GPWAWSNIDT SKVNYGVTVL PTFKGQPSKP FVGVLSAGIN AASPNKELAK
EFLENYLLTD EGLEAVNKDK PLGAVALKSY EEELAKDPRI AATMENAQKG EIMPNIPQMS AFWYAVRTAV
INAASGRQTV DEALKDAQTS SGENLYFQGS EQWRSSFMRC NRDPQLNERV HRVRALQSTL KAKLQELQVL
EEVLGDPELT GEKFRQWKEQ
```

Overview of all purified proteins

In order to show the purity of all proteins used in this study, approximately 1 µg of the proteins were applied to SDS-PAGE and stained with Coomassie blue (supporting fig. A-1).

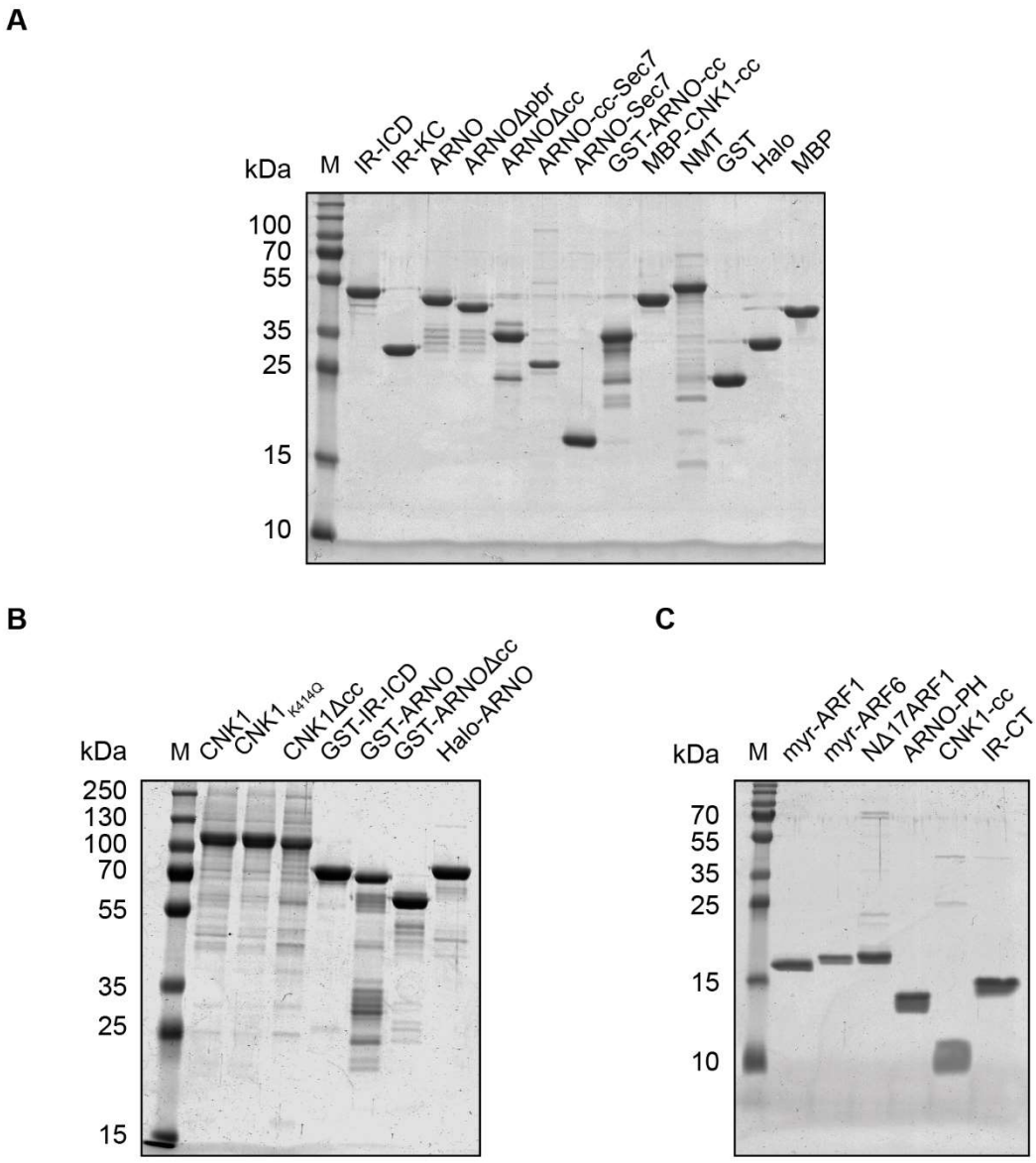

Supp. fig. A-1: Overview of all purified proteins. Approximately 1µg of the proteins were applied to SDS-PAGE and stained with Coomassie blue. **A** | 12.5 % SDS-PAGE, **B** | 10 % SDS-PAGE, **C** | 15 % SDS-PAGE.

Influence of $CNK1_{K414Q}$ on ARNO/myr-ARF1 exchange

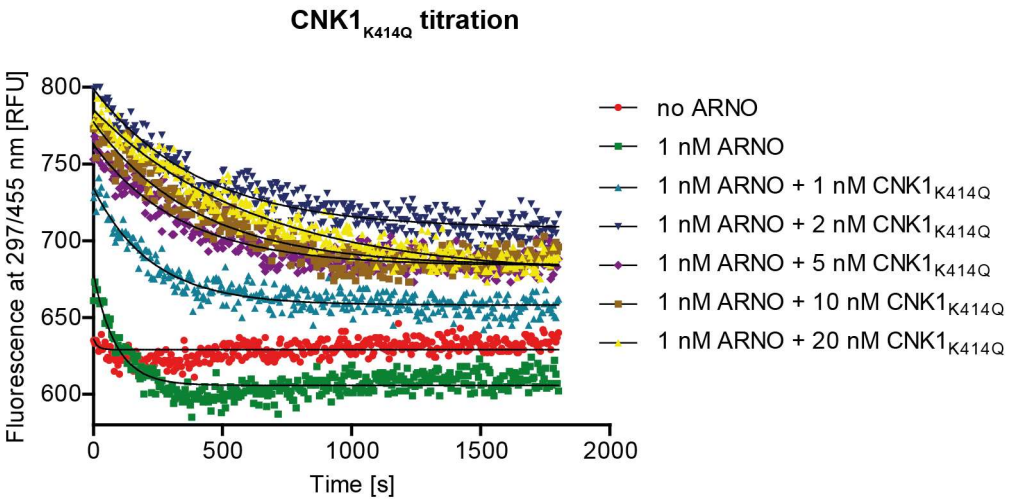

Supp. fig. A-2: $CNK1_{K414Q}$ does not enhance ARNO exchange on myr-ARF1. 400 nM myr-ARF1 was pre-loaded with 1 µM Mant-GDP. The exchange reaction in presence of liposomes (2 % PIP_2, 200 µM total lipid concentration) and 100 µM GTP was initiated by the addition of 1 nM ARNO or mixtures of 1 nM ARNO and the indicated $CNK1_{K414Q}$ concentrations. The reaction was performed at 37 °C and monitored by the decreasing Mant-FRET signal. The black lines show the mono-exponential fits of the data assuming pseudo-first order kinetics.

DLS analysis of liposomes containing DGS-NTA(Ni)

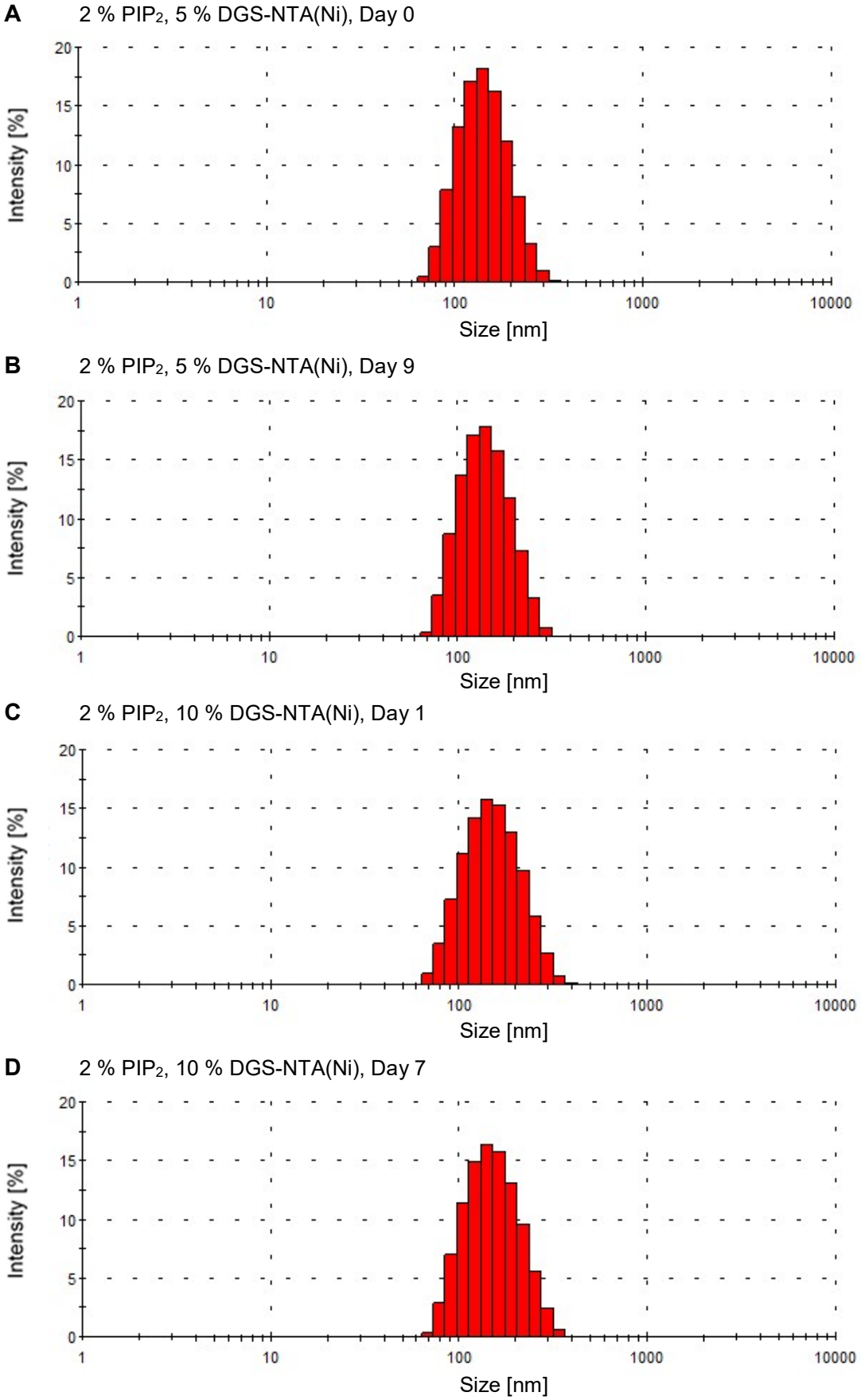

Supp. fig. A-3: DLS analysis of liposomes containing DGS-NTA(Ni). Description on next page.

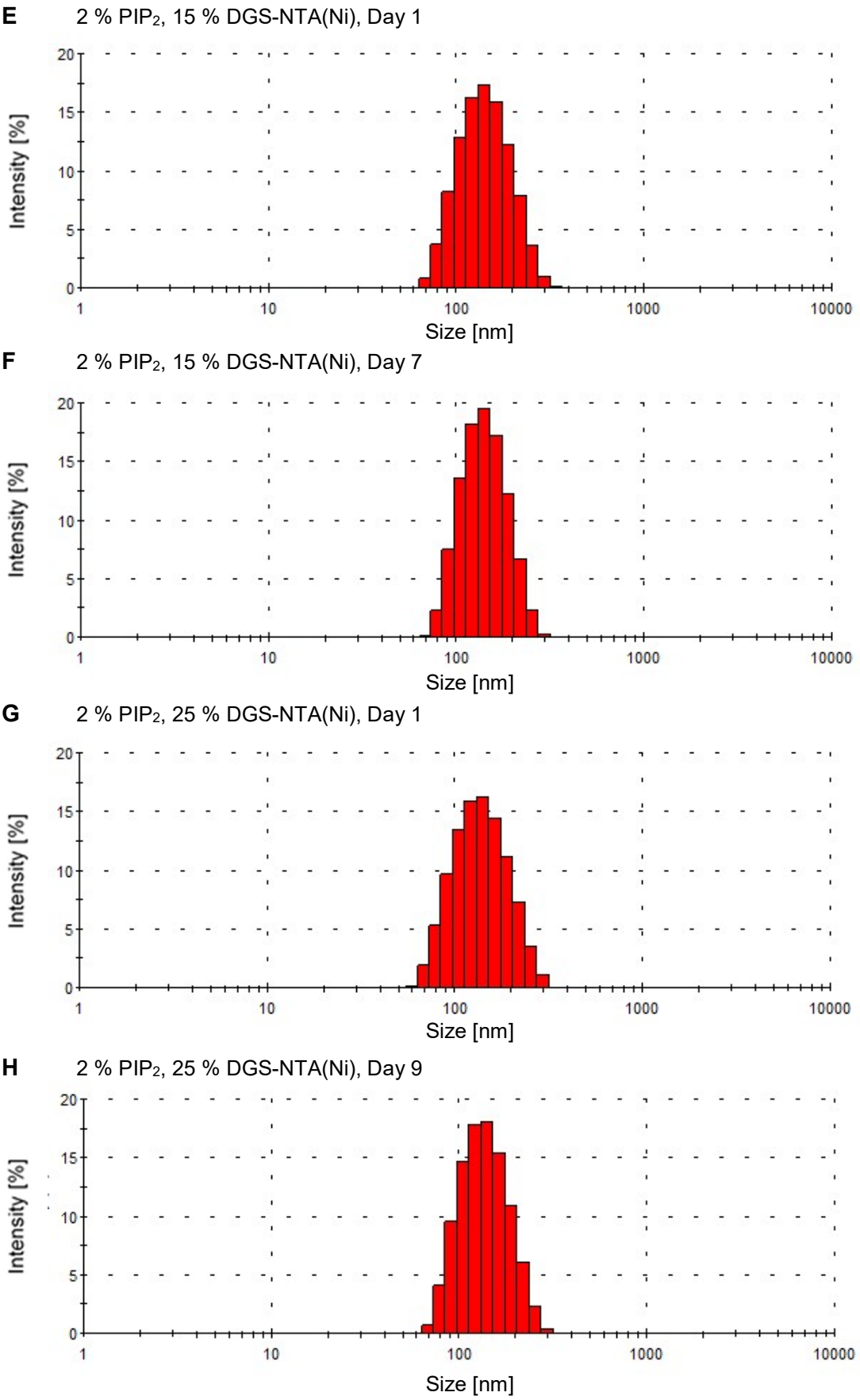

Supp. fig. A-3: DLS analysis of liposomes containing DGS-NTA(Ni). The prepared liposomes were diluted 1:100 and measured in the DLS Zetasizer nano Series S. The averages of 3 measurements, each consisting of 15 runs of the same sample are shown in the intensity representation.

Original Coomassie stained SDS gels and western blots

All Coomassie stained SDS gels as well as western blots, which are depicted in a cropped version in the results part, are shown completely here. Gels and western blots, which are depicted fully in the results section, are not shown again. The same applies to gels and western blots, where only empty lanes at the left or right gel/blot edges were cut.

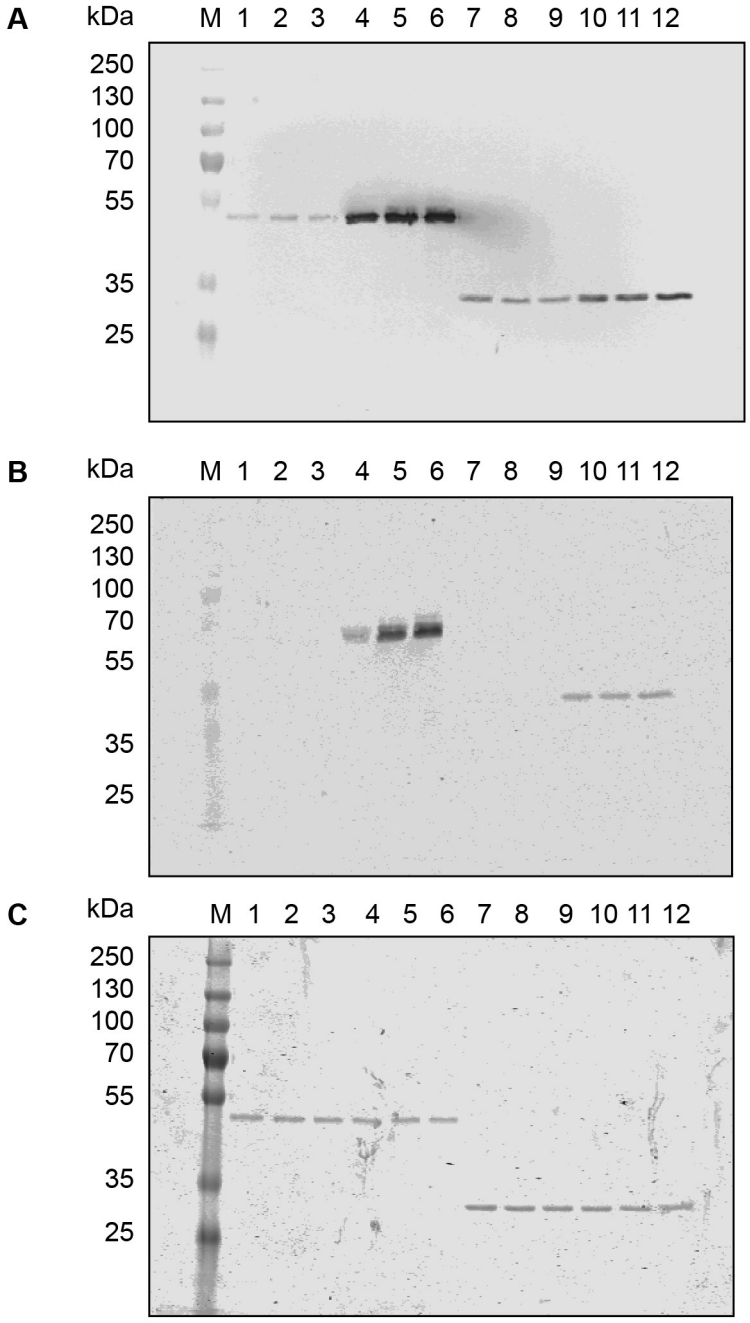

Supp. fig. A-4: IR-ICD and ARNO are catalytically active, unmodified original of figure 3-1. **A** | Lanes 1-6 correspond to the lanes shown in the results part, α-pY. **B** | Lanes 1-6 correspond to the lanes shown in the results part, α-pY1162/1163. **C** | Lanes 1-6 correspond to the lanes shown in the results part, Coomassie stain.

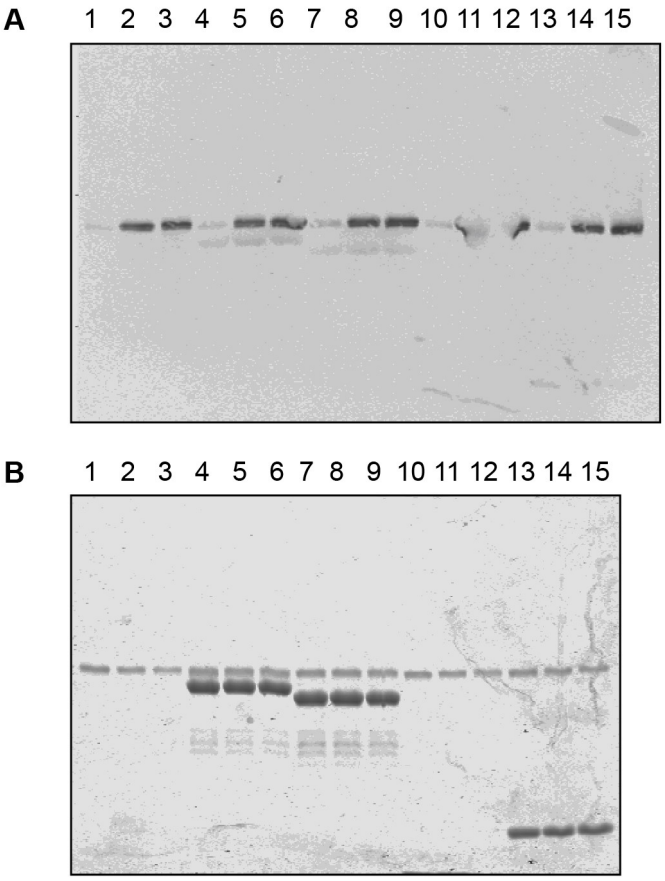

Supp. fig. A-5: IR-ICD autophosphorylation remains constant upon ARNO addition, unmodified original of figure 3-2. A | Lanes 1-9 correspond to the lanes shown in the results part, α-pY. **B** | Lanes 1-9 correspond to the lanes shown in the results part, Coomassie stain.

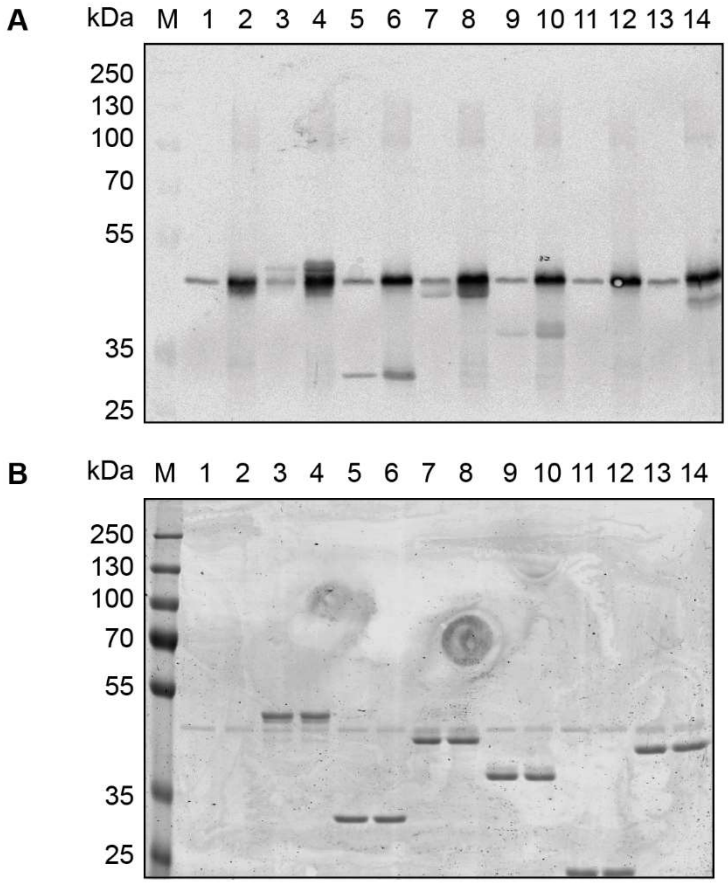

Supp. fig. A-6: Label transfer suggests interaction between ARNO and IR-ICD, unmodified original of figure 3-3. A | Lanes 1-6 and 13-14 correspond to the lanes shown in the results part, streptavidin blot. **B** | Lanes 1-6 and 13-14 correspond to the lanes shown in the results part, Coomassie stain. Since fig. 3-3 B contains uncropped pictures, no additional figure is shown here.

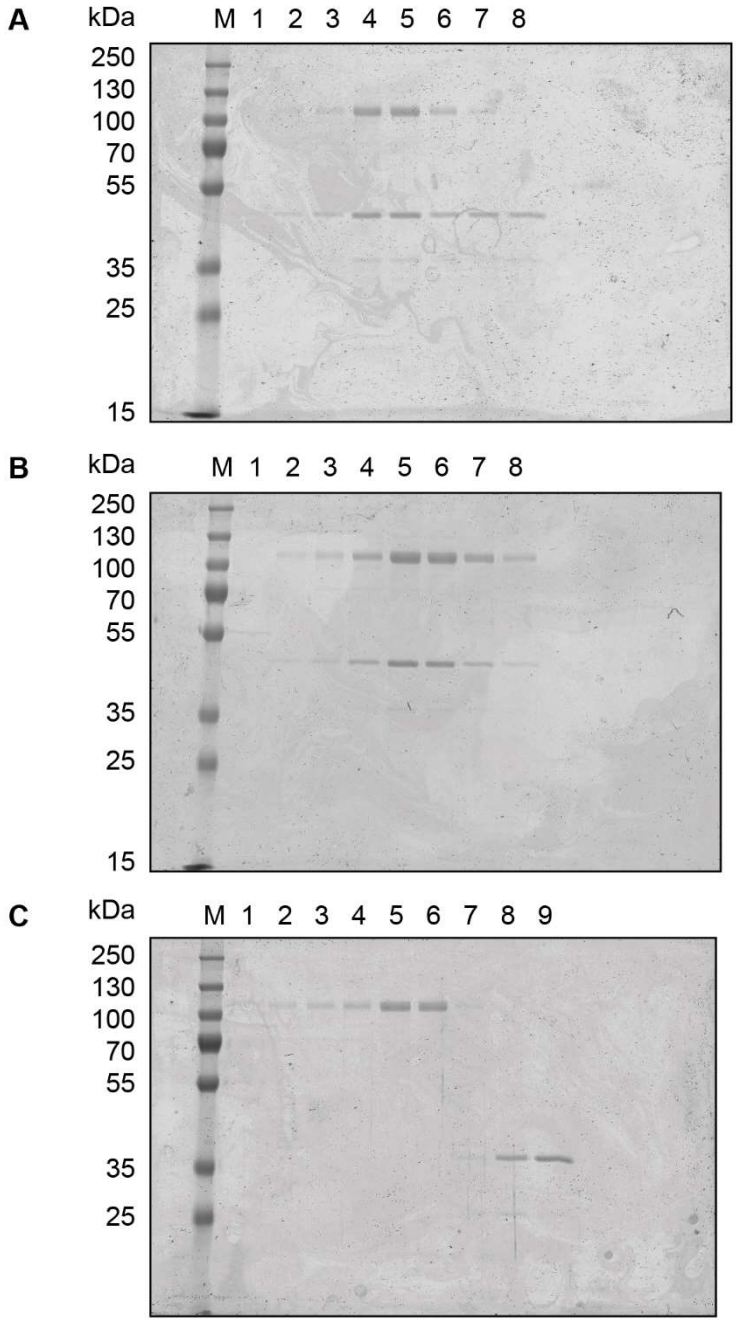

Supp. fig. A-7: Analytical SEC confirms the interaction of ARNO and CNK1, unmodified original of figure 3-12. A | Lanes 1-8 correspond to the lanes shown in the results part, 7.5 µM ARNO + 7.5 µM CNK1, Coomassie blue stain. **B** | Lanes 1-8 correspond to the lanes shown in the results part, 7.5 µM ARNO + 15 µM CNK1, Coomassie blue stain. **C** | Lanes 1-9 correspond to the lanes shown in the results part, 7.5 µM ARNOΔcc + 7.5 µM CNK1, Coomassie blue stain.

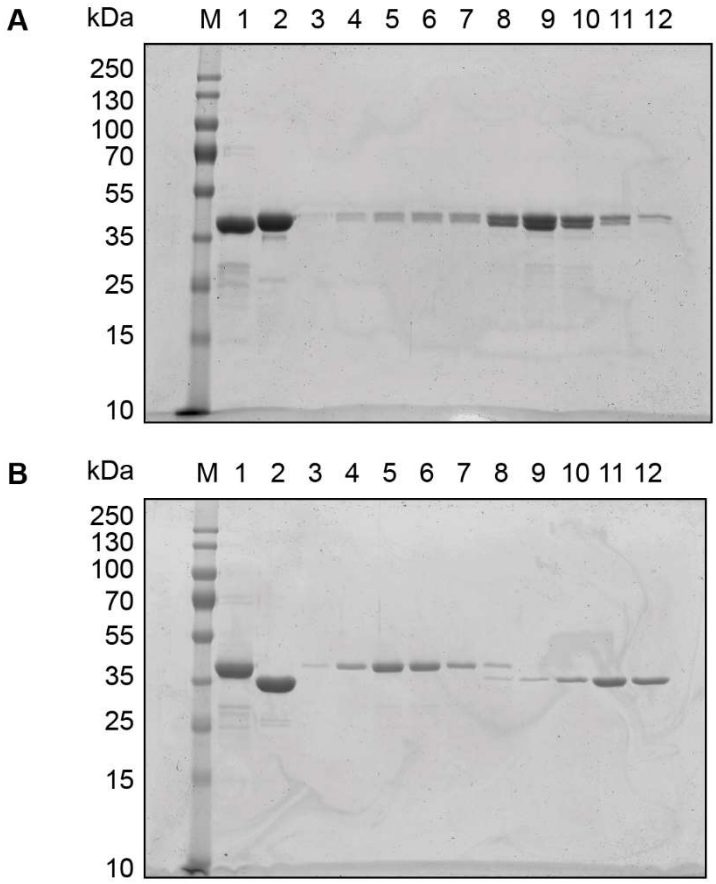

Supp. fig. A-8: Analytical SEC confirms that the CNK1 cc domain is sufficient for ARNO interaction, unmodified original of figure 3-13. A | Lanes 3-12 correspond to the lanes shown in the results part, MBP-CNK1-cc/ARNO interaction. Lane 1 shows an ARNO sample, lane 2 an MBP-CNK1-cc sample. **B** | Lanes 3-12 correspond to the lanes shown in the results part, MBP/ARNO interaction. Lane 1 shows an ARNO sample, lane 2 an MBP sample.

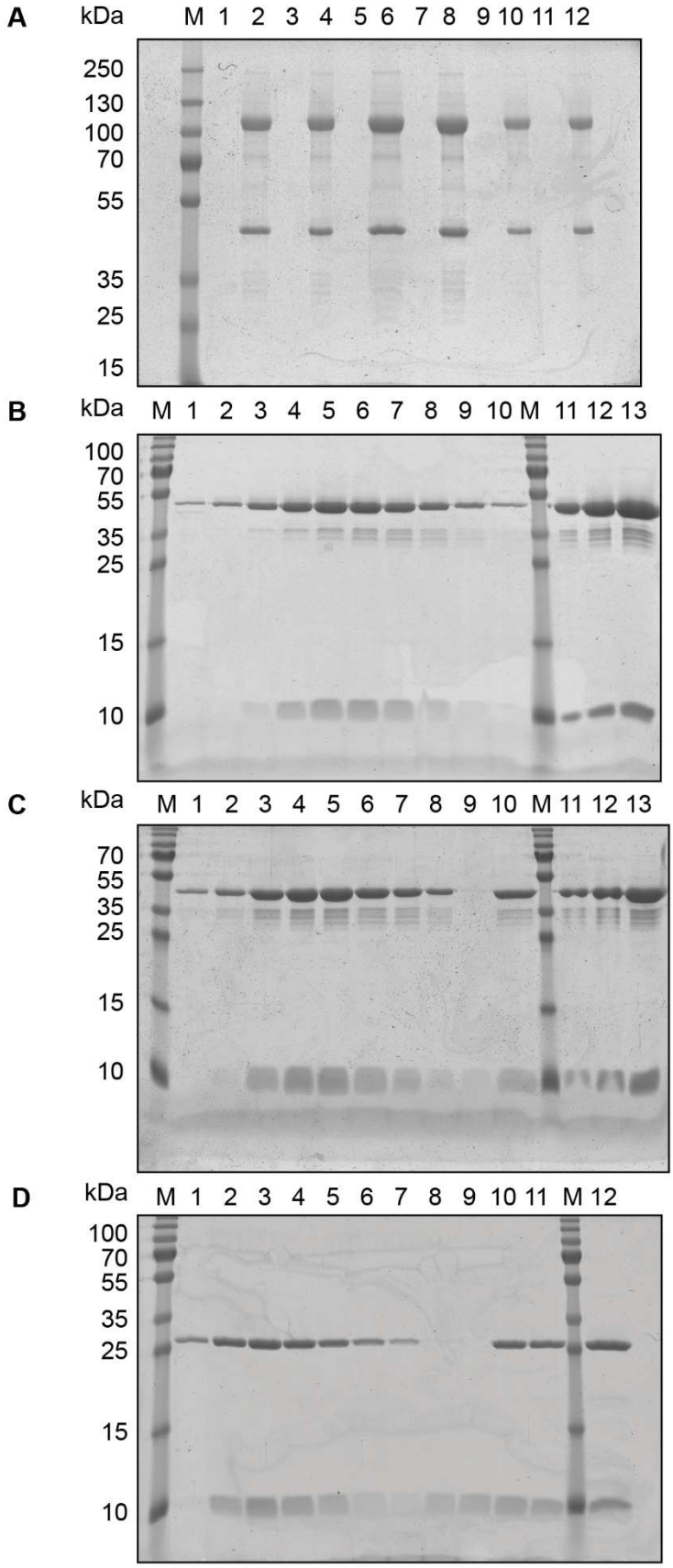

Supp. fig. A-9: Crystallisation of diverse ARNO-CNK1 complexes, unmodified original of figure 3-15. A | Lane 2 corresponds to the lane shown in the results part, ARNO:CNK1. **B** | Lane 11 corresponds to the lane shown in the results part, ARNO:CNK1-cc. **C** | Lane 11 corresponds to the lane shown in the results part, ARNOΔpbr:CNK1-cc. **D** | Lane 12 corresponds to the lane shown in the results part, ARNO-cc-Sec7:CNK1-cc.

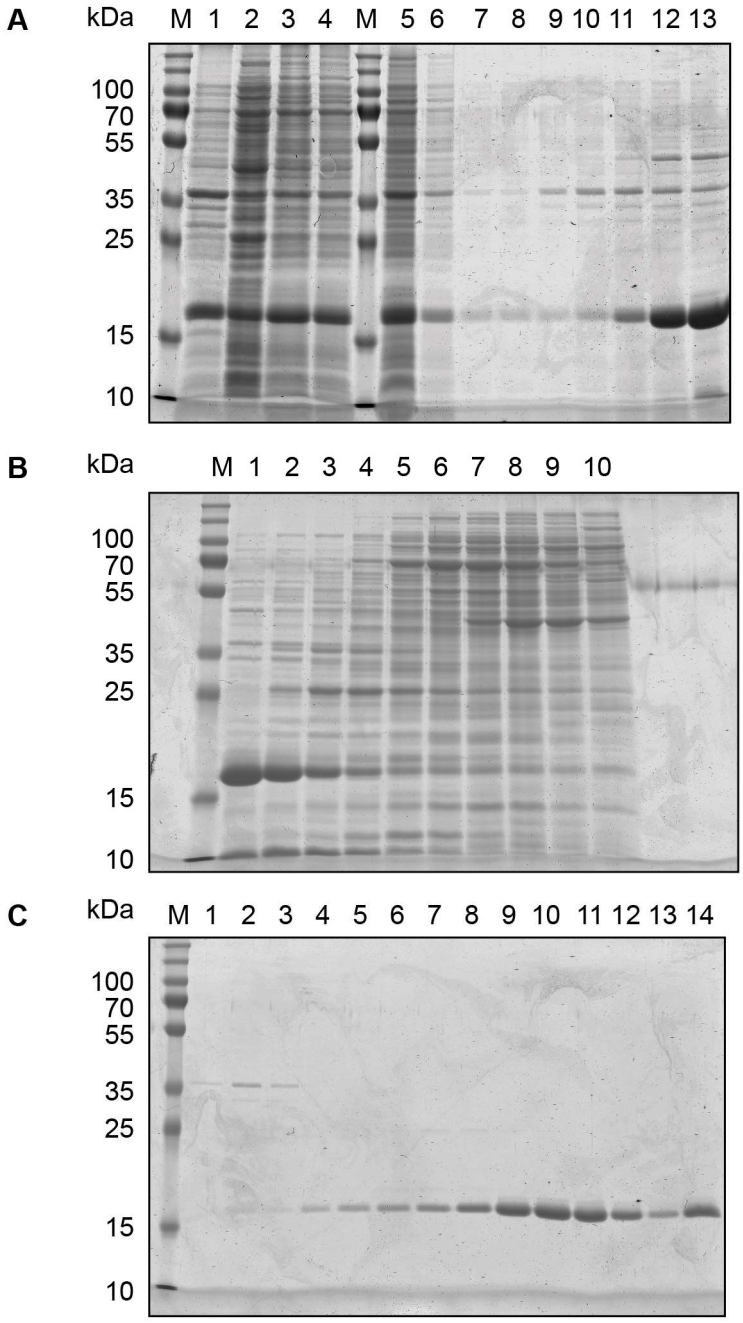

Supp. fig. A-10: Purification of myr-ARF1, unmodified original of figure 3-16. A | Lanes 1-4 correspond to the cell debris, lysate, resolubilised precipitate and rebuffered lysate lanes shown in the results part. The rest of the gel depicts fractions of the anion exchange chromatography. **B** | Lane 1 corresponds to the IEX first peak lane shown in the results part. The rest of the gel depicts more fractions of the anion exchange chromatography. **C** | Lane 14 corresponds to the final after SEC lane shown in the results part. The rest of the gel depicts more SEC fractions.

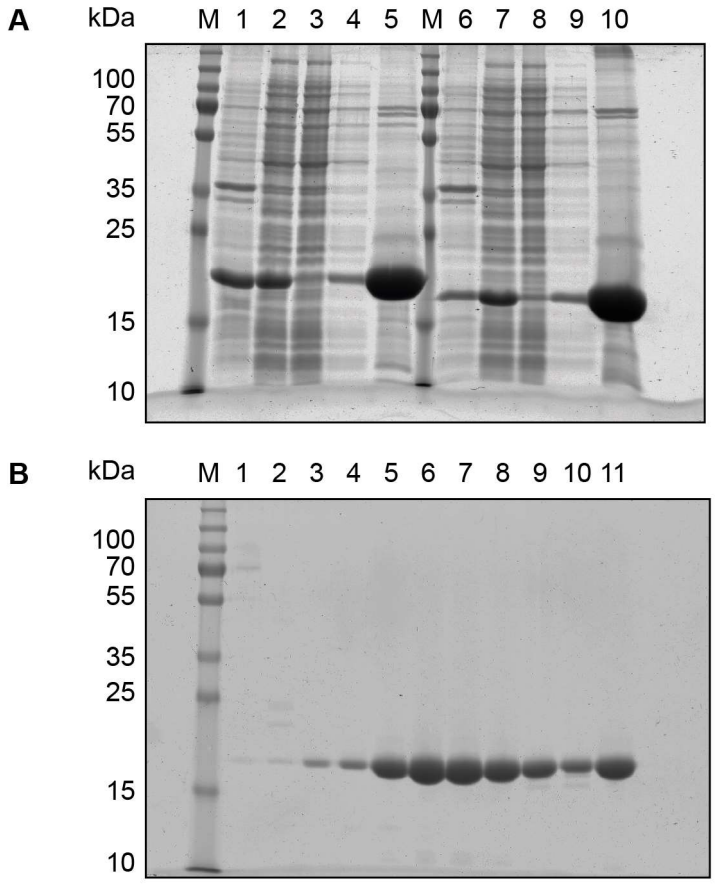

Supp. fig. A-11: Purification and *in vitro* myristoylation of ARF6, unmodified original of figure 3-17 part 1. A | Lanes 6-10 correspond to the cell debris, lysate, flow through, wash and eluate lanes for ARF6 shown in the results part. **B** | Lane 11 corresponds to the final after SEC lane for ARF6 shown in the results part. The rest of the gel depicts more fractions of the SEC.

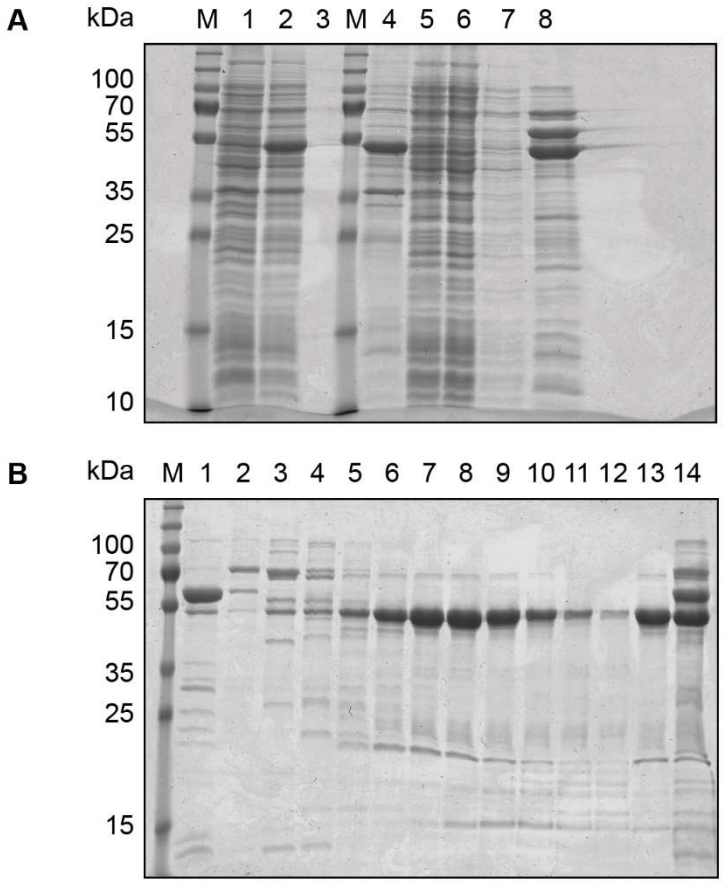

Supp. fig. A-12: Purification and *in vitro* myristoylation of ARF6, unmodified original of figure 3-17 part 2. A | Lanes 4-8 correspond to the cell debris, lysate, flow through, wash and eluate lanes for NMT shown in the results part. Lanes 1 and 2 show a sample of lysed bacteria before and after expression induction, respectively. **B** | Lane 13 corresponds to the final after SEC lane for NMT shown in the results part. The rest of the gel depicts more fractions of the SEC as well as the IMAC eluate fraction for comparison.

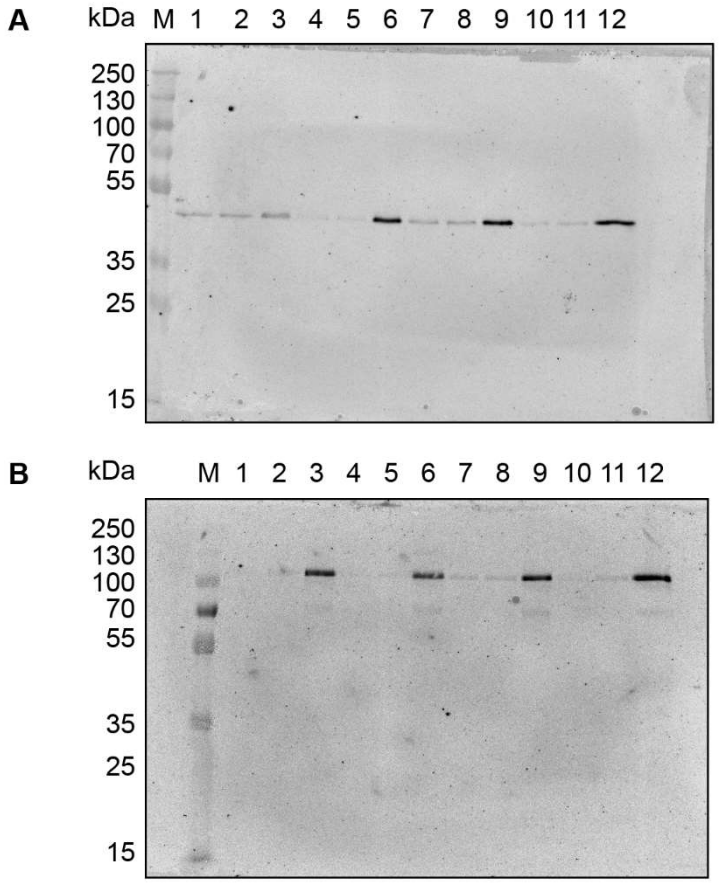

Supp. fig. A-13: CNK1 does not recruit ARNO to the liposome fraction, unmodified original of figure 3-22. A | Lanes 1-12 correspond to the lanes shown in the results part, α-ARNO. **B** | Lanes 1-12 correspond to the lanes shown in the results part, α-CNK1.

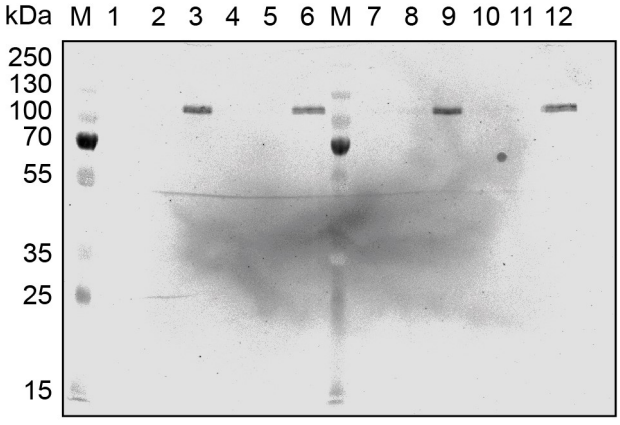

Supp. fig. A-14: CNK1$_{K414Q}$ does not bind to liposomes, unmodified original of figure 3-23. Lanes 1-6 correspond to the lanes shown in the results part, α-CNK1. Lanes 7-12 show a replicate of the experiment.

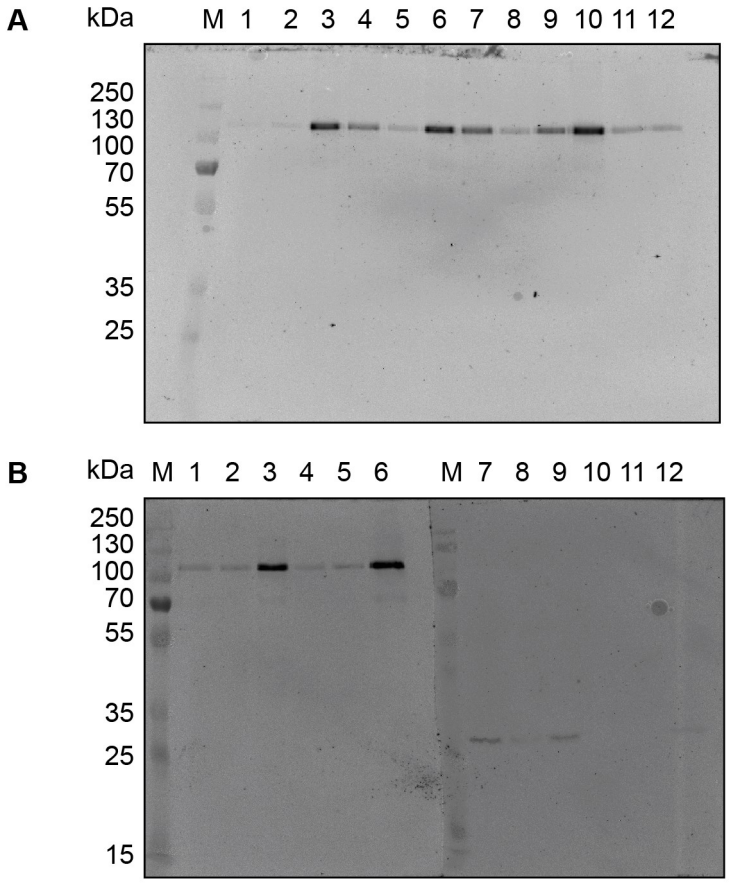

Supp. fig. A-15: Binding of His-tagged CNK1 to liposomes with increasing concentration of DGS-NTA(Ni), unmodified original of figure 3-24. A | Lanes 1-12 correspond to the lanes shown in the results part, 0-25 % DGS-NTA(Ni). **B** | Lanes 1-3 correspond to the lanes shown in the results part, 5 % DGS-NTA(Ni).

Acknowledgements

I would like to express my gratitude to all the people who helped me during the project in many different ways. First, I need to thank Prof Michael Famulok for having me in his group, giving me constant advice and discussing various aspects of the project.

Further, I thank Prof Matthias Geyer for being my second examiner, giving me the chance to perform crystallography in his lab, always being interested in my project and open for discussion. At this point, a big thank you to Dr Kanchan Anand who conducted most of the crystallography part in Karlsruhe and advised me on experimental planning. I am very grateful to Prof Waldemar Kolanus and Prof Olav Schiemann for being my referees from related and non-related fields, respectively.

Dr Anton Schmitz was always there to help interpret confusing data and plan the next steps; I especially want to thank him for his patience and constant support as well as a lot of DNA-related work.

I thank Yvonne Aschenbach for taking over a lot of cloning and Sf-9 expression work and Volkmar Fieberg for practical help and advice in all situations as well as the occasional stunning story on a Friday afternoon. I am grateful for having access to the DLS instrument of Prof Eckhard Mandelkow and thank Dr Senthil Kaniyappan for teaching me how to use it. Thank you to Prof Christoph Thiele for giving me advice on lipid-related topics and to Philipp Leyendecker for being a great student. I also thank Frank Eggert for teaching me how to handle the LC-MS.

I enjoyed the work environment a lot which is largely dependent on the positive atmosphere created by the lab members of the Famulok, Geyer, Mayer and Kath-Schorr groups – thanks a lot. I especially want to thank the caesar group members, Martina Bettio, Maren Hamann, Nora Karnowski and Max Yin for practical help and sticking together in sometimes difficult waters.

All this would not have been possible without the encouragement of my family, my close friends Robert Schröder and Alexander Timm as well as the great people I got to know during table tennis course, Italian evenings and the ImmunoSensation blog. Special thanks to my parents and grandparents who always believed in me and to Martina, who became a fantastic friend.